BIOMECHANICS APPROACH AND MECHANICAL BIOMARKERS FOR CANCER DETECTION: A CASE STUDY OF TRIPLE-NEGATIVE BREAST CANCER

KILLIAN ONWUDIWE

ID #: 70172

A DISSERTATION

PRESENTED TO THE DEPARTMENT OF MATERIALS SCIENCE AND ENGINEERING

AFRICAN UNIVERSITY OF SCIENCE AND TECHNOLOGY

IN PARTIAL FULLFILMENT OF THE REQUIREMENTS FOR THE AWARD OF THE DEGREE OF DOCTOR OF PHILOSOPHY

ADVISOR: PROFESSOR WINSTON O. SOBOYEJO

NOVEMBER 2021

Abstract

This thesis explores the cytoskeletal structures and the statistical variations in the cell-protein fluorescence intensities/volume densities, creep characteristics, and viscoelastic properties of non-tumorigenic breast cells and triple-negative breast cancer cells at different stages of metastases. Most of the cytoskeletal proteins, such as actin contents of the cell cytoskeletal structures are shown to decrease significantly with cell progression from non-tumorigenic to more metastatic states. The corresponding creep and viscoelastic properties of the nuclei and the cytoplasm (Young's moduli, viscosities, and relaxation times) of the cells are also measured using Digital Image Correlation (DIC) and shear assay techniques. The study reveals significant differences between the creep and viscoelastic properties of non-tumorigenic breast cells versus tumorigenic cells. These are shown to exhibit statistical variations that are well characterized by normal distributions. The changes in the mean properties of individual cancer cells are tested using Fisher pairwise comparisons and the analysis of variance (ANOVA). The probabilistic implications of the results are then discussed for the development of shear assay techniques and mechanical biomarkers for the detection of triple-negative breast cancer at different stages of progression.

Acknowledgments

I want to kindly acknowledge the guidance and assistance of several people, who in many ways have been of great support to me, and have given their unmatched contributions, advice, and prayers.

To my supervisor and mentor, Prof. Wole Soboyejo, whose unrequited love for his students and passion for human development got me thus far. My idea of a PhD journey was scary, but with his kind words and encouragement he showed me how interesting and adventurous the journey can be, not without its hurdles, but with a good support system and mentorship. Aside the knowledge, and the deep-rooted skill for independent thought, I also gained tenacity and resilience, key skills I am sure will take me through life. Over these past years, I have worked with my supervisor not in the very conventional professor-student relationship manner, but a father-son relationship, as a mentor and a friend. I greatly appreciate how this journey had gone by working with Prof. Wole. The time I had with was well spent.

Special gratitude to my committee members, who have in many ways been a wonderful support system. Prof. Jingjie, for the countless times I have sought for your time, for a meeting and for your guidance, you showed relentless effort to help and was always too willing to offer

your assistance. Dr. John Obayemi, who for the most time was my go-to person for anything and everything, from research to personal and other extracurricular activities, you made the research life more interesting and have immensely contributed to my success today. I want to extend my gratitude to Prof. Nima, who was ever willing to provide technical insights and helped me a lot with modeling and ABAQUS simulation, your efforts and assistance have given me a good edge to being better. I also extend my gratitude to Dr. Shola Odusanya, who in his capacity as our group supervisor at AUST, has provided support to the group and which has provided an environment for excellence, I sincerely appreciate your effort.

To my friends and colleagues, Clare Nwazojie, Sr. Chinyerem Onyekanne, Josephine Oparah, Stanley Eluu, Canice Ezeala, Toyin Aina and all the Wole Soboyejo Bio group members at AUST and WPI, I am very grateful for a time together.

I want to thank my family, my mum and sister who have been the most supportive, with their kind words, prayer, and support. We made it!!

This research was supported by Pan African Materials Institute (PAMI) funding, the African University of Science and Technology, Abuja and the Worcester Polytechnic Institute, USA. Special thanks to the former department head and acting president of AUST, Prof. Peter Onwualu for these opportunities.

This research was supported by the Pan African Materials Institute (PAMI) with a grant from the African Centers of Excellence (ACE) Program (Grant No. P126974) that was funded by the World Bank. The authors are also grateful to the Worcester Polytechnic Institute for the financial support of the work.

Table of Contents

Table of Contents *6*

Table of figures *9*

List of Tables *13*

Introduction *14*

1.1. overview and Motivation 14

1.2. Scope and Organization of Thesis 16

Literature Review *18*

2.1. Cell as a Material 18

2.2. Cytoskeletal structure of the cell 18

2.2.1. Actin Filament 19

2.2.2. Intermediate Filament 20

2.2.3. Micro tubulin 20

2.2.4. Relative Volume density of the cell cytoskeleton 20

2.3. The Tensegrity Structure of the Cell 20

2.4. Cell Mechanics 21

2.4.1. Cell Mechanics Techniques. 22

2.4.2. Shear assay Technique 23

2.4.3. Strain and Displacement Mapping of the Cell 26

2.4. Fatigue and fracture in cells 30

Chapter 3 ..... *31*

Actin Cytoskeletal Structure and the Statistical Variations of the Mechanical Properties of Non-Tumorigenic Breast and Triple-Negative Breast Cancer Cells *31*

3.1. Introduction 31

3.2. Experimental Methods 34

3.2.1. Analytical Modeling and Statistical Analysis 34

3.2.2. Statistical Analysis 35

3.3. Results and Discussion 36

3.3.1. Actin Cytoskeletal Structure 36

3.3.2. Viscoelastic Properties of Non-Tumorigenic Breast Cells and TNBC cells Using the Shear Assay Technique 39

3.3.3. Comparison between the Cell Mechanical Properties Using Shear Assay and AFM Measurement Technique 41
3.4. Statistical Distributions and Analysis 43
Analysis of Variance (ANOVA) and Fisher Pairwise Comparison (FPC) 49
3.4.1. Probability and Cumulative Density Functions of Cell Fluorescence Intensities and Viscoelastic Properties 52
3.5. Actin Cytoskeletal Structure and the Variations in Cell Viscoelastic Properties 55
3.6. Implications 60
Chapter 4 ..... *61*
Investigation of Creep Properties and the Cytoskeletal Structures of Non-Tumorigenic Breast Cells and Triple-Negative Breast Cancer Cells *61*
4.1. Introduction 61
4.2. Materials and Methods 65
4.2.1. Cell Culture 65
4.2.2. Immunofluorescence Cell Staining 65
4.2.3. Confocal imaging and analysis 67
4.2.4. Shear Assay Experiments 68
4.2.5. Strain Mapping 72
4.2.6. Viscoelastic modeling 72
4.2.7. Statistical Analysis 74
4.3. Results 74
..... 74
4.3.1. Single-Cell Strain Mapping and Strain Evolution 74
4.3.2. Cell Viscoelastic Properties 82
4.3.3. Relative volume density distributions of the different proteins 83
4.3.4. Strain evolution analysis, the relative volume density of cell cytoskeletal structure, and correlation with cell mechanics. 92
4.4. Discussion 94
Chapter 5 ..... *96*
A Shear Assay Study of the Viscoelastic Deformation and Interfacial Fracture Behavior of Non-tumorigenic and Triple-Negative Breast Cancer Cells *96*
5.1 Introduction 96
5.2. Materials and Methods 99
5.2.1 Cell Culture Experiments 99
5.2.2. Shear Assay Experiments 100
5.2.3. Strain Mapping 102
5.2.4. Immunofluorescence Staining of the ECM 103

5.2.5. Finite Element Analysis 104
5.3. Results and Discussion 105
5.3.1. Cell Detachment Behaviors and Characteristic Creep Profiles 105
5.3.2. Detachment of Cells from the Extra Cellular Matrix 106
5.3.3. Effects of strain Evolution on Cell Orientation and Viscoelastic/Creep Behavior 108
5.3.4. Focal Adhesion/ Cytoskeletal Protein Staining of the ECM 112
5.3.5. Contribution of the cell Cytoskeleton to strengthening and Cell Deformation 114
5.3.6. Finite Element Modeling 115
5.4. Implications 125
6.0 Chapter Conclusion *126*
General Conclusion and Recommendation for Future Work. *130*
Reference: *131*

Table of figures

Figure 1:Schematic image of the cell cytoskeletal structure 19

Figure 2: Cell tensegrity structure (Adapted from [49])..... 21

Figure 3: (a) Programmable syringe pump (b) 35x10mm Petri dish for cell culture (c)Microfluidic flow chamber (d) rubber gasket (e) complete experimental set-up (f) schematic of laminar flow over cell..... 26

Figure 4: strain mapping of cell deformation 28

Figure 5: (a) Cell deformation process in response to applied of shear stress. (b) displacement gradient due to deformation. (c) Strains in terms of displacement gradient. 29

Figure 6: (a) and (b) Representative confocal microscopy images of MCF-10A normal breast cells; (c) and (d) MDA-MB-468 less metastatic TNBC cells; (e) & (f). MDA-MB-231 highly metastatic TNBC cells, obtained by confocal microscopy. All cells were stained and imaged under similar conditions..... 38

Figure 7: Variations in the actin fluorescence intensity for the different cells..... 39

Figure 8: Frequency distribution of the actin fluorescent intensity per unit area for the different cell types. 44

Figure 9: Frequency distribution curve for (a) The modulus of elasticity of the nucleus of the 3 cell types. (b) The modulus of elasticity of the cytoplasm of the 3 cell types. 46

Figure 10: Frequency distribution curve for (a) The viscosity of the nucleus between the 3 cell types. (b) The viscosity of the cytoplasm between the 3 cell types. 47

Figure 11: Frequency distribution curve for (a) The relaxation time of the nucleus between the 3 cell types (b) The relaxation time of the cytoplasm between the 3 cell types 49

Figure 12: Relationship between the variation in the density of actin fluorescence and the cell viscoelastic properties. (a) Modulus of the nucleus (b) modulus of the cytoplasm (c) viscosity of the nucleus (d) viscosity of the cytoplasm (e) relaxation time of the 58

Figure 13: (a) Stained images showing the different protein structures of the cell cytoskeleton (Figure insets adapted. (b) Schematic of cytoskeletal structures in a biological cell. 63

Figure 14: (a) Programmable syringe pump (b) 35x10mm Petri dish for cell culture (c)Microfluidic flow chamber (d) rubber gasket (e) complete experimental set-up (f) schematic of laminar flow over cell..... 71

Figure 15: Schematic of the three-element generalized maxwell model..... 73

Figure 16: A five-data plot representative of (a) Single-cell strain evolution for the nucleus of the cells at the primary (elastic) creep stage. (b) Single-cell strain evolution for the cytoplasm of the cells at the primary (elastic) creep stage. (c) Single cell..... 77

Figure 17:Frequency distribution at the onset of creep (Primary creep), for (a) the nucleus of the MCF-10A cell (b) the nucleus of the MDA-MB-231(c) cytoplasm of the MCF-10A, and (d) the cytoplasm of the MDA-MB-231..... 79

Figure 18: Frequency distribution at the onset of creep (Primary creep), for (a) the nucleus of the MCF-10A cell (b) the nucleus of the MDA-MB-231(c) cytoplasm of the MCF-10A, and (d) the cytoplasm of the MDA-MB-231..... 80

Figure 19:The fluorescence intensities/ area for the normal MCF-10A and cancerous MDA-MB-231 for the different proteins (a) Keratin 19 (b) keratin 18 (c) keratin 8 (d) keratin 7 (e) vimentin (f) tubulin (g) actin..... 86

Figure 20: Frequency distribution of the different cytoskeleton proteins for the MCF-10A and MDA-MB-231 cells: (a) Keratin 19 (b) Keratin 18 (c) Keratin 8 (d) Keratin 7 (e) Vimentin (f) Tubulin (g) Actin 88

Figure 21:Confocal images of the cell cytoskeletal proteins and the nucleus for MCF-10A..... 90

Figure 22:Confocal images of the cell cytoskeletal proteins and the nucleus for MDA-MB-231. 90

Figure 23: (a) Confocal images of the F-actin and G -actin structures for MCF-10A. (b) Confocal images of the F-actin and G -actin structures for MDA-MB-231. 91

Figure 24: (a) Shear assay set-up (b) Schematic of a cell under laminar flow 99

Figure 25: Deformation mechanisms for different cells: (a) Before the deformation of cancerous MD-MB-231 cells (b) Peel-off (tensile failure) and in-plane shear-off (shear failure) of cancerous MD-MB-231 cells (c) Before the deformation of normal MCF-10A cells and (d) Micro-buckling of the internal structure of the Normal MCF-10A cells..... 106

Figure 26: Description of Cell-ECM detachment revealing the ECM and cohesive material post - shear 108

Figure 27: (a) Displacement evolution and mapping for the Normal MCF-10A cells (I) Cell structure at t=0, and without deformation (II) A gradual buildup of stress around the cell cytoplasm and nucleus (III) Uniform stress distribution within the cytoplasm and nucleus (IV) The onset of micro buckling within the cell structure and onset of tertiary creep (V) Increased failure progression (VI) Final failure/Detachment of the cell. 110

Figure 28: (b)Displacement evolution and mapping for cancerous MDA-MB-231 cells (I) Cell structure at t=0, and without deformation (II) Larger displacements within the cell membrane than in the cell cytoplasm and nucleus, preceding the early peel-off/shear-off of cells (III)

Increased stress and displacement within the cell structure (IV) Onset of failure (V) Failure progression within the structure of the cell (VI) Final failure by shearing off and peeling-off of cell 111

Figure 29:Creep curve for the deformation of the Cell nucleus for the normal and cancerous cell (b) Creep curve for the deformation of the cell cytoplasm for the normal and cancerous cell .. 112

Figure 30: Fluorescence imaging of the vinculin and actin structures of the (a) Normal MCF-10A cell (b) Cancerous MDA-MB-231 cell 114

Figure 31: Schematic of the contribution of cell cytoskeleton in the strengthening and deformation/detachment of the cell 115

Figure 32: Different traction-separation laws: (a) Bilinear form (b) linear-exponential form (c) trapezoidal form (d) trilinear form 117

Figure 33: Finite element modelling of (a) MCF-10A (b) MDA-MB-231 122

Figure 34: Force- traction curve and energy release rate for (a) MCF-10A cell at a displacement magnitude of 3 (U=3) (b) MCF-10A cell at a displacement magnitude of 5 (U=5) (c) MDA-MB-231 cell at a displacement magnitude of (U=3) (d) MDA-MB-231 cell at a displace displacement magnitude of 5 (U=5) 123

List of Tables

Table 1: Viscoelastic properties of normal and cancerous TNBC cells 41

Table 2: Mechanical properties of the breast cells using AFM measurement technique 42

Table 3(a): Fisher Pairwise Comparison (FPC) for the means of actin density of the cells..... 50

Table 4: Statistical analysis for strain evolution of the cells at the onset of deformation (Primary creep regime) 80

Table 5:Viscoelastic properties of normal and cancerous TNBC cells [25]..... 82

Table 6: The relative volume densities of the cell cytoskeleton..... 91

Table 7: Properties of the cohesive zone 119

Table 8: Fracture toughness of the cells computed experimentally and theoretically..... 124

Introduction

1.1. overview and Motivation

In the last few decades, there have been an increased emphasis on the diagnosis and treatment of difficult-to-treat diseases. Cancer which is one of the leading causes of death globally, is one of such diseases with difficult diagnostic and treatment options [1], [2]. Breast cancer is however, one of the most commonly diagnosed cancers in women and records the highest rate of mortality of death by cancer in women worldwide, second in Africa and fifth in the west pacific[3]–[5].

The incidence rate, recurrence and mortality rate vary from region to region. While there is a recorded high incidence of cancers in the western world, the recurrence and mortality rates of cancer is relatively higher in the developing and third world countries[6]. This is to a large extent attributed to the delayed or poor diagnosis of these cancers in these nations, where most cancers are diagnosed at the later stages of cancer progression[1], [7].

In most third world countries and developing nations of the world, there is a huge deficiency in diagnostic methods peculiar to the variance of cancers or other diseases suffered by people of those regions. Triple-negative breast cancer (TNBC) for example, is a type of breast cancer pertinent to most women of African descent, and thus requires specific attention in understanding its peculiarities and uniqueness, and ways to effectively, target, diagnose and treat it. It has thus been found that TNBC compared to all other types of breast cancer, has a poorer prognosis and poor clinical outcomes, and as such constitutes the low survival rates associated with TNBC[8], [9]. TNBCs tests negative for the expression of estrogen receptor (ER)

progesterone receptor (PR) and human epidermal growth factor receptor-2 (HER-2) [10]–[13]. This therefore limits its responsiveness to established therapies such as the hormone therapies (ER or PR positive) and the anti-HER2 targeted therapy that are designed to target these receptors. Due to the lack of targeted therapy in the treatment of TNBCs, the existing therapies used such as the chemotherapy and radiation therapy or a combination of both serve more as adjuvant therapies, which in most cases have both long term and short-term side effects[14], [15]

TNBC in the past is diagnosed via a two-step procedure, which involves imaging and immunohistochemistry, which are rather operator-dependent and time consuming[16]. In most cases, TNBCs may exhibit benign features in mammography and ultrasound screening, and thus would require more sonographic features for its imaging and diagnosis[17], [18]. There is therefore, a crucial need for the development of more effective and advanced diagnostic method for the detection and treatment of TNBC.

In this thesis, we explored more interesting and effective techniques for the classification of non-tumorigenic breast cells from triple negative breast cancer cells (TNBC) and thus the diagnosis and detection of triple negative breast cancer cells.

We explored the mechanical properties of the normal breast cells and the tumorigenic breast cancer cells using a unique shear assay technique and consequent image correlation to understudy these properties, therefore leading to the development of a mechanical biomarker for the cancer diagnosis. We also explored the physiological and microstructural differences between the non-tumorigenic breast cells and tumorigenic TNBCs, using confocal microscopy and different image analysis techniques and thus, determining ways these properties differ during the onset and progression of tumors, and at varying stages of the cancer progression.

Lastly, with the aid of finite element analysis, we also analyzed cell detachment mechanisms, and the fracture properties of the different types of cells. We correlated the results from these techniques to make a sound judgment on the properties of the cells and ways they can be differentiated in its different states (cancerous and non-cancerous).

1.2. Scope and Organization of Thesis

This thesis presents the results of a combined experimental and theoretical study of the different cell mechanical properties, and their physiological and microstructural properties.

A combined approach using shear assay technique, strain mapping, viscoelastic models, and finite element models (cohesive zone model) was used to study the viscoelastic properties (Elastic Modulus, Viscosity and Relaxation times) and the fracture properties (fracture toughness, energy release rates) of the different cells.

The thesis consists of seven chapters:

- Chapter1 (Introduction): This gives a perspective to the motivation of the work and underlying challenges in the field of study.
- Chapter 2 (literature review): This includes relevant literature and published works on mechanical properties of breast cells and TNBCs using of varying mechanical techniques and the structures and roles of the cell cytoskeleton. It also describes use of different models in the study of cell detachment mechanisms.
- Chapter 3: A published work on “Actin cytoskeletal structure and the statistical variations of the mechanical properties of non-tumorigenic breast and triple-negative breast cancer” cells

- Chapter 4: A published work on “Investigation of Creep Properties and the Cytoskeletal Structures of Non-Tumorigenic Breast Cells and Triple-Negative Breast Cancer Cells”

- Chapter 5: A published work on “Shear Assay Study of the Viscoelastic Deformation and Interfacial Fracture Behavior of Non-tumorigenic and Triple Negative Breast Cancer Cells”
- Chapter 6: Concluding Remarks and Suggestions for Future Work

This thesis is based on the following publications:

- **Actin cytoskeletal structure and the statistical variations of the mechanical properties of non-tumorigenic breast and triple-negative breast cancer cells**
- **Investigation of Creep Properties and the Cytoskeletal Structures of Non-Tumorigenic Breast Cells and Triple-Negative Breast Cancer Cells**
- **A Shear Assay Study of the Viscoelastic Deformation and Interfacial Fracture Behavior of Non-tumorigenic and Triple-Negative Breast Cancer Cells**

Literature Review

2.1. Cell as a Material

The human cell and other biological cells under microscopic conditions behave like viscoelastic materials [19]–[25]. The respond directly and indirectly to external influences such as external forces, pressure, change in temperature[26]–[33] and other physiological and environmental factors. These factors influence their activities, functionalities, and performances in biological systems, and therefore, the cells can be analyzed in response to these factors. Viscoelastic materials are materials that exhibit viscous and elastic properties. Therefore, the cell as a viscoelastic material is such that it processes viscous and elastic properties and will respond to either viscous or elastic forces. Within the cell, are proteins called the cell cytoskeleton, that play vital roles in the movement, structure, and architecture cell[34]–[36]. These proteins are also materials that influence the functions and performances of the cell. They are strands of ligaments and rod-like structures that define the cell.

2.2. Cytoskeletal structure of the cell

Eukaryotic cells possess different proteins that make up its structures. These proteins are called the cell cytoskeletal structures and play vital roles in cellular activities. The cell cytoskeletal proteins consist of actin microfilaments, intermediate filaments, and micro tubulin[37].

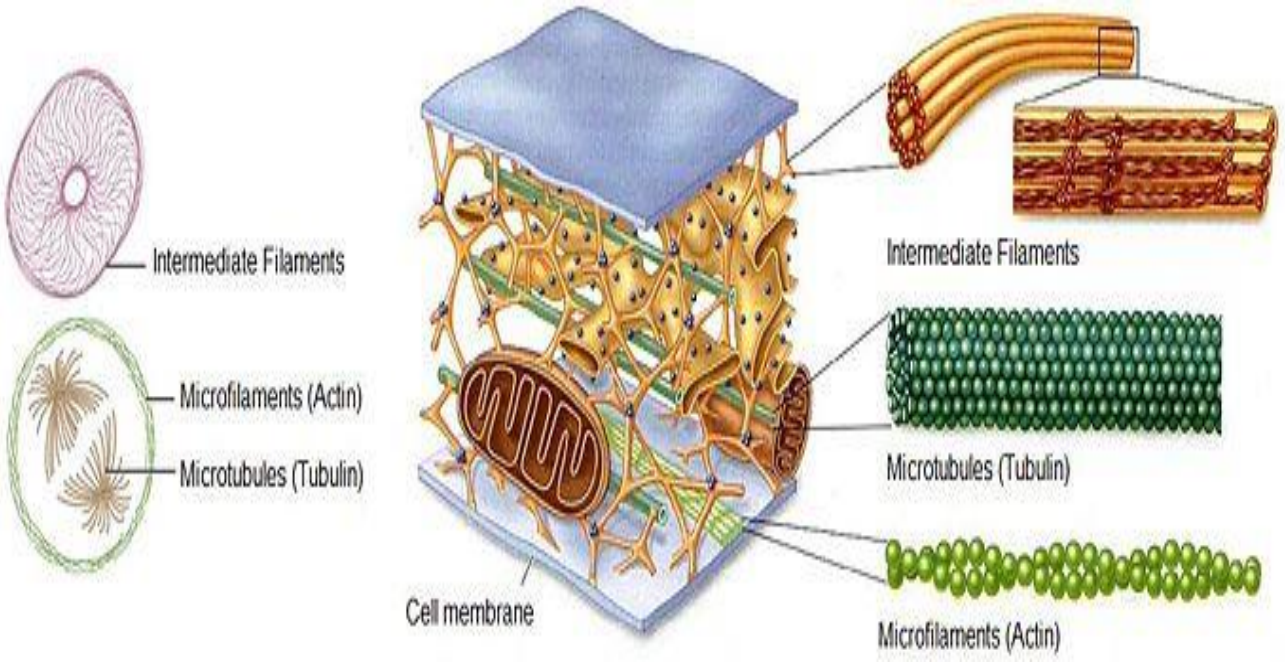

Figure 1:Schematic image of the cell cytoskeletal structure

2.2.1. Actin Filament

The actin filament are the most abundant component of the cell cytoskeleton[25], [38], they are strands of fiber bundles that contribute greatly to the functionality and activity of the cell. They are the smallest of the cytoskeleton with a diameter of about 6nm and are made of proteins called actin. The Actin structure is of two subunits, the filamentous actin (F-actin) and the globular actin (G-actin). Both have specific functions in cell's activities. The globular actin is a monomeric form of actin, which is expected to polymerize into the filamentous actin structure.

The actin structure provides the cell with the rigidity, mechanical support and driving forces for movement. It also contributes to biological processes such as sensing environmental forces, moving over surfaces, and dividing the cell in two [39].

2.2.2. Intermediate Filament

The intermediate filaments which consist of several proteins (the cytokeratin proteins and vimentin) are mid-sized, with a diameter between 8-10nm. The organization of intermediate filaments and their association with plasma membranes suggest that their principal function is structural. They help in the reinforcement of the cells, help to organize cells into tissues, cell signaling, and regulating cell shape [40]–[43]. These intermediate filaments consist of various cytokeratin structures (keratin 7, keratin 8, keratin 18 and Keratin 19) and vimentin.

2.2.3. Micro tubulin

Microtubules are highly dynamic structures which consist of α- and β-tubulin heterodimers, and are involved in cell movement, intracellular trafficking, cell stress responses and mitosis [44], [45]. The micro tubulin has a diameter of about 25nm and consists of a protein called tubulin.

2.2.4. Relative Volume density of the cell cytoskeleton

The determination of the relative volume densities of the cell cytoskeletal proteins at varying stages of cancer progression, can give great insights to the cell states and as biomarkers for cancer detection[34], [37], [46], [47]. In this thesis, the relative volume densities of the cell cytoskeletal proteins were quantified by analyzing their immunofluorescence expressions under the confocal microscope and by measuring their respective fluorescence intensities (gray scale values) using Leica Las fite, an image analysis software.

2.3. The Tensegrity Structure of the Cell

The tensegrity analogy of the cell cytoskeleton brings into perspective, the combined role of the proteins of the cytoskeleton. This explains the cell structure, in which continuous tension within the members forms the basis for mechanical and structural integrity. The cell tensegrity, known

in structural design to maintain tension and structural integrity within members of a structure. They are made of compressive trusses, which in our case are microtubules, tied together by tensile ropes, which are actin and intermediate filaments. The stability of tensegrity structures is due to the way in which their compressive ad tensile-loading components interact[48]. The cables which are the intermediate filaments and actin filaments pull in on both ends of the struts, which are microtubules, and place them under compression, while the microtubules push out and tense the actin and intermediate filaments. This happens continuously within the cell to maintain structural stability and explains the specific roles of these proteins in the activities of cells.

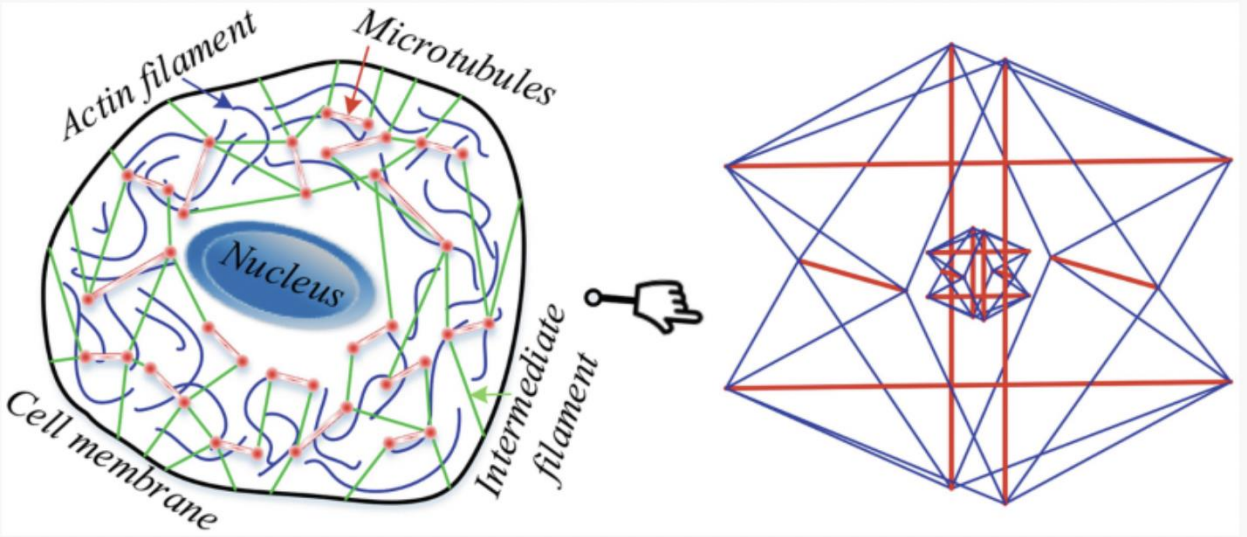

Figure 2: Cell tensegrity structure (Adapted from [49])

2.4. Cell Mechanics

The human eukaryotic cells/biological cells can be idealized as a material only due to their inert material properties. These properties, however, can be characterized using different

mechanical characterization techniques, owing to their behavior under microstructural conditions. These mechanical behaviors of the cell are very unique, such that it provides some useful inert properties that helps in the classification into different characteristic cell state, (benign or cancerous)[50]–[53]. Different techniques have been used for the study of the mechanical properties of cells. These techniques are the use of atomic force microscopy [20], [54]–[57], optical tweezers[58]–[62], rheometer[63], micro pipepte aspiration[64], [65] shear assay technique [23], [25], [66]–[69], and other microfluidic devices[70]–[73]. Results from studies using these techniques strongly suggest that deviations in the cell properties (viscosities and elastic moduli) correspond to the onset and progression of cancers and other related diseases in humans. In this thesis, we studied the mechanical properties of the normal breast cells and cancerous triple negative breast cancer cells using the shear assay technique and correlates these properties to the cytoskeletal structures of the cell as tumor progresses.

2.4.1. Cell Mechanics Techniques.

In recent years, there have been considerable research on the characterization of mechanical properties of cells. These techniques utilize various functionalities of the cells, their orientation, their response to external forces, cytoskeletal variations, interaction between cells and with the environment, and their structural behaviors during migration or movement. These various approaches have been reported using the atomic force microscopy (AFM)[20], [54]–[56], Optical tweezers [59], [61], [62], [74], microfluidics [72], [75], micropipette aspiration [64], [65], magnetic twisting cytometry, shear flow[23], [25], [67]–[69], etc. Studies using these techniques have shown similar trends in the mechanical properties of the cells. Generally, the normal cells are shown to be stiffer and less viscous compared to cancer cells. Our group has, however, utilized the principles of shear assay technique (A flow-based study) and image correlation using

the digital image correlation, to study the mechanical behavior of cells under certain conditions, and correlate them to their modulus of elasticity, viscosities, and relaxation time.

2.4.2. Shear assay Technique

The shear assay experiment as one of the cell mechanics tools that utilize the principle of shear flow, was used in this thesis. This technique was used to exert mechanical forces in the form of fluid pressure to biological cells (MCF-10A and MDA-MB-231), and hence the mechanical response of these cells to an applied force was subsequently observed. This, however, translates to the further determination of the cell viscoelastic properties of the non-tumorigenic and tumorigenic breast cells using other mechanical techniques such as strain mapping and the use of viscoelastic models. An average of 20 single cells per cell line was sampled for this study. Fig 2 below shows the experimental setup involved in the determination of the mechanical response of the cells as a function of the external forces. The cells were cultured in a Petri dish (35x10mm) (CELL TREAT scientific products, MA, USA) as shown in Fig 2b. The process further involves the fitting of the microfluidic device chamber, together with the rubber gasket in between. This set up is connected to the syringe pump with the help of tubing, and then placed on the optical microscope for imaging and monitoring. The programmable syringe pump (Fig 2a), then infuses and withdraws the fluid medium using syringes and tubing and is kept at a constant flow rate (3ml/min), ensuring a continuous flow of fluid over the surface of the cell. This controlled flow of fluid is carried out within a microfluidic flow chamber as shown in Fig 2 c, fitted unto the Petri dish with the help of the rubber gasket (Fig 2d), which helps ensure controlled fluid flow between the microfluidic device and the Petri dish. The rubber gasket is circular, with tiny holes, and serves as vacuum suction. It has a rectangular channel in the middle (20.5 mm - length, 2.5 mm - width, and 0.254 mm height) that determines the flow profile. The controlled

flow of fluid within the parallel flow chamber generates the desirable wall shear stresses. The process of shearing off of the cells and determining how the fluid flow affects the mechanical and structural integrity of the cells is captured by the optical microscope and displayed on a computer monitor as shown in Fig 2e.

Formula for the determination of the wall shear stress is given as

$$\sigma = \frac{6\mu Q}{wh^2} \quad (1)$$

where is σ is the wall shear stress, μ is the viscosity of the fluid medium, Q is the flow rate, W is the width of the channel (rubber gasket), and H is the height of the channel (rubber gasket).

To prevent non-specific binding of the extracellular matrix protein, a serum-free culture media was used for cell culture. In most cases, methylcellulose which is non-toxic and non-allergenic is added to the serum-free media to increase the viscosity of the cell culture medium. This is the case in MCF-10A cells, where 3.5wt% methylcellulose is added to the culture media to obtain a viscosity of 0.16Pa.s. For the MDA-Mb-231 cells, no cellulose was added, and hence the viscosity of the media was 0.02 Pa.s. This is because less shear stress is required to deform or shear off the MDA-MB-231 cells. However, the shear rates for both the MCF-10A and MDA-MB-231 cells are similar (2500 $s^{=1}$), and the wall shear stress for the shearing-off of MCF-10A and MDA-MB-231 was 410 Pa and 10 Pa, respectively. The Reynolds number was ensured to be within the laminar flow regime (Re<100).

To ensure that the same fluid temperature is maintained and delivered to the cells, and to avoid disturbance of the cells during the experiments, the flow medium was pre-heated to 37^{o}C in a water bath, and residual bubbles in the flow line were evacuated by pre-flushing the tubing alongside the medium. The cells were subjected to controlled shear stresses by keeping the flow

and velocities uniform. The response of the cells to shear stresses was observed *in situ* using an optical microscope and a video camera. The movements and detachment of isolated single cells from their substrates without the interference of the adjacent neighboring cells were monitored using the 40 X objective lens from Nikon. The detachment/dislocation of the cells (nucleus and cytoplasm) were recorded and stopped when the cells detached from the substrate. The individual frames from the recordings were extracted for the digital image correlation analysis. This technique proves to be a potential mechanical means for cell characterization and is proposed for the characterization of cells into their component cell states.

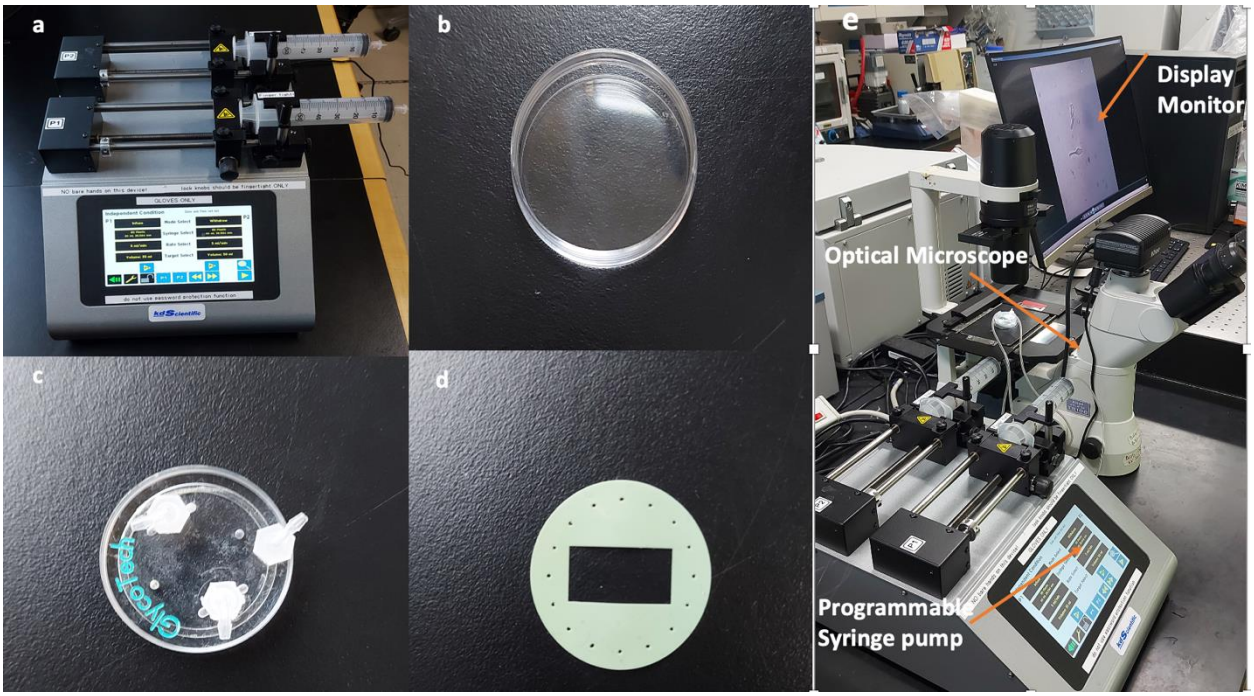

(f)

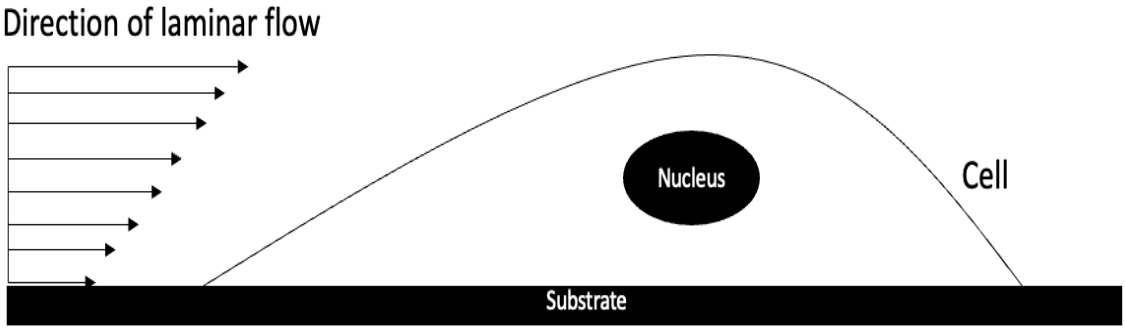

Figure 3: (a) Programmable syringe pump (b) 35x10mm Petri dish for cell culture (c)Microfluidic flow chamber (d) rubber gasket (e) complete experimental set-up (f) schematic of laminar flow over cell

2.4.3. Strain and Displacement Mapping of the Cell

Displacement and strain are resulting effects of deformation of any given material. The response of any material subjected to an external stress/force, generates associated displacement and strain within the structure of the material and in general the material itself. The response to applied forces/stresses by materials enables the determination of the materials' strength and other associated mechanical properties. In this thesis, the strain deformation of the cells was determined using the digital image correlation software (DIC), by tracking the deformation of each marked point on the nucleus and cytoplasm images within the cell as shown in Figure 2a [25]. After the background images of the cell were digitally masked, DIC was performed on the images, where the deformation of the patterned nucleus and cytoplasm are being tracked. The cell deformation at every given time, yielded a displacement-time data for the calculation of the maximum shear strain and creep

After deformation of the cells, the corresponding displacement-gradient data was obtained as the cells were deformed with respect to time. Strain values were further obtained using strain mapping techniques. Fig 2A-C shows the evolution from applied shear stress to the determination of the shear strain. Fig 1A represents the shear deformation of the breast cell due to the application of shear stress. The nucleus and cytoplasm as shown are marked and are tracked to monitor the deformation of the cells from a given point to another till complete detachment /deformation of the cells from the base matrix (culture dish). This was done using the La-Vision DIC software by Hu *et al.*, 2017[25].

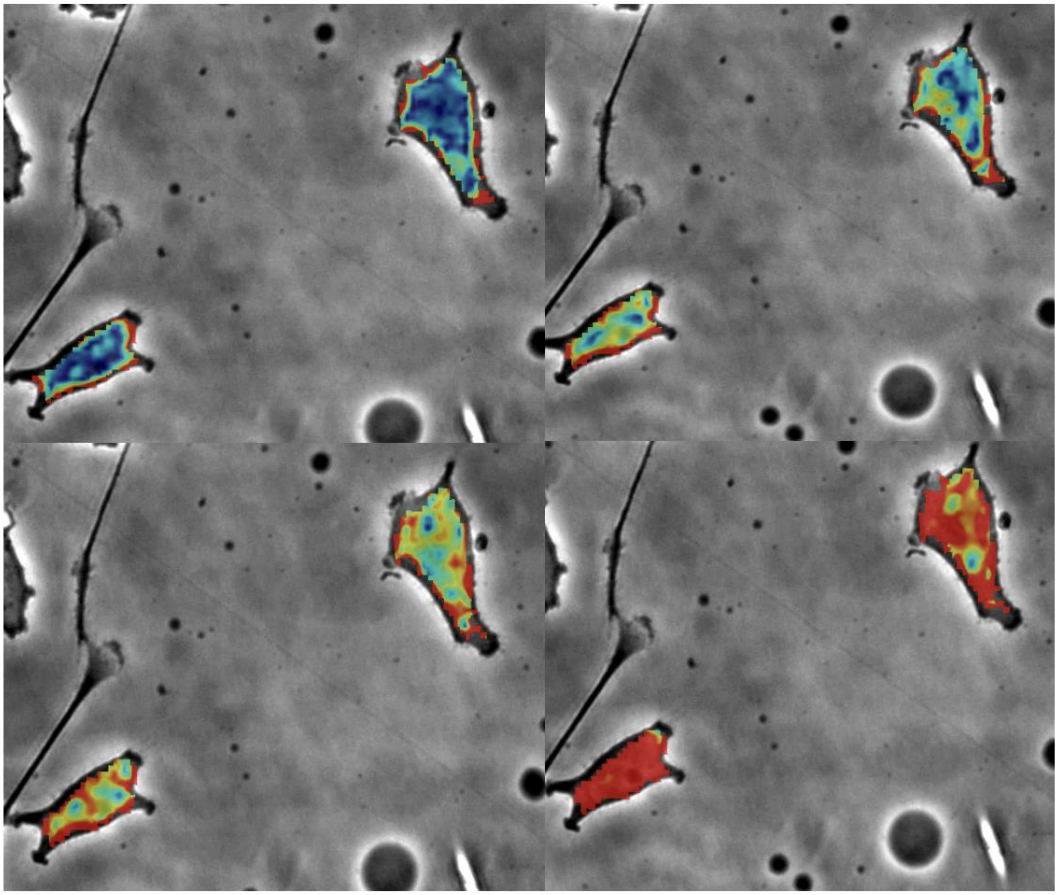

Figure 4: strain mapping of cell deformation

By considering a line element of length Δ *x*, denoted as AB as shown in Fig 2B, the element assumes the new position A'B' after deformation due to translation, extension and rotation. Therefore, strain which is defined as change of length/original length ($\frac{\Delta l}{l_o}$ will thus be:

$$\frac{A'B' - AB}{AB} = \frac{u_x(x+\Delta x,y) - u_x(x,y)}{\Delta x} = \varepsilon_{xx} \; ; \qquad (2)$$

As the limit $\Delta x \longrightarrow 0$; $\varepsilon_{xx} = \frac{\partial u_x}{\partial x}$(displacement gradient with respect to the x- axis).

Provided that the angle of rotation is small, and the displacement gradient is also small, the Shear strain as shown in Fig 2C can be written in terms of displacement gradients as.

$\varepsilon_{xx} = \frac{\partial u_x}{\partial x}$ (Displacement gradient with respect to the x- axis)

$\varepsilon_{yy} = \frac{\partial u_y}{\partial y}$ (Displacement gradient with respect to the y- axis) (3)

$\varepsilon_{xy} = \frac{1}{2}\left(\frac{\partial u_x}{\partial y} + \frac{\partial u_y}{\partial x}\right)$ displacement gradient with respect to the x-y plane)

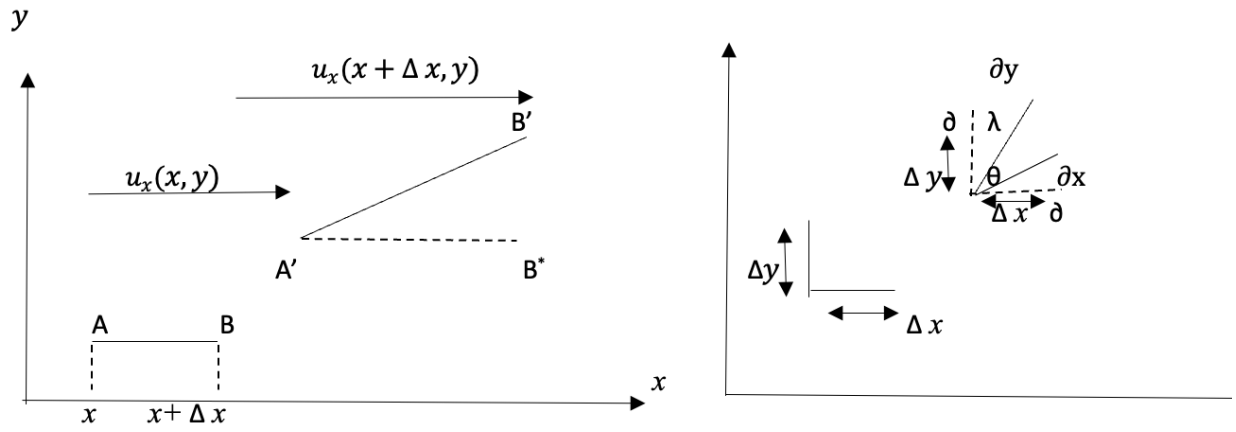

Figure 5: (a) Cell deformation process in response to applied of shear stress. (b) displacement gradient due to deformation. (c) Strains in terms of displacement gradient.

$$\Delta y = \frac{\partial u_y}{\partial y}; \quad \Delta x = \frac{\partial u_x}{\partial x}; \quad \partial y = \frac{\partial u_x}{\partial y}; \quad \partial x = \frac{\partial u_y}{\partial x} \tag{4}$$

2.4. **Fatigue and fracture in cells**

Several fracture mechanics models have been used to characterize the fracture behaviors in biological cells[68]. In a previous research, linear elastic fracture mechanics (LEFM) have been used to analyze the deformation/detachment processes in normal breast cells and cancerous cells. This, however, helps the classification of cells using the variance in the fracture toughness, and critical energy release rates. During the deformation of cells, there exist certain point of stress concentration, inert inconsistencies that bring about surface or internal cracks and can however be points of crack growth, propagation, and detachment/failure. These mechanisms, however, help in the quantification of the failure and fracture properties of the cell. Section 5 of this work utilizes the cohesive zone fracture mechanics model and thuss, provides insight on the fracture properties of normal breast cells and tumorigenic triple-negative breast cancer cells. Variation in these properties can thus be used for the diagnosis of cancer.

Chapter 3

Actin Cytoskeletal Structure and the Statistical Variations of the Mechanical Properties of Non-Tumorigenic Breast and Triple-Negative Breast Cancer Cells

3.1. Introduction

Breast cancer is the second leading cause of death in women [76]. It is mostly considered as a pathology that emanates from the breast tissue, especially in the milk duct (ductal carcinoma, representing 80% of all cases) and lobules [77]. In the case of Triple-Negative Breast Cancer (TNBC), which represents about 10-15% of all diagnosed breast cancer cases [76], the tumorigenic cells are deficient in estrogen, progesterone, and the erythroblasts oncogene B (ERBB2) receptors [77] that are typically used to detect breast cancer. They are also known to have a poor prognosis and limited treatment options [4], [76].

Hence, to explore alternative approaches for the detection of breast cancer cells, several researchers [7]; [8][9][10][11][12] have used cell mechanics approaches to study the viscoelastic properties of cells in non-tumorigenic and tumorigenic states. These studies have shown that the average viscoelastic properties (Young's moduli, viscosities, and relaxation times) of the cytoplasm and nuclei of such cells generally degrade with increasing metastases [12][10]. However, since the viscoelastic properties of non-tumorigenic and tumorigenic cells can exhibit significant statistical variations [25], there is a need to study the statistical distributions associated with individual cancer cells and cancer tissue. There is also the potential need to correlate the measured cell viscoelastic properties to the underlying cell cytoskeletal structure [46].

The cytoskeletal structure of cells serve as an intricate structural polymer network that supports the shape and structure of the cell and also ensures cell mechanical rigidity [79]. It is also interesting to note that changes in the mechanical properties of cells have been associated with structural changes in the cell cytoskeleton [82].

Actin filaments for example, represent a significant part of the cytoskeletal structure, which also includes microtubules and intermediate filaments. They provide the scaffold or supporting structure for the cell [20], [54], [81], and are also implicated in the formation of filopodia and lamellipodia during cell locomotion and spreading [83]. Recent work has also shown that the actin cytoskeletal structure can evolve significantly during cancer cell progression from less metastatic to more metastatic states [20], [54], [81]. This has been attributed to the disruption of the actin cytoskeletal structure. This contributes significantly to the viscoelastic properties of cells, as described by Kubitschke *et al*. [84]], reducing the relaxation times for small and large strains, and other mechanical properties [84]. In any case, new insights have been obtained from biomechanics studies of non-tumorigenic and tumorigenic cells [18], [19]. The insights have also provided some basis for the development of novel mechanical biomarkers for early cancer detection [9], [10][12]

Since the development of mechanical biomarkers involves the development of experimental techniques for the determination of single-cell mechanical properties, such as the atomic force microscopy, nanoindentation, optical tweezer, and micropipette aspiration [74], [87], [88], it is important to note here that there are attendant challenges in the effective use of these methods [25]. For example, the atomic force microscopy probes can damage the intracellular structure of the cell, as a result of their complex tip geometries. Results from other measurement techniques

such as nanoindentation and micropipette aspiration can be affected by the indentation depth and substrate/contact stiffness respectively. Similarly, laser/materials interactions can affect the local properties obtained from optical tweezers [25]. There is, therefore, a need for soft contact methods for the measurement of cell viscoelastic properties.

Thus, in recent years, shear assay methods have been used by our research group to study the viscoelastic properties of individual cells and tissue [13], [19], [23]. These rely on the shear flow of cell culture fluid in the shear deformation and detachment of single cells or clusters of cells (tissue) under well-controlled flow conditions. The integration of *in-situ* cell observations and strain mapping has also been used to determine the temporal and spatial evolution of strains within the cell membranes and nuclei of non-tumorigenic and tumorigenic cells in prior experiments [25] by our group. However, the statistical variations in the individual cell mechanical properties have not been explored in detail. Furthermore, the variations in the actin cytoskeletal structure have not been related to the statistical variations in the viscoelastic properties of normal cells and cancer cells at different stages of tumor development.

Hence, in this work, cytoskeletal structure and the statistical variations in the viscoelastic properties of non-tumorigenic and tumorigenic cells are studied using the results of shear assay experiments on non-tumorigenic breast cells (MCF-10A), less metastatic triple-negative breast cancer cells (MDA-MB-468), and highly metastatic breast cancer cells (MDA-MB-231). The statistical variations in the viscoelastic properties of the non-tumorigenic and tumorigenic triple-negative breast cancer cells (TNBC) are compared using the analysis of variance (ANOVA) and the Fisher pairwise comparison (FPC). Normal distributions are also shown to describe the statistical distributions of viscoelastic properties in non-tumorigenic and tumorigenic breast cells. The measured viscoelastic properties are related to changes in the actin cytoskeletal structure

(obtained for non-tumorigenic and tumorigenic cells) before discussing the implications of the current work for the development of mechanical biomarkers for the detection of breast cancer from biopsies.

3.2. Experimental Methods

This paper builds on prior shear assay work that was done in our group [25] on breast cancer cells and non-tumorigenic cells. Details of the experiments and the analyses of the data are already presented in the supplementary text. They are, however, only summarized here to provide some context for the statistical analyses that are the focus of this work.

3.2.1. Analytical Modeling and Statistical Analysis

In this section, the viscoelastic properties of the different cells were determined using an analytical model. The variations in these properties were further analyzed using statistical means and techniques.

The viscoelastic properties of the cells (Young's moduli, viscosities, and relaxation times) were determined using a three-element generalized Maxwell model as shown in Figure 2 of the supplementary text. The strain-time data obtained from the DIC analysis was fitted to the corresponding expressions for the strain-time dependence in the primary, secondary, and tertiary regimes. The three-element generalized Maxwell model contains a dashpot and a Voigt model arranged in series. Within this model, $(\sigma/\eta 1)t$ represents the strain in the dashpot after time, t, while $\sigma/E(1-\exp(-t/\tau))$ corresponds to the strain associated with the Voigt model in series with the dashpot [77]. The general equation for the three-element generalized Maxwell model is given by:

$$\varepsilon = \left(\frac{\sigma}{\eta 1}\right) t + \frac{\sigma}{E}\left(1 - exp\left(\frac{-t}{\tau}\right)\right) \quad (1)$$

where ε represents the total strain, σ is the applied shear stress, $\eta 1$ represents the viscosity of the cells, E is young's modulus, t is the time and τ is the relaxation time, which is given by η2/E. These viscoelastic properties were determined by fitting the measured strain-time data to the above equation. This was done using the MATLAB 2013b software package (The MathWorks Inc., Natick, MA, USA), as described by Hu *et al.* [25].

3.2.2. Statistical Analysis

The statistical analyses of the viscoelastic properties of the non-tumorigenic and tumorigenic TNBC cells were carried out using the Minitab 18 software package (Minitab LLC, State College, PA). For each cell type (MCF 10A, MDA-MB-468, and MDA-MB-231), 10 different cells and 30 locations in the nucleus and cytoplasm of the cells were analyzed. These were used to determine the statistical variations in the viscoelastic properties within each cell, and between the different cell types. The similarities and variations in the properties of the nuclei and the cytoplasm were established using the frequency distribution curves. The differences between the distributions obtained for individual cells and groups of cells were then analyzed using the analysis of Variance (ANOVA) and Fisher pairwise comparisons (FPC).

One-way Analysis of Variance Analysis (ANOVA) was used to establish the statistical differences between the different types of cells, and to classify the different classes of cells (non-tumorigenic, less metastatic, and highly metastatic). The differences between the mean properties were also compared using the Fisher Pairwise Comparisons (FPC). In the case of the analysis of variance (ANOVA) between the different cell lines, the analysis was done for equal variances at a confidence level (CL) of 95%. A significance level (SL) (α) of 0.05 was adopted for the analysis.

The null hypothesis (H_0) proposed that the means of the actin fluorescent intensity per unit area and the viscoelastic properties of the different cells were equal (suggesting that there were insignificant differences in the properties of the different cells that were examined in this study. If this is true, then the P-values for the means must be >0.05. The complementary alternative hypothesis (H_a) assumes that the means are not all equal (suggesting that there are significant differences between the mean properties of the different cells), and as such the P-values must be <0.05. The pairwise comparisons were further authenticated using the Fisher Pairwise Comparison (FPC).

3.3. Results and Discussion

In this section, the viscoelastic properties of the normal and TNBC cells are discussed in correlation with the variation in the density of the actin cytoskeleton. Statistical variations of the viscoelastic properties and the density of action for the different types of cells are also discussed.

3.3.1. Actin Cytoskeletal Structure

The actin cytoskeleton which plays a major role in cellular processes like cell migration, organelle transport, axonal growth, structural support, and phagocytosis, has been extensively studied in this work. A clear difference was observed in the actin density and structure in three types of breast cells. The normal MCF-10A breast cells exhibited a compact actin cytoskeletal network, as shown in Figs. 1a-b and Fig 2. In contrast, the highly metastatic MDA-MB-231 TNBC cells exhibited a more dispersed actin cytoskeletal structure (Figures 1c-d and Fig 2), while the less metastatic MDA-MD-468 cells had a less dense actin cytoskeletal structure (Fig. 1e-f and Fig 2). These results were consistent with our prior studies [13], [19].

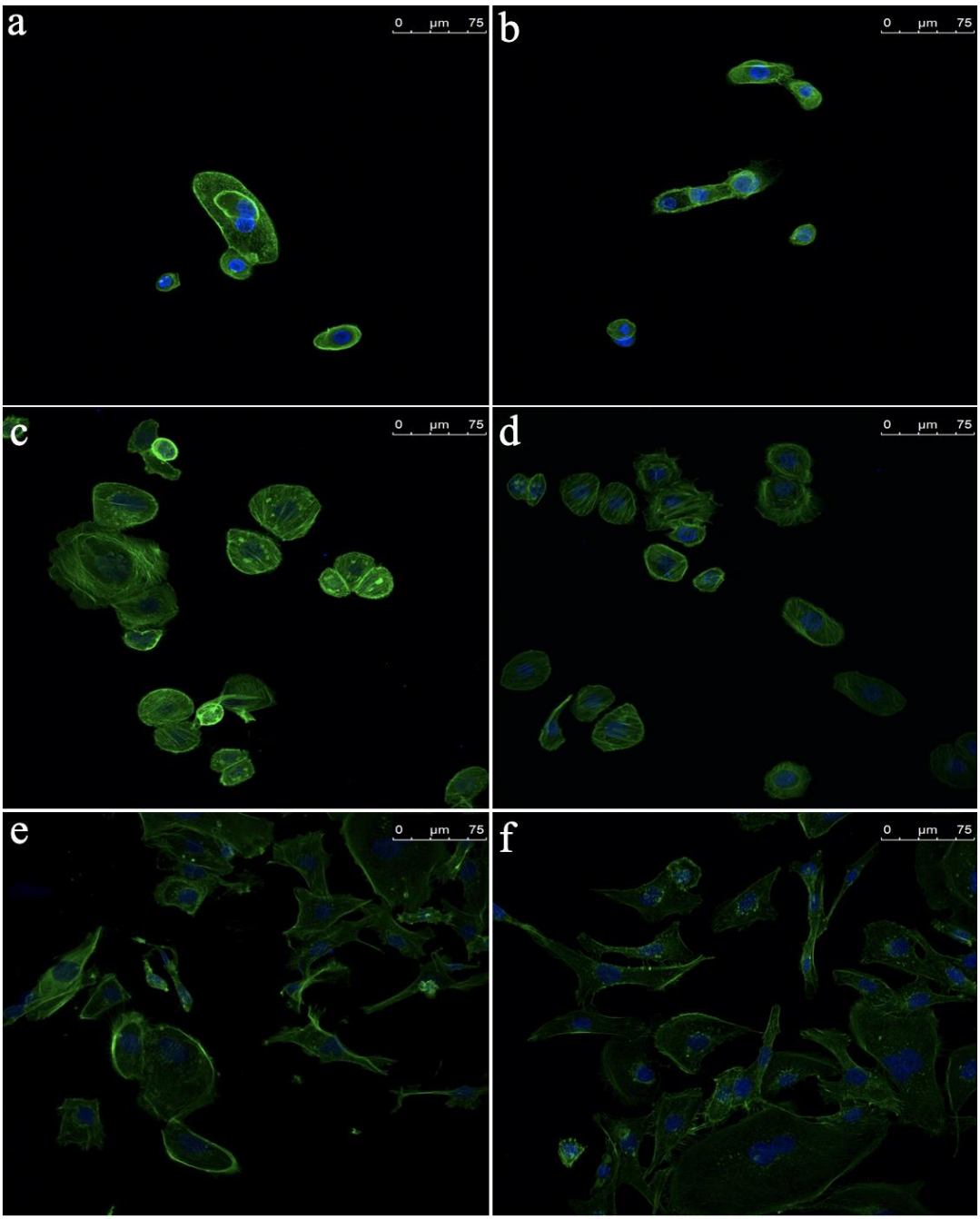

Figure 6: (a) and (b) Representative confocal microscopy images of MCF-10A normal breast cells; (c) and (d) MDA-MB-468 less metastatic TNBC cells; (e) & (f). MDA-MB-231 highly metastatic TNBC cells, obtained by confocal microscopy. All cells were stained and imaged under similar conditions

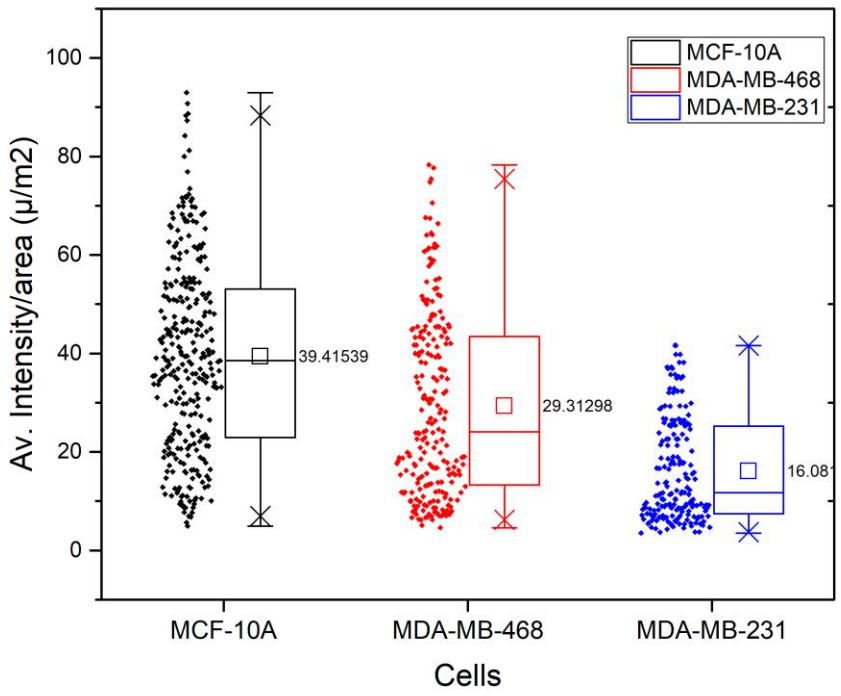

Figure 7: Variations in the actin fluorescence intensity for the different cells

3.3.2. Viscoelastic Properties of Non-Tumorigenic Breast Cells and TNBC cells Using the Shear Assay Technique

In previous works by different authors, these mechanical properties of the cell have been modeled using various viscoelastic models, and thus, certain elements of the model have been attributed to the cell intracellular structure. [21] Their study used the Voigt model, whereby the spring constants of the model were considered as linear approximations to the elasticity of the inner cell. All springs were subject to a damping force due to the viscosity of the cytoplasm and the linear dashpots were used to approximate the viscosity of the cytoskeleton. In this study, the viscoelastic properties were obtained through an empirical fit of the stress-strain data using the

three-element generalized maxwell model, which combines the spring and dashpot model in series to characterize stress-strain behavior.

The average viscoelastic properties were obtained from the same data sets that were used in [25] and are summarized in table 1 below. However, unlike [25]in which the trends in the average data were mostly considered, this paper explores the statistical variations in the induced viscoelastic properties that were obtained from the curve fitting of the strain-time data at discrete points within the cytoplasm and the nuclei of individual cells that were examined in shear assay experiments.

No obvious trends were observed in the relaxation times, although the relaxation times of the nuclei were generally greater than those of the cytoplasm. However, the average young's moduli and the viscosities of the nuclei were generally greater than those of the cytoplasm. Furthermore, the highest average young's moduli and viscosities were obtained for the non-tumorigenic (MCF-10A) cells. These were generally greater than those of the MDA-MB-468 TNBC cells (less metastatic cancer cells). The Young's moduli and the viscosities of the nuclei and the cytoplasm of the MDA-MBA-468 cells were also greater than those of the most metastatic cells (MDA-MB-231 cancer cells). The results, therefore, suggest that the average young's moduli and the viscosities of the cells can be used to identify individual TNBC cells or non-tumorigenic breast cells. However, the corresponding errors in the measurements are quite significant. It is, therefore, important to examine the statistical distributions associated with the measured viscoelastic properties (Young's moduli, viscosities, and relaxation times).

Table 1: Viscoelastic properties of normal and cancerous TNBC cells

Cell Type	Av. Modulus, E, [Pa] Nucleus	Av. Modulus, E [Pa] Cytoplasm	Av. Viscosity, η [Pa*s] Nucleus	Av. Viscosity, η [Pa*s] Cytoplasm	Av. Relaxation Time, τ [s] Nucleus	Av. Relaxation Time, τ [s] Cytoplasm
MCF-10A	7966 ± 2536	3598 ± 1511	6868 ± 3095	3132 ± 1745	0.514 ± 0.290	0.583 ± 0.415
MDA-MB-468	5632 ± 2089	3334 ± 1764	5616 ± 2887	3390 ± 2106	0.597 ± 0.424	0.662 ± 0.840
MDA-MB-231	622 ± 399	261 ± 148	325 ± 234	215 ± 135	0.309 ± 0.353	0.409 ± 0.355

3.3.3. Comparison between the Cell Mechanical Properties Using Shear Assay and AFM Measurement Technique.

Various measurement techniques have been used to characterize the mechanical properties of the cell. Table 2 below shows the results from the AFM measurement technique and their corresponding cell mechanical properties.

Table 2: Mechanical properties of the breast cells using AFM measurement technique

Author	Cell	Modulus [Pa]	Technique
[89]	MDA-MB-231	1004±100	AFM
	MCF-7	3431±377	
[54]	MCF-7	310-810	AFM
	MCF-10A	610-1610	
[22]	MDA-MB-231	856±356	AFM
	MCF-7	963±277	
	MCF-10A	1195±397	
[90]	MDA-MB-231	120-620	AFM
	MCF-10A	1100-1960	
[91]	MCF-7	100-400	AFM
	MCF-10A	200-800	
[24]	MDA-MB-231	4000-6000	AFM
	MCF-7	2500-3500	
	MCF-10A	10,000-30,000	

Most of the measurement of the mechanical properties of breast cells was carried out using the AFM technique. There were varying mechanical properties associated with the normal breast cell (MCF-10A) and the cancerous cells, less metastatic (MCF-7), and highly metastatic (MDA-MB-231). This can be attributed to the variation in indentation rates and depth implored in the various studies. In our current study, it is of note that the values for the mechanical properties of the cell

using the shear assay technique was generally higher than those obtained using the AFM technique.

3.4. Statistical Distributions and Analysis

The frequency distribution curves (probability density functions) obtained for the actin filament intensity per unit area for the different cell types is shown in Figure 3, and that of the viscoelastic properties of the nuclei and the cytoplasm are presented in Figures 4, 5 and, 6 for the different cell types. Figure 3 shows distinct differences in the actin filament intensity. Figures 4 and 5 show that there are distinct statistical distributions of the viscosities and moduli of the nuclei and cytoplasm of the different cell lines.

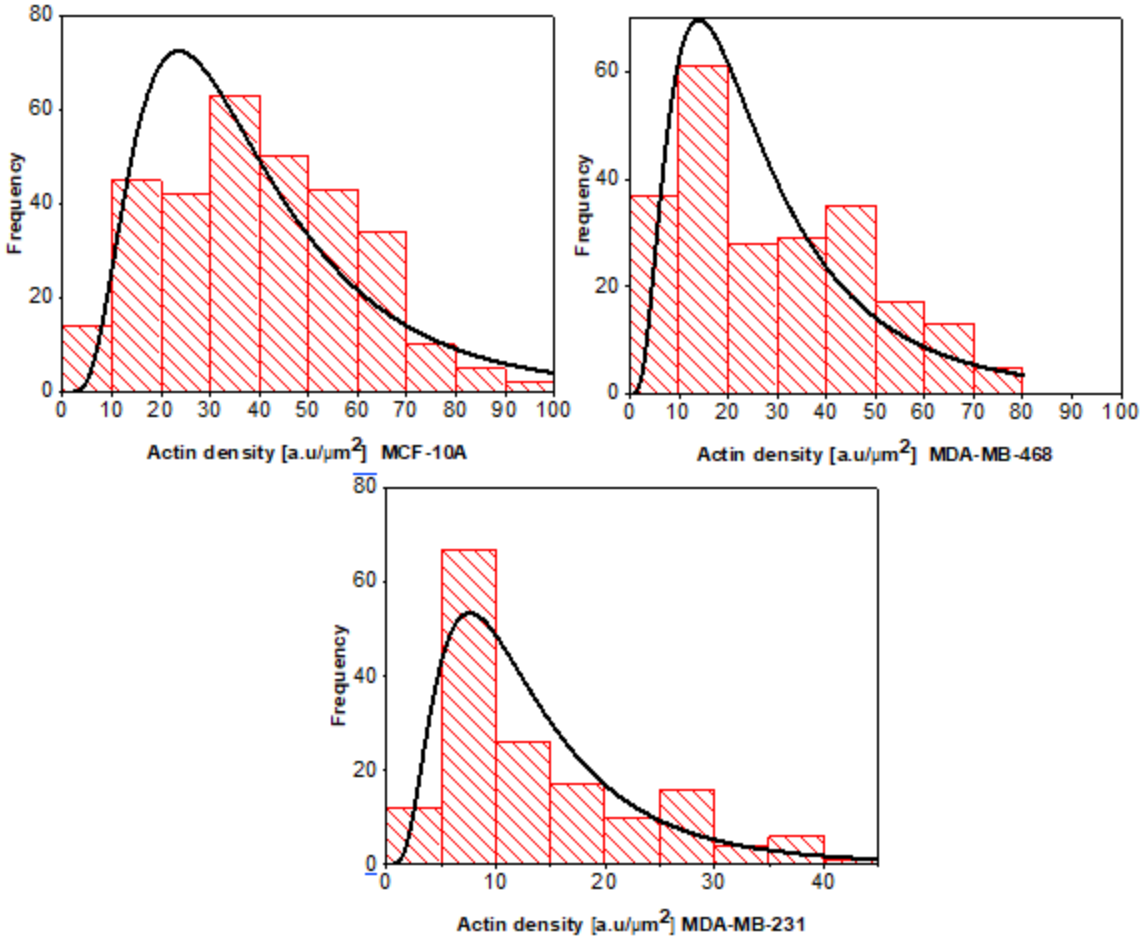

Figure 8: Frequency distribution of the actin fluorescent intensity per unit area for the different cell types.

However, the statistical distributions of the actin fluorescence intensities, young's moduli, and viscosities of the non-tumorigenic breast cells (MCF-10A) were closer to those of the less metastatic MDA-MB-468 cells. Very distinct statistical distributions were obtained for the most metastatic MDA-MB-231 cell lines, which were found to have the lowest fluorescence intensities, young's moduli, and viscosities with high frequencies of occurrence (Figures 3, 4, 5, 6). In the case of the relaxation times, no clear trends were obtained in the statistical

distributions. However, the results in Figures 6a and 6b show that characteristic distributions were obtained for the nuclei and the cytoplasm.

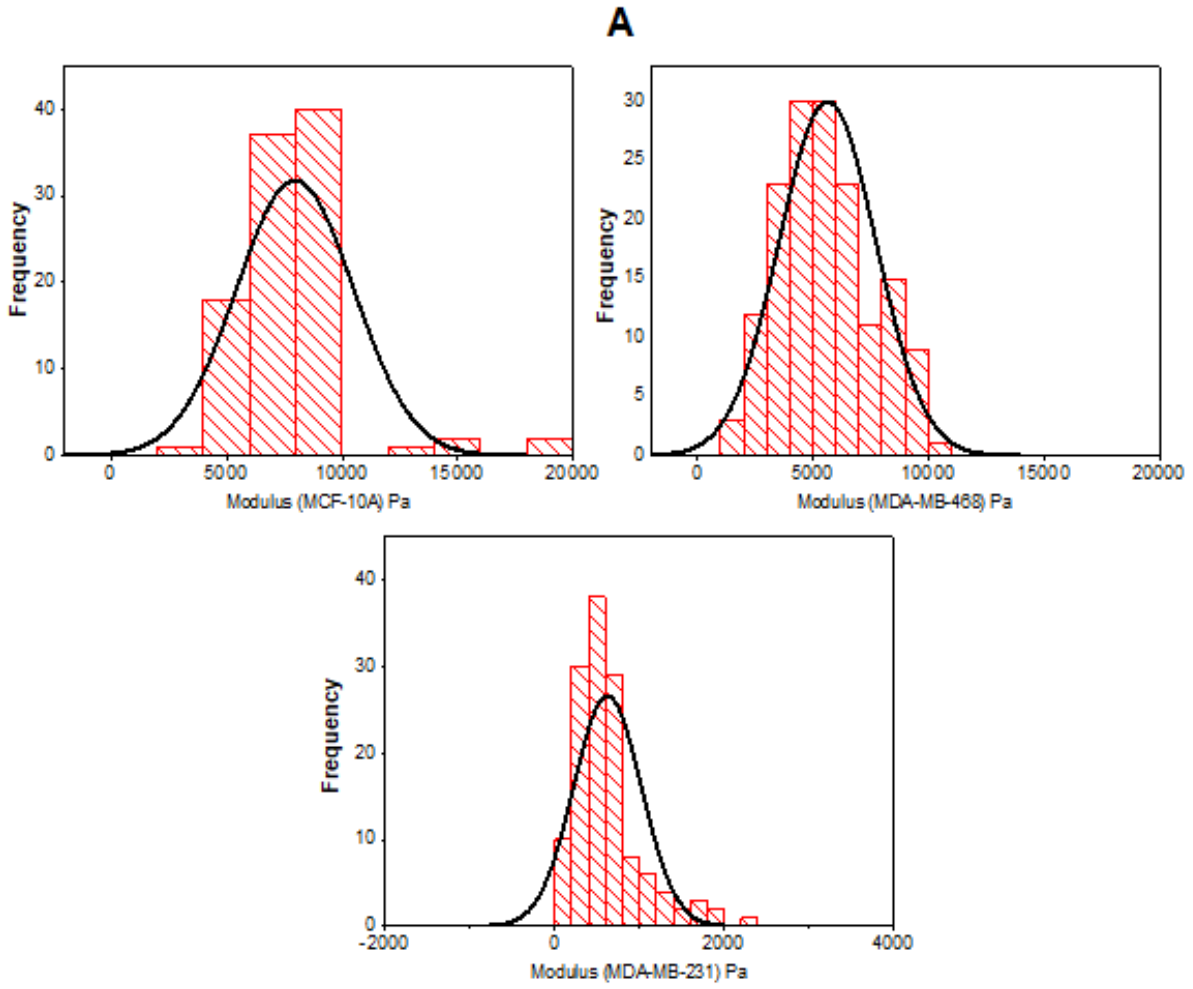

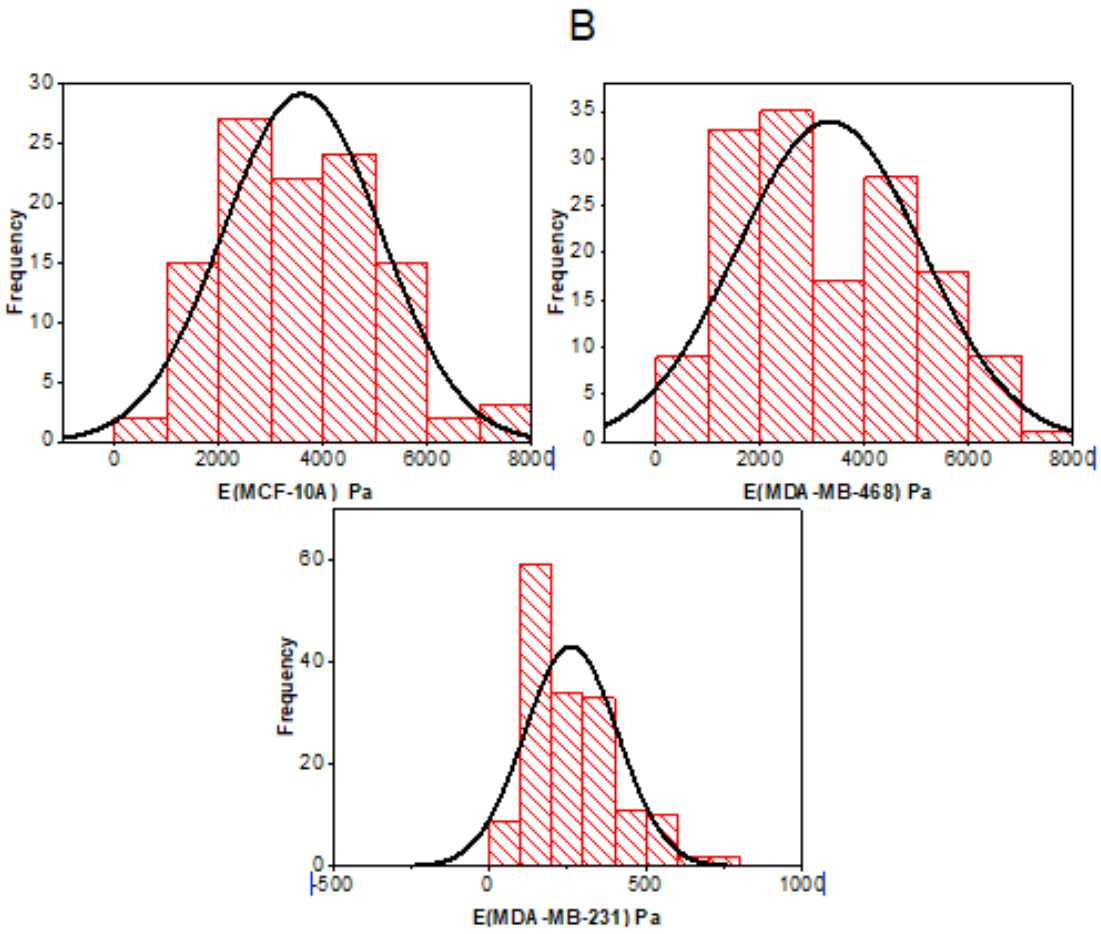

Figure 9: Frequency distribution curve for (a) The modulus of elasticity of the nucleus of the 3 cell types. (b) The modulus of elasticity of the cytoplasm of the 3 cell types.

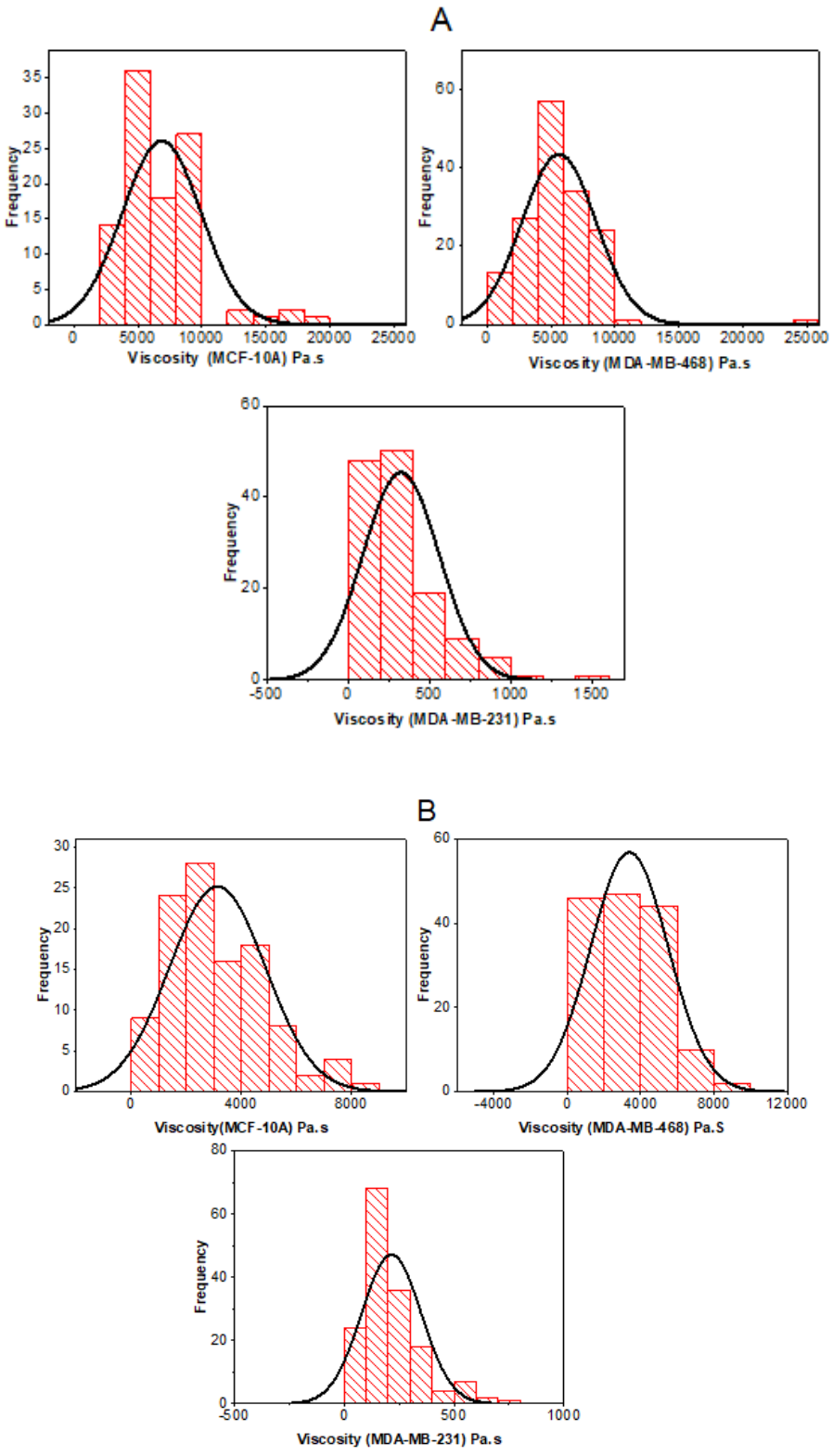

Figure 10: Frequency distribution curve for (a) The viscosity of the nucleus between the 3 cell types. (b) The viscosity of the cytoplasm between the 3 cell types.

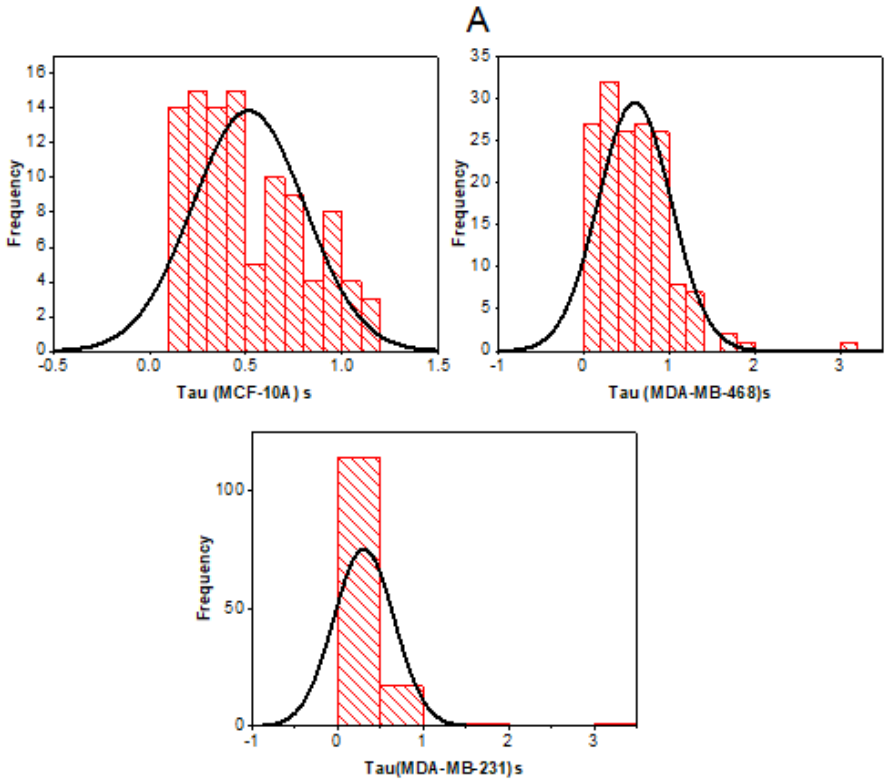
A
Frequency
Tau (MCF-10A) s
Frequency
Tau (MDA-MB-468)s
Frequency
Tau(MDA-MB-231)s

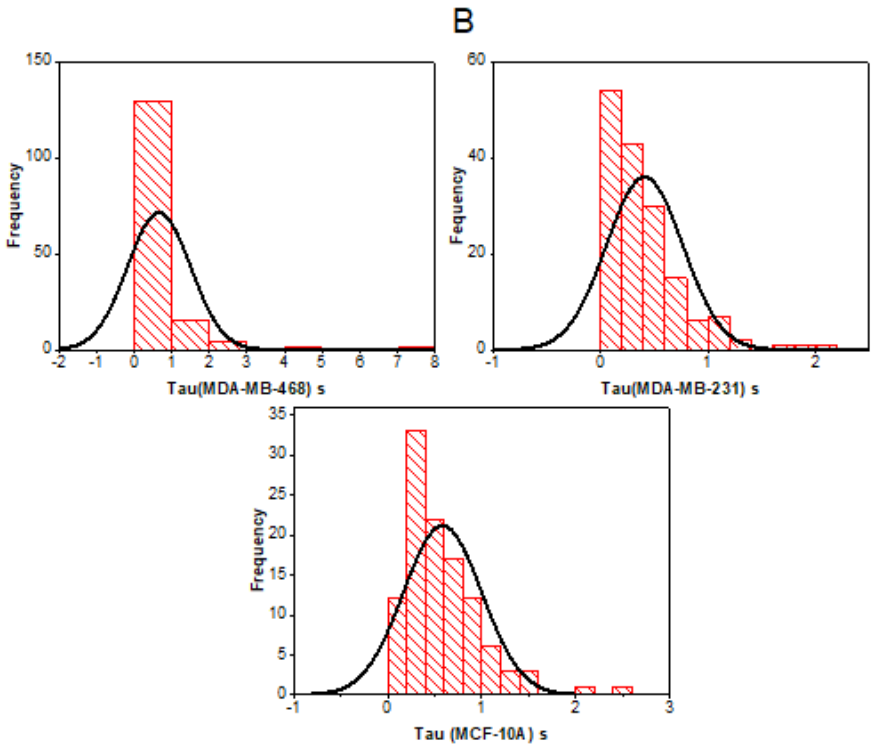

Figure 11: Frequency distribution curve for (a) The relaxation time of the nucleus between the 3 cell types (b) The relaxation time of the cytoplasm between the 3 cell types

Analysis of Variance (ANOVA) and Fisher Pairwise Comparison (FPC)

The results of the FPC analysis are presented in tables 3a, 3b, and 3c. Note that, if an interval does not contain zero, the corresponding means are significantly different.

H_0: $\mu_1 = \mu_2 = \mu_3$

H_a: $\mu_1 \neq \mu_2 \neq \mu_3$ (2)

where μ_1, μ_2, μ_3 are the means for the corresponding properties of the different cells.

The analysis of variance (ANOVA) revealed significant differences between the intensity of the actin filament in the different cell types and the viscoelastic properties (Young's moduli, viscosities, and relaxation times) of the nuclei and cytoplasm obtained for the different cell lines. With P-values < 0.05, their mean values reject the null hypothesis (H_0) and hence accept the

alternative hypothesis (H_a). However, the relaxation time values had P-values < 0.05 for the nucleus of the cells but was greater than 0.005 (>0.05), which means the relaxation times were similar. We, therefore, accept the null hypothesis and reject the alternative hypothesis, in the case of the comparison of the relaxation times.

Table 3(a): Fisher Pairwise Comparison (FPC) for the means of actin density of the cells

Cell	Av. Actin density	FPC grouping
MCF-10A	39.42	A
MDA-MB-468	29.31	B
MDA-MB-231	13.97	C

Table 3b: Fisher Pairwise Comparison (FPC) for the means of the viscoelastic properties of the nucleus

Cell (Nucleus)	Av. Modulus [Pa]	FPC grouping	Av. Viscosity [Pa. s]	FPC grouping	Av. Relaxation time [s]	FPC grouping
MCF-10A	7966	A	6868	A	0.5143	A
MDA-MB-468	5632	B	5617	B	0.5974	A
MDA-MB-231	622	C	325	C	0.3096	B

Table 3c: Fisher Pairwise Comparison (FPC) for the means of the viscoelastic properties of the cytoplasm

Cell (Cytoplasm)	Av. Modulus [Pa]	FPC grouping	Av. Viscosity [Pa. s]	FPC grouping	Av. Relaxation time [s]	FPC grouping
MCF-10A	3598	A	3133	A	0.5831	A
MDA-MB-468	3334	A	3391	A	0.4100	A
MDA-MB-231	261	B	215	B	0.6619	B

N/B: Means that do not share a letter are significantly different

The results of the FPC analysis are presented in Tables 3a, b &c. Table 3a shows the comparison between the actin filament intensity between the different cell types. The statistical analysis shows that there were significant differences in the intensity of the actin filaments observed in the different cell types. On the other hand, tables 3b & 3c, show the comparisons in the viscoelastic properties of the nuclei and the cytoplasm, respectively, for the different cell lines. In table 3b. FPC shows that the means of the moduli and viscosities of the cells do not share a letter, and hence their means were significantly different for different cell states (normal, less metastatic, and highly metastatic). However, the relaxation time does not share the same trends, as it shows no significant difference between the normal cell (MCF-10A) and less metastatic cells (MDA-MB-468), but a significant difference exists between both cell line (MCF-10A & MDA-M-468) and the highly metastatic cells (MDA-MB-231). Table 3c shows the FPC for the

viscoelastic properties of the cytoplasm. The results show that there exists only a significant difference between the highly metastatic cell and less metastatic, and the highly metastatic

3.4.1. Probability and Cumulative Density Functions of Cell Fluorescence Intensities and Viscoelastic Properties

The statistical analysis of individual distribution is shown in Table 1 in the supplementary text file. This was carried out using the Minitab 18 software package (Minitab LLC, State College, PA). The test revealed that the normal distribution best characterizes the statistical variations in young's moduli, viscosities, and the relaxation times (for the normal breast cells and the TNBC cell lines, while for the distribution of the cell actin density, the log normal best characterizes the data. The criteria for selection of the distribution type were based on the distribution with the least P-value and highest AD-value. The normal distribution for the viscoelastic properties of the cell gave a P-value less than 0.005 and an AD-value of 2.386 and was however used to determine the distribution of the viscoelastic properties of the cell. However, for the actin density distribution of the cells, the log normal distribution was used. The lognormal distribution had a P-Value of less than 0.005 and a higher AD-value of 5.915. This was also evident in the frequency distribution curves (probability density functions) presented in Figures 3-6. The normal distribution is, therefore, proposed for the characterization of the probabilities of occurrence of the viscoelastic properties (Young's moduli, viscosities, and relaxation times) and the actin density distribution that were obtained in this study.

The probability density function (PDF) for the normal distribution, which corresponds to the frequency distribution curve for the different properties of the cell is given by

$$f(x) = \frac{1}{\sigma\sqrt{2\pi}} \exp[\frac{-[x-\mu]^2}{2\sigma^2}], \sigma > 0 \quad (3)$$

where f(x) is the frequency of occurrence, σ and μ^2 are the scale parameters and the location parameter of the distribution, corresponding to the standard deviation and the mean respectively. Therefore, to determine the probability of occurrence of a given cell viscoelastic property, the cumulative density function (CDF) is determined from the area under the PDF curve, which is thus given by:

$$F(x) = \int_{-\infty}^{x} \frac{1}{\sigma\sqrt{2\pi}} \exp[\frac{-[x-\mu]^2}{2\sigma^2}]\, dx,\ \sigma > 0 \quad (4)$$

On the other hand, the probability density function (PDF) for the lognormal distribution, which corresponds to the frequency distribution curve for the actin density of the cell is given by

The cumulative density function (CDF) is determined from the area under the PDF curve, which is thus given by:

$$F(x) = \int_{\lambda}^{x} \frac{1}{\sigma\sqrt{2\pi}(x-\lambda)} \exp[\frac{-[\ln(x-\lambda)-\mu]^2}{2\sigma^2}]\, dx, x > \lambda\ \ \sigma > 0 \quad (6)$$

where the above variables have their usual meaning and λ represents the threshold parameter. Furthermore, the probability of non-occurrence for both the normal and lognormal distribution is given by:

$$F'(x) = 1\text{-}CDF = 1 - F(x) \quad (7)$$

In the case of the current work, the expressions in equations 3 and 4 can be used to compute the PDFs and CDFs of Young's moduli, viscosities, and the relaxation times, while equations 5 and 6 can be used to compute the PDFs and CDFs of the actin densities of the cell. These are presented in Figures 3-6 (For the PDFs) in the main text and Figures 4-7 (For the CDFs) in the supplementary text, respectively. These can be used to determine the probabilities of occurrence or non-occurrence, for different viscoelastic properties (of the nuclei and cytoplasm) that are associated with the shear deformation of non-tumorigenic and TNBC cells at different stages of metastases.

The current results can also be extended generally to the development of mechanical biomarkers that can distinguish clearly between normal breast cells and non-tumorigenic breast cells (using accepted probabilities of occurrence or non-occurrence that are associated with tumor biopsies) at different stages of tumor progression. Finally in this section, it is important to note that Bayesian statistics may be used to improve the PDFs and CDFs as additional data becomes available for the non-tumorigenic (MCF-10A cells) and tumorigenic (MDA-MB-468 and MDA-MB-231) cancer cells that were examined in this study.

3.5. Actin Cytoskeletal Structure and the Variations in Cell Viscoelastic Properties

Before closing, it is important to re-examine the confocal microscopy images that were presented earlier in Figures 1a-1f. These show the actin cytoskeletal structures of the non-tumorigenic and tumorigenic cancers cells that were examined in this study. Note that the intensity of the fluorescence signal directly correlates with the actual amount of actin. Since the actin cytoskeletal structure of the cell plays a major role in the stiffening of the cell, it is not surprising to see that a higher actin content correlates with increased young's moduli and viscosities of the cells.

The variations in the actin cytoskeletal structure have a direct correlation to the variations in the cell viscoelastic properties as shown in Figures 7a-f. The moduli and viscosities (Nuclei and cytoplasm) in Fig 7a-c decrease with decreasing density of actin cytoskeletal structure, which also corresponds to more metastatic conditions. Hence, the highest fluorescence intensities and cytoplasm/nuclei young's moduli were observed in the normal MCF-10A cells, while the lowest fluorescence intensities and cytoplasm/nuclei Young's moduli occurred in the most metastatic MDA-MB-231 cell line (MDA-MB-231), and the less metastatic MDA-MB-468 cell line had intermediate fluorescence intensities and cytoplasm/nuclei Young's moduli. However, there were no clear continuous trends in the relationships between the fluorescence intensities and the relaxation times or viscosities obtained for the cytoplasm and the nuclei of the different cells that were examined in this study.

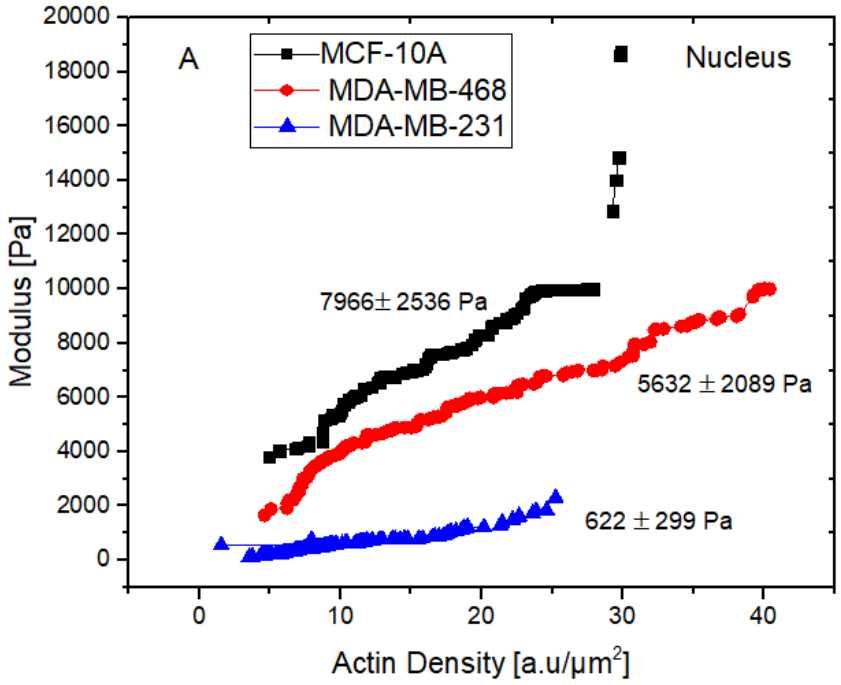
A
MCF-10A
MDA-MB-468
MDA-MB-231
Nucleus
7966± 2536 Pa
5632 ± 2089 Pa
622 ± 299 Pa
Modulus [Pa]
Actin Density [a.u/μm²]

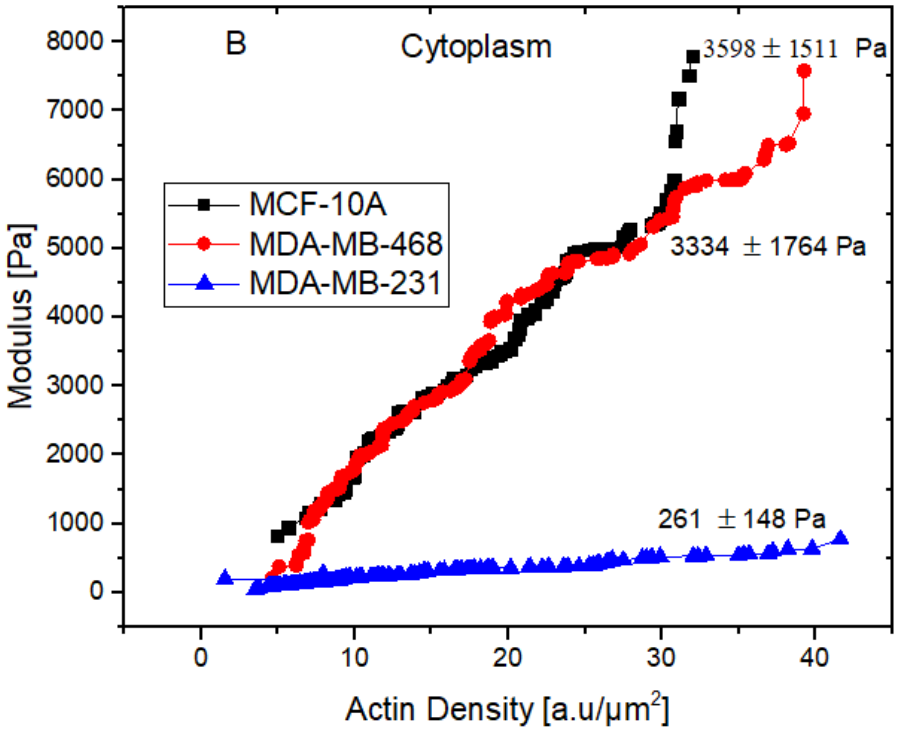
B
Cytoplasm
3598 ± 1511 Pa
3334 ± 1764 Pa
261 ± 148 Pa
MCF-10A
MDA-MB-468
MDA-MB-231
Modulus [Pa]
Actin Density [a.u/μm²]

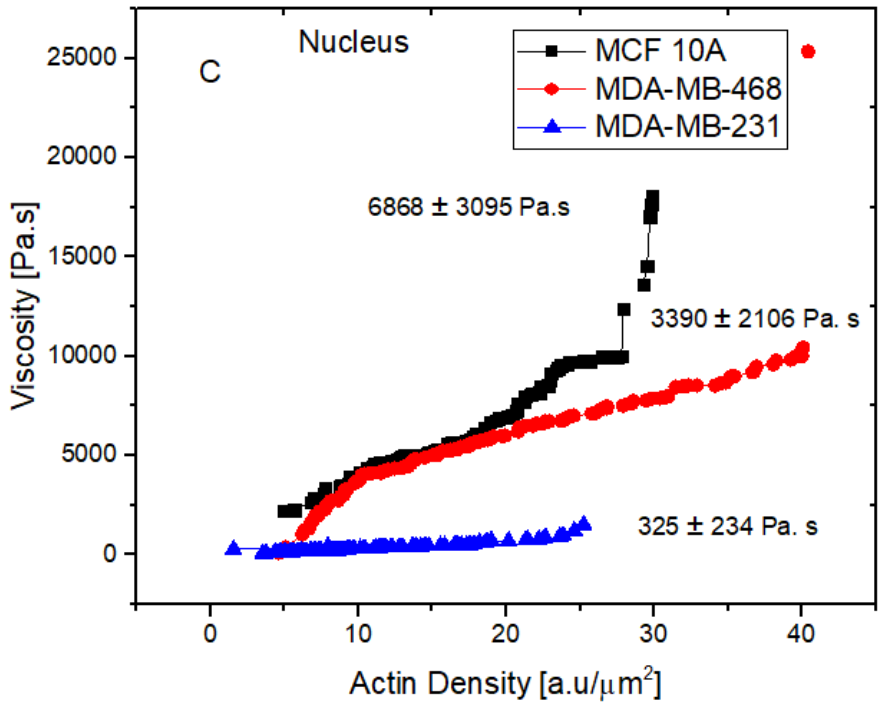
C
Nucleus
MCF 10A
MDA-MB-468
MDA-MB-231
6868 ± 3095 Pa.s
3390 ± 2106 Pa. s
325 ± 234 Pa. s
Viscosity [Pa.s]
Actin Density [a.u/μm²]
25000
20000
15000
10000
5000
0
0
10
20
30
40

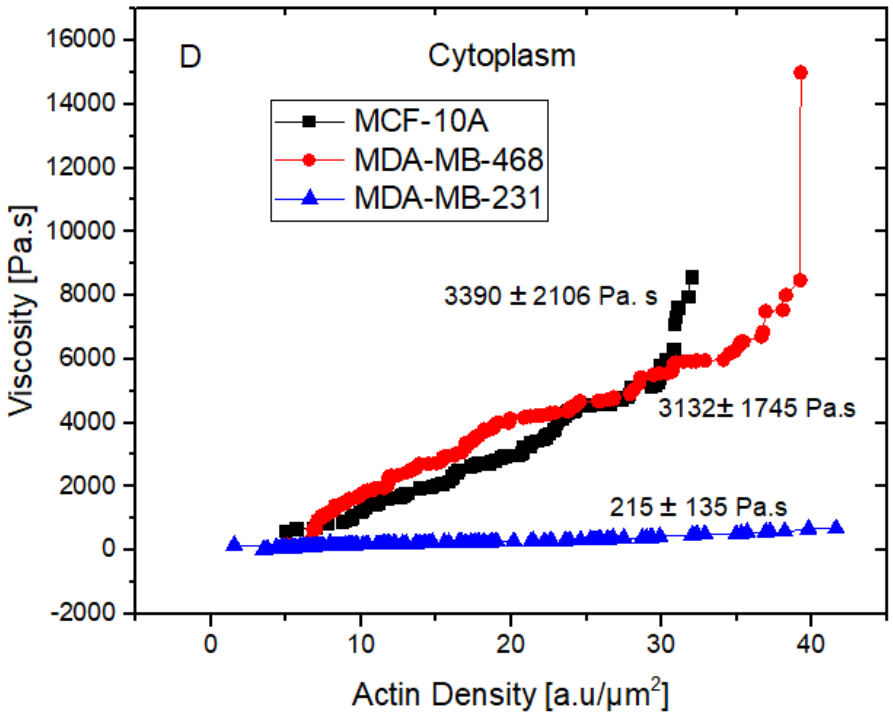
D
Cytoplasm
MCF-10A
MDA-MB-468
MDA-MB-231
3390 ± 2106 Pa. s
3132± 1745 Pa.s
215 ± 135 Pa.s
Viscosity [Pa.s]
Actin Density [a.u/μm²]
16000
14000
12000
10000
8000
6000
4000
2000
0
-2000
0
10
20
30
40

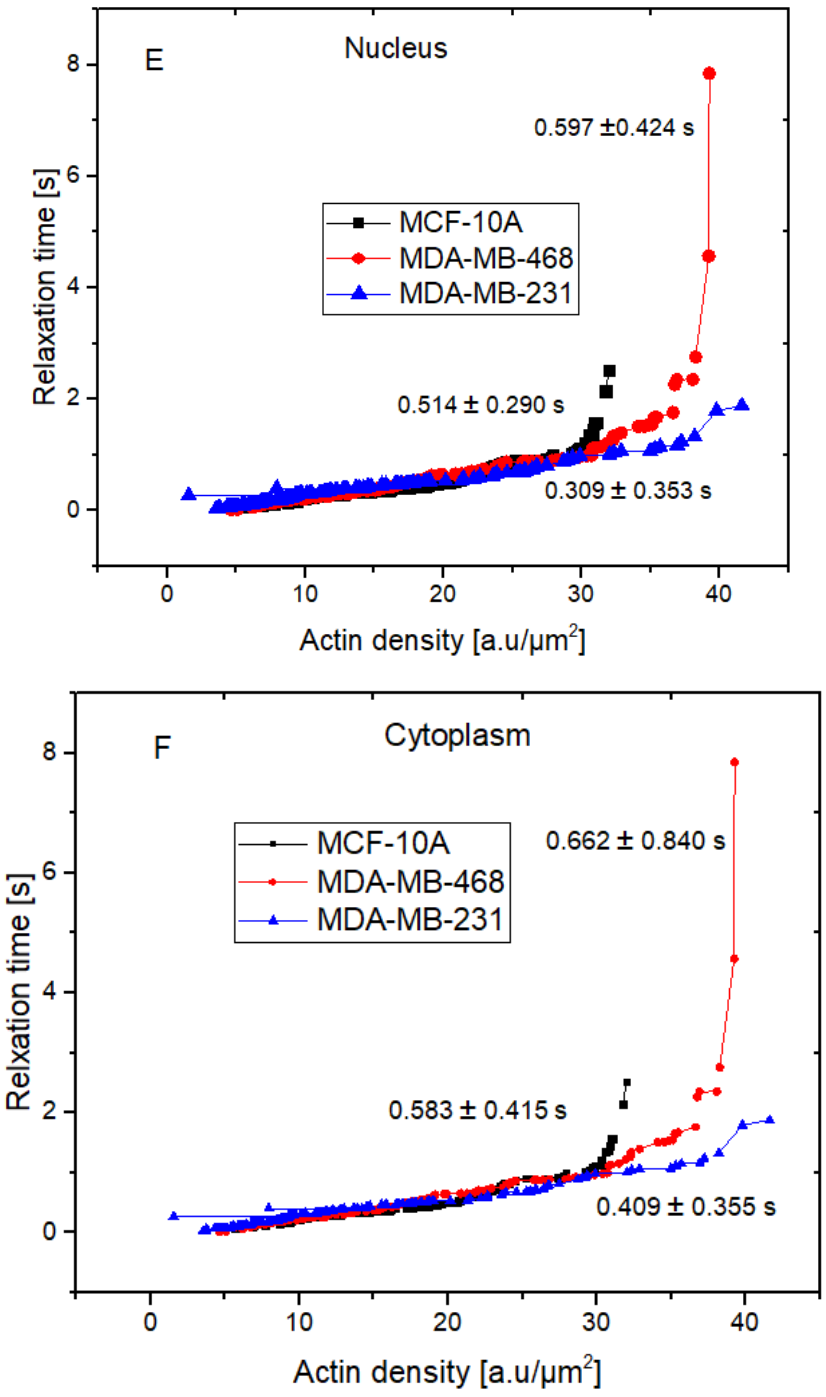

Figure 12: Relationship between the variation in the density of actin fluorescence and the cell viscoelastic properties. (a) Modulus of the nucleus (b) modulus of the cytoplasm (c) viscosity of the nucleus (d) viscosity of the cytoplasm (e) relaxation time of the

Furthermore, since the variabilities in the fluorescence intensities within the pixels in each image correspond to variabilities in the actin content, it is of interest to compare the PDFs of the pixel fluorescence intensities that were associated with the fluorescence images of the non-tumorigenic breast cells (MCF-10A cells) and the metastatic TNBC cells (MDA-MB-468 and MDA-MB-231 cells). The results are shown in Figure 3 for the nuclei and the cytoplasm. The corresponding CDF plots are also presented in Figures 4 in the supplementary text.

It is also of interest to compare the CDFs for the means that correspond to CDF of 0.5 (Figure 4, 5, 6, and 7 in the supplementary text). These, of course, correspond to the mean fluorescence intensities for the images obtained from the non-tumorigenic MCF-10A cells and the TNBC cells. The current results show that young's moduli and viscosities of the nuclei and cytoplasm decrease with decreasing mean fluorescence intensity of the actin cytoskeletal structure. Furthermore, very large reductions in young's moduli and viscosities of the cells can occur, with the progression of cancer from less metastatic to more metastatic states. Such reductions could make it easier for cells to squeeze through pores/capillaries during transport in the blood to metastatic organs.

Similar comparisons of PDFs and CDFs can also be made for other probabilities of occurrence or non-occurrence. In such cases, the probabilities of occurrence or non-occurrence can be compared for known stress states due to laminar flow or applied shear stresses. In this way, the viscoelastic responses of the non-tumorigenic and TNBC cells can be compared, for known probabilities of occurrence or non-occurrence. The approaches developed in this paper could,

therefore, provide the basis for the development of probabilistic approaches to the characterization of single cell/tissue viscoelastic properties.

3.6. Implications

The implications of the current result are quite significant for the characterization of statistical variations in the structure and the viscoelastic properties of the non-tumorigenic cell (MCF-10A) and tumorigenic TNBC cells (MDA-MB-468 and MDA-MB-231). First, the results show that the statistical variations in pixel fluorescence intensity can be related to the local variations in actin cytoskeletal density, which in turn can be related to the variations in the viscoelastic properties of the nuclei and cytoplasm of non-tumorigenic and TNBC cells.

The above results also show that normal distributions can be used to determine the PDFs and the CDFs associated with the occurrence of cell viscoelastic properties (Young's moduli, viscosities, and relaxation times). Furthermore, the results obtained from ANOVA and FPC reveal significant differences between the different cells, and, slight similarities between the MCF-10A and MDA-MB-468 cells. The statistical analysis also shows that the young moduli of the cells provide the clearest indicators of the states of the non-tumorigenic and tumorigenic states.

Finally, it is important to note that the current work shows that the statistical analysis of the viscoelastic properties of non-tumorigenic breast cells and tumorigenic breast cells can be used to enable the development of mechanical biomarkers for the detection and classification of breast cells and TNBC cells at different stages of tumor progression. Further work is needed to test the shear assay approach on biopsies obtained from cancer and non-cancer patients in clinical scenarios.

Chapter 4

Investigation of Creep Properties and the Cytoskeletal Structures of Non-Tumorigenic Breast Cells and Triple-Negative Breast Cancer Cells

4.1. Introduction

In the last few decades, there has been an increased emphasis on the diagnosis and treatment of difficult-to-treat diseases such as cancer, which is one of the leading causes of death globally.[1], [2]. Breast cancer, on the other hand, has been recorded as the most diagnosed cancer in women and constitutes the highest rate of mortality by cancer in women worldwide, second in Africa, and fifth in the west pacific[3]– [5]. Triple-negative breast cancer, which is prevalent in most women of African descent, tests negative for estrogen receptor (ER), progesterone receptor (PR), and human epidermal growth factor receptor-2 (HER-2) [10]–[13], and therefore poses a more imminent threat to these women in Africa, owing to its difficult prognosis and clinical outcomes [8], [9]. Therefore, there is a strong need for a more targeted diagnostic technique and treatment pathway, to help combat the challenges posed by this type of cancer.

To address the challenges in cancer diagnosis, recent studies have demonstrated the role of cell mechanics in the characterization of cells into benign, less metastatic, c, and highly metastatic cells, using different mechanical techniques [54], [55], [59], [62], [64], [65], [70], [72], [75], [92], [93]. It was observed that in most cases, normal cells had relatively higher mechanical properties compared to cancerous cells[23], [25], [68], [69]. The variations in the mechanical properties of the cells were, however, linked to the different compositions of the cell cytoskeletal structures at varying stages of cancer progression[25], [37], [46], [55], [81], [94], [95]. The

cytoskeletal structure of the cell (Fig 1) is a heterogeneous structure that consists of different cell proteins, the actin filaments, microtubules, and intermediate filament [36], [45], [96], [97], and it is primarily responsible for structural support, localization, and transport of organelles in the cell, and intracellular trafficking [23], [25]. The cell cytoskeleton plays an important role in the study of the mechanical properties of the cell, and in the development of mechanical biomarkers for the detection of diseases such as cancer, a disease characterized by marked tumor heterogeneity and diverse molecular orientations[25], [34], [98]. Figures 1a and 1b show the schematic of the cytoskeletal structures of a cell and the stained images for the different protein structures of the cell cytoskeleton respectively. In Figure 1b, the staining of the actin cytoskeletal proteins and the nucleus are shown in red and blue, while the intermediate filaments and microtubules are shown in green. Prior research has also shown that the over-expression of some cytoskeletal proteins can provide indicators of tumor progression [34].

(a)

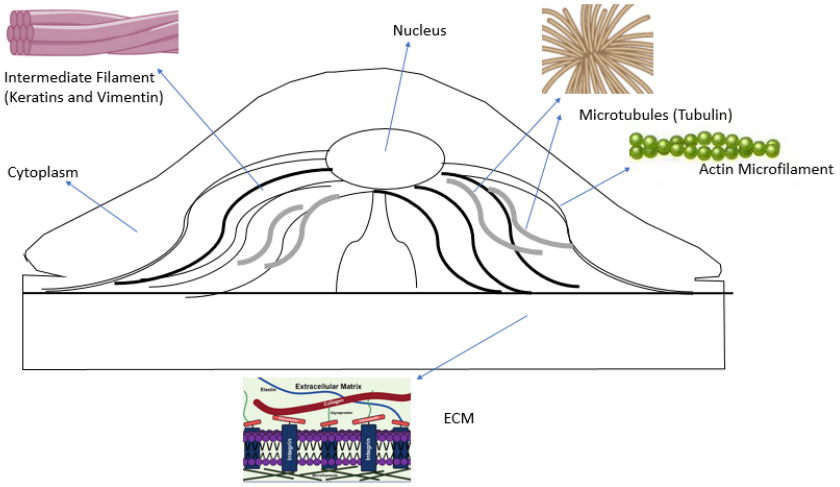

(b)

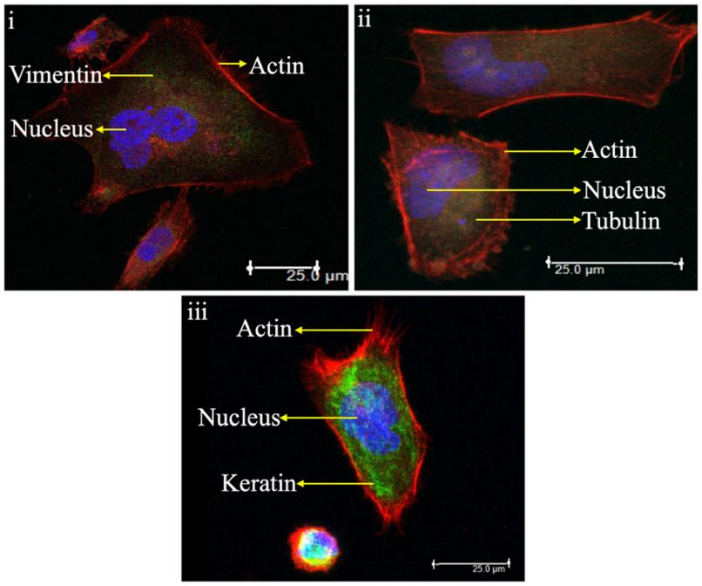

Figure 13: (a) Stained images showing the different protein structures of the cell cytoskeleton (Figure insets adapted. (b) Schematic of cytoskeletal structures in a biological cell.

In a prior work by our research group, we studied the viscoelastic properties of non-tumorigenic breast cells and tumorigenic triple-negative breast cancer cells and their relationship with actin cytoskeletal structure [25], [69]. The mechanical properties of the cell were seen to reduce relatively with cancer progression, and the fluorescence intensities of actin filaments in the breast cells were found to decrease with increasing metastasis of breast cancer [23], [25], [38]. The reduction in the actin filament of the cell cytoskeleton was, however, correlated with the reduction in cell stiffness[69].

However, the role of creep in cell deformation studies and the contributions of the other components of the cytoskeletal structure (keratin 7, 8, 18, and 19; vimentin, and microtubules such as tubulin) have not been considered in our prior work.

In this study, local variations in the viscoelastic and creep properties of the cell were studied using shear assay technique and strain mapping techniques with digital image correlation software, which can distinguish between the local properties of the cells at different regions within the cell. The variations in the strain rates and strain evolution of the cells are good indicators of the contributions of the cell proteins/structure to the deformation and mechanical properties of the cell. The effects of the cell cytoskeleton on the spatial variations of cell creep and viscoelastic properties were also studied. The implications of the current work are discussed for the study of discrete cell behaviors, strain and viscoelastic responses of the cell, and the role of cell cytoskeleton in the onset and progression of cancers.

4.2. Materials and Methods

4.2.1. Cell Culture

The normal breast cell (MCF-10A) and the metastatic breast cell (MDA-MB-231) were cultured under conditions described previously in a study by[68]. The cells were cultured in 60 x 15 x 35 mm falcon Petri dishes (Corning Inc., Corning, NY, USA) for a duration of 48hours. This was done at 37°C in 5% CO_2, at atmospheric pressure, to allow adequate time for the attachment and growth of the cells on the substrate. Under these conditions, the MCF-10A cells were grown using Dulbecco's modified eagle medium (DMEM)/Ham's F-12 medium (Invitrogen, Carlsbad, CA, USA) at an equal mix ratio of 1:1, together with a supplemented 5% horse serum (Invitrogen, Carlsbad, CA, USA), 0.2% amphotericin (Gemini Bio-Products, West Sacramento, CA, USA), 30 ng/ml insulin (Sigma-Aldrich, St. Louis, MO, USA), 100ng/ml cholera toxin (Sigma Aldrich), 30 ng/ml murine epidermal growth factor (Peprotech), 0.5 g/ml hydrocortisone (Sigma Aldrich) and 1% Penicillin Streptomycin (Invitrogen, Carlsbad, CA, USA). On the other hand, the MDA-MB-231 cells were grown at the same conditions in a 10% fetal bovine serum (FBS) from the American Type Culture Collection (ATCC) (Manassas, VA, USA) and in an L-15 base media, with a supplemented 100 I.U/ml penicillin/100µg/ml streptomycin respectively.

4.2.2. Immunofluorescence Cell Staining

The cytoskeletal structures of the different cells MCF-10A and MDA-MB-231 were stained to reveal the distribution and relative volume density of the different cytoskeletal proteins (actin, Keratin, vimentin, and tubulin). Each cell was stained to reveal: the nucleus; actin filaments; intermediate filaments, and microtubules (tubulin). The staining protocols are the same as

summarized in our previous work [68]. A 4% high-grade paraformaldehyde (4% in 0.1 PBS, Electron Microscopy Science, Hatfield, PA, USA) was used to fixate the cells after culturing for 48 hours. This was followed by the aspiration of the paraformaldehyde and rinsing thoroughly with a Phosphate Buffer Solution (PBS) diluted with deionized water. The cells were each permeabilized for 10 minutes with 1 ml of 0.1% Triton X-100 solution (Life Technologies Corporation, Carlsbad, CA, USA).

Furthermore, the cells were then incubated in PBS with 1% of Bovine Serum Albumin (BSA) (Sigma-Aldrich, St. Louis, MO, USA) at room temperature (25^{o}C) for 1 hour, after which they were rinsed thoroughly with PBS. Staining for any of the cell proteins was done using the protein's specific antibody. For Keratin 7, 8, 18 & 19, cytokeratin 7, 8, 18 & 19 (TSI) Mouse Monoclonal Antibody at 2µg/ml in 0.1% BSA was used. Tubulin alpha Rabbit Polyclonal Antibody (Thermo Fisher Scientific) at 2µg/ml in 0.1% BSA was used for the tubulin staining, and lastly, for vimentin, Vimentin Mouse Monoclonal Antibody (Thermo Fisher Scientific, Waltham, MA, USA) was used at 2µg/ml in 0.1% BSA. The labeled proteins were incubated for 3 hours at room temperature (25 C), before rinsing with PBS. The cells were then further labeled with Goat anti-Mouse IgG (H+L) superclonal^{TM} secondary antibody Alexa Fluor® 488 conjugate (Thermo Fisher Scientific, Waltham, MA, USA) at a dilution of 1:2000, after which the cells were further rinsed properly in PBS and incubated in a dark environment for 25 minutes, at room temperature. The resulting structures were further stained in PBS with F-actin stain Rhodamine Phalloidin (Thermo Fisher Scientific, Waltham, MA, USA), followed by proper rinsing with PBS.

The MCF-10A and MDA-MB-231 cells were sub-cultured on coverslips and fixed with 4% (v/v) paraformaldehyde for 15 minutes and at room temperature. A mixture of diluted water and

Dulbecco's phosphate-buffered saline (DPBS) was used to wash the cells three times. The cells were blocked using 1%(w/v) pharmingen Stain Buffer (BSA) prepared with PBS for 15 minutes at room temperature. The samples were then rehydrated in PBS for 10 minutes and washed again with DiH_20 + DPBS.

The resulting cells were then stained simultaneously with Alexa-488 phalloidin (A12379) and Alexa-594 DnaSe1-deoxyribonuclease 1, Alexa flour^{TM} 594 conjugates (D12372) (Invitrogen, USA) for staining F-actin and G-actin, respectively. This was done by adding 200□L of a 9 □g/mL solution of fluorescent DNase 1in a buffer to the coverslip. I unit (200 □L of a 0.165 □M solution) of fluorescent phallotoxin was used to simultaneously label F-actin, for 20minutes. The cells were washed with DiH_20 + DPBS. The nuclei of the cells were stained using SlowFade® Gold Antifade Mountant with DAPI (Thermo Fisher Scientific, Waltham, MA, USA) for 2 minutes. The samples were mounted on a clean glass slide in a medium of Fluoro Guard Reagent drop. The imaging of the stained cell samples was done using a 60X oil immersion objective, and an inverted Leica SP5 point Scanning Confocal Microscope (Leica Microsystems, Heidelberg, Germany). Leica LAS AF Lite software was used to determine the total intensity per given area for the tubulin, keratins, actin, and vimentin.

4.2.3. Confocal imaging and analysis

The stained cells were imaged under a confocal microscope (an inverted Leica SP5 point scanning confocal microscope, Leica microsystems, Heidelberg, Germany) using a 40X oil immersion objective. The actin cytoskeleton was imaged with a wavelength of 565nm excitation, while the other intermediate filaments (vimentin, keratin 19, keratin 18, keratin 8, keratin 7) and microtubulin, were imaged with a wavelength of 488nm excitation. The nucleus was also imaged with a wavelength of 488nm excitation. The cells were imaged under identical system parameter

settings, at a z stack height of 1µm, and an average of 20-30 slices per cell. The fluorescence intensities (intensity per unit area) of the proteins of each cell line were estimated using the three-dimensional confocal image stacks. However, the variation in intensities for the individual proteins of the normal cell was compared with that of the cancer cells. The image visualization and analysis were carried out using the Leica software. The total amount of fluorescence was measured according to the protocol reported in a previous study[99], [100]

4.2.4. Shear Assay Experiments

The shear assay experiment was used in this study to exert mechanical forces in the form of fluid pressure to biological cells (MCF-10A and MDA-MB-231), and hence the mechanical response of these cells to an applied force was subsequently observed. This, however, translates to the further determination of the cell viscoelastic properties of the non-tumorigenic and tumorigenic breast cells using other mechanical techniques such as strain mapping and the use of viscoelastic models. An average of 20 single cells per cell line was sampled for this study. Fig 2 below shows the experimental setup involved in the determination of the mechanical response of the cells as a function of the external forces. The cells were cultured in a Petri dish (35x10mm) (CELL TREAT scientific products, MA, USA) as shown in fig 2b. The process further involves the fitting of the microfluidic device chamber, together with the rubber gasket in between. This set up is connected to the syringe pump with the help of tubing, and then placed on the optical microscope for imaging and monitoring. The programmable syringe pump (Fig 2a), then infuses and withdraws the fluid medium using syringes and tubing and is kept at a constant flow rate (3ml/min), ensuring a continuous flow of fluid over the surface of the cell. This controlled flow of fluid is carried out within a microfluidic flow chamber as shown in fig 2 c, fitted unto the Petri dish with the help of the rubber gasket (fig 2d), which helps ensure controlled fluid flow

between the microfluidic device and the Petri dish. The rubber gasket is circular, with tiny holes, and serves as vacuum suction. It has a rectangular channel in the middle (20.5 mm - length, 2.5 mm - width, and 0.254 mm height) that determines the flow profile. The controlled flow of fluid within the parallel flow chamber generates the desirable wall shear stresses. The process of shearing off of the cells and determining how the fluid flow affects the mechanical and structural integrity of the cells is captured by the optical microscope and displayed on a computer monitor as shown in fig 2e.

formula for the determination of the wall shear stress is given as

$$\sigma = \frac{6\mu Q}{wh^2} \qquad (1)$$

where is σ is the wall shear stress, μ is the viscosity of the fluid medium Q is the flow rate W is the width of the channel (rubber gasket) H is the height of the channel (rubber gasket).

To prevent non-specific binding of the extracellular matrix protein, a serum-free culture media was used for cell culture. In most cases, methylcellulose which is non-toxic and non-allergenic is added to the serum-free media to increase the viscosity of the cell culture medium. This is the case in MCF-10A cells, where 3.5wt% methylcellulose is added to the culture media to obtain a viscosity of 0.16Pa.s. For the MDA-Mb-231 cells, no cellulose was added, and hence the viscosity of the media was 0.02 Pa.s. This is because less shear stress is required to deform or shear off the MDA-MB-231 cells. However, the shear rates for both the MCF-10A and MDA-MB-231 cells are similar (2500 $s^{=1}$), and the wall shear stress for the shearing-off of MCF-10A and MDA-MB-231 was 410 Pa and 10 Pa, respectively. The Reynolds number was ensured to be within the laminar flow regime (Re<100).

To ensure that the same fluid temperature is maintained and delivered to the cells, and to avoid disturbance of the cells during the experiments, the flow medium was pre-heated to 37^{o}C in a water bath, and residual bubbles in the flow line were evacuated by pre-flushing the tubing alongside the medium. The cells were subjected to controlled shear stresses by keeping the flow and velocities uniform. The response of the cells to shear stresses was observed in situ using an optical microscope and a video camera. The movements and detachment of isolated single cells from their substrates without the interference of the adjacent neighboring cells were monitored using the 40 X objective lens from Nikon. The detachment/dislocation of the cells (nucleus and cytoplasm) were recorded and stopped when the cells detached from the substrate. The individual frames from the recordings were extracted for the digital image correlation analysis. This technique proves to be a potential mechanical means for cell characterization and is proposed for the characterization of cells into their component cell states.

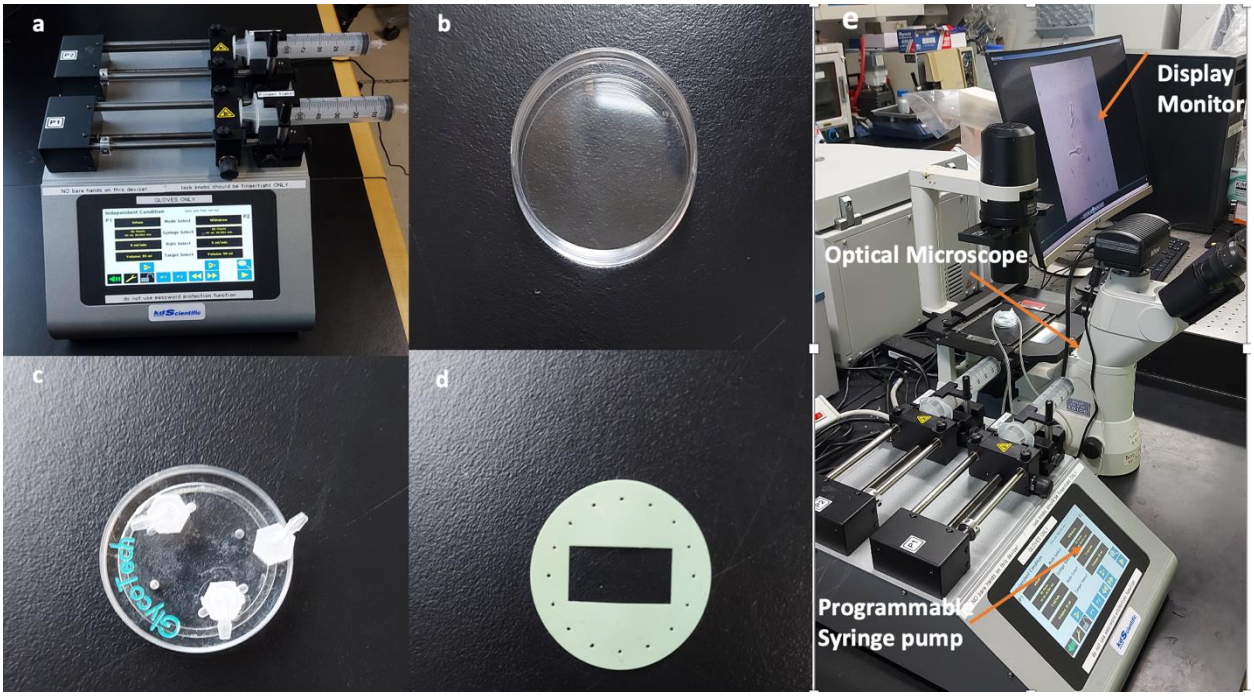

(f)

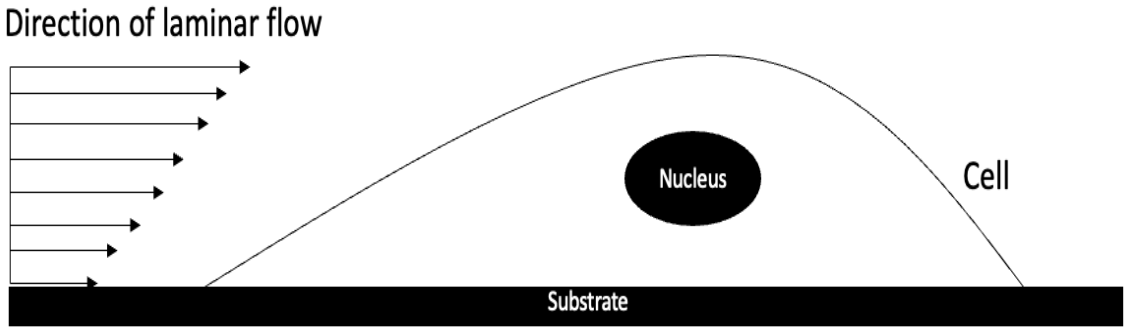

Figure 14: (a) Programmable syringe pump (b) 35x10mm Petri dish for cell culture (c)Microfluidic flow chamber (d) rubber gasket (e) complete experimental set-up (f) schematic of laminar flow over cell

4.2.5. Strain Mapping

To determine the mechanical behavior of these cells (MCF-10A and MDA-MB-231), their deformation images obtained during the shear assay experiment were analyzed using the digital image correlation (DIC) software. The changes in the cell structure (nucleus and cytoplasm) were tracked by locating each pixel block in the images of the deformed cell structure. From the images of the cell as obtained during the shear assay experiment, a position in the nucleus and cytoplasm of the cell is marked and tracked to determine the magnitude of strain experienced during deformation. As the cell deforms, the displacement of the cell with respect to time is determined as the position of the cell structure changes during deformation from the marked position to a new position. For an optimized correlation value, a subset size of 31 x 31 pixels and a step size of 8 pixels were chosen. The step size defines the difference in the distance of the subset before the next correlation.

4.2.6. Viscoelastic modeling

The viscoelastic properties of the cell define the cell as both viscous and elastic material. In our study, the cells were subjected to constant stress and thus experienced creep. The creep region was, however, analyzed using the three-element generalized Maxwell model as shown in fig 3. This model describes a time-dependent strain due to viscoelastic effects and can be defined by equation 2, which shows the relationship between the various parameters.

$$\varepsilon = \left(\frac{\sigma}{\eta 1}\right) t + \frac{\sigma}{E}\left(1 - exp\left(\frac{-t}{\tau}\right)\right) \qquad (2)$$

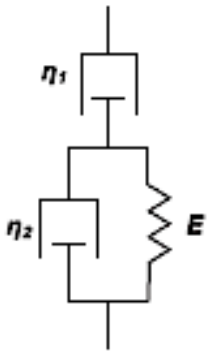

Figure 15: Schematic of the three-element generalized maxwell model

The viscous behavior is accounted by the top dashpot and is thus represented by$\left(\frac{\sigma}{\eta 1}\right) t$. The combination of the spring and dashpot in parallel represents the Voigt model. The spring component on the right of the model represents the elasticity of the material. The effective viscosity of the cell is obtained by the top dashpot value $\eta 1$, and the relaxation time (τ is given by the ratio of the elasticity and the viscosity of the dashpot $\eta 2$, in the Voigt component, and hence it is given as$\frac{\eta 2}{E}$.

The viscoelastic properties of the cell were thus determined by using the equation for the viscoelastic model as shown in eq. 2 to fit the strain-time data with the curve fitting tool in MATLAB. The fitting parameters ($\frac{\sigma}{\eta 1}$, $\frac{\sigma}{E}$, $\frac{E}{\eta 2}$) were adjusted to yield high R-square. The viscoelastic properties, therefore, were extracted from the fitting parameters. From the parameters, ε represents the strain, σ represents the wall shear stress, E represents the elastic modulus, $\eta 1$ represents the viscosity and τ represents the relaxation time.

4.2.7. Statistical Analysis

The statistical analyses of the creep properties and the fluorescence intensities of the different cytoskeleton proteins of the non-tumorigenic and tumorigenic TNBC cells were carried out using the Minitab 18 software package (Minitab LLC, State College, PA). For each cytoskeletal protein, the statistical variations of the fluorescence intensities were determined for the two cell types (MCF-10A and MDA-MB-231) using a one-way analysis of variance (ANOVA) and Fisher Pairwise Comparisons (FPC). The analysis of variance was done for equal variances at a confidence level (CL) of 95%, and a significance level (SL) of 0.05 that was adopted for the analysis.

For the analysis of variance, the null hypothesis (H_0) assumes equal means between the different cell types of the proteins, suggesting that the variation between the cell types (MC-10A and MDA-MB-231) was insignificant, and therefore the P-value must be >0.05. The alternative hypothesis (H_a) assumes that the means of the different cell types are not equal, which suggests that there are significant differences between the mean properties of the different cells, and as such the P-values must be <0.05. Furthermore, the similarities and variations in their intensities were established using the frequency distribution curves.

4.3. Results

4.3.1. Single-Cell Strain Mapping and Strain Evolution

The single-cell images of the different types of cells were analyzed using the digital image correlation machine (DIC), and hence, the differences in the strain evolution between the nucleus and the cytoplasm of different cell types were obtained at different stages of deformation. The evolution of strain under constant stress for both the normal and tumor cell resulted to creep. In

Figures 4a-d, the difference in the strain evolution between the nucleus and cytoplasm of the normal MCF-10A cells and the tumorigenic MDA-MB-231 cells are shown at different creep stages.

Figures 4a and 4b shows the initial creep stages of the cells for the nucleus and cytoplasm of both the normal and cancerous cells. At this stage, both types of cells, the normal and cancer cells exhibit fairly the same strain trends, where creep starts at a relatively rapid rate and slows with time. In this creep regime, the cells exhibit an instantaneous elastic phase before deformation, and their profiles are relatively similar, and thus their mechanical properties can be fairly compared. For the cancerous MDA-MB-231 cells, it was observed that they experienced more strain at shorter periods than the normal MCF-10A cells. Figures. 4c and 4d, show the secondary creep stage, and the strain during deformation of the structure of the cell. At this stage, the MDA-MB-231 cells experiences a rather steady creep followed by a sudden failure/detachment of the cell, in most cases, at the onset of the secondary creep stage, the MDA-MB-231 cells were fully deformed/detached from the substrate. For the normal MCF-10A cells, there is an increased resistance to deformation, giving rise to slower strain rates and increased strength. Most MCF-10A cells only experience failure or detachment, beyond the secondary creep stage.

(a)

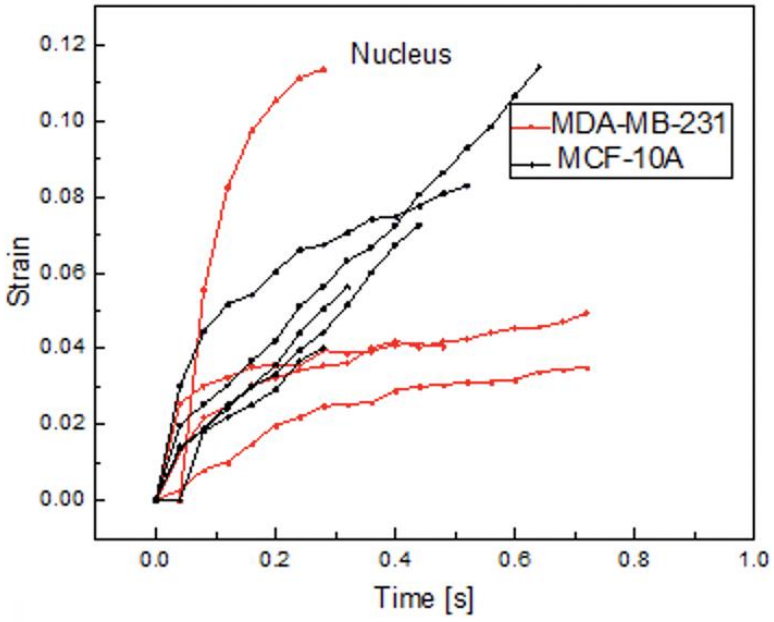
Nucleus
MDA-MB-231
MCF-10A
Strain
Time [s]
0.00
0.02
0.04
0.06
0.08
0.10
0.12
0.0
0.2
0.4
0.6
0.8
1.0

(b)

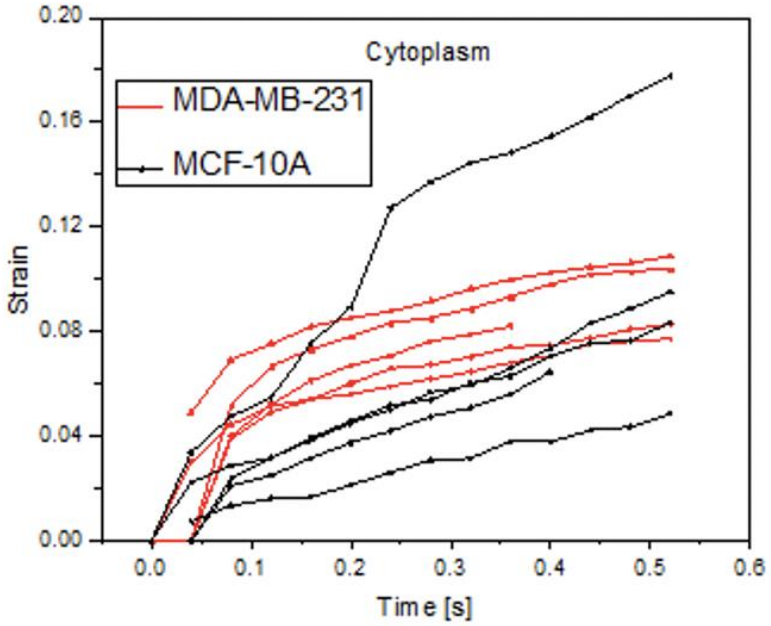
Cytoplasm
MDA-MB-231
MCF-10A
Strain
Time [s]
0.00
0.04
0.08
0.12
0.16
0.20
0.0
0.1
0.2
0.3
0.4
0.5
0.6

(c)

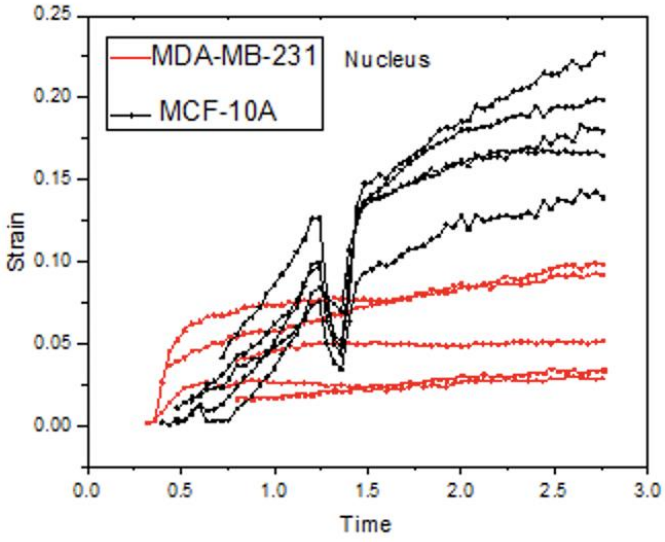

(d)

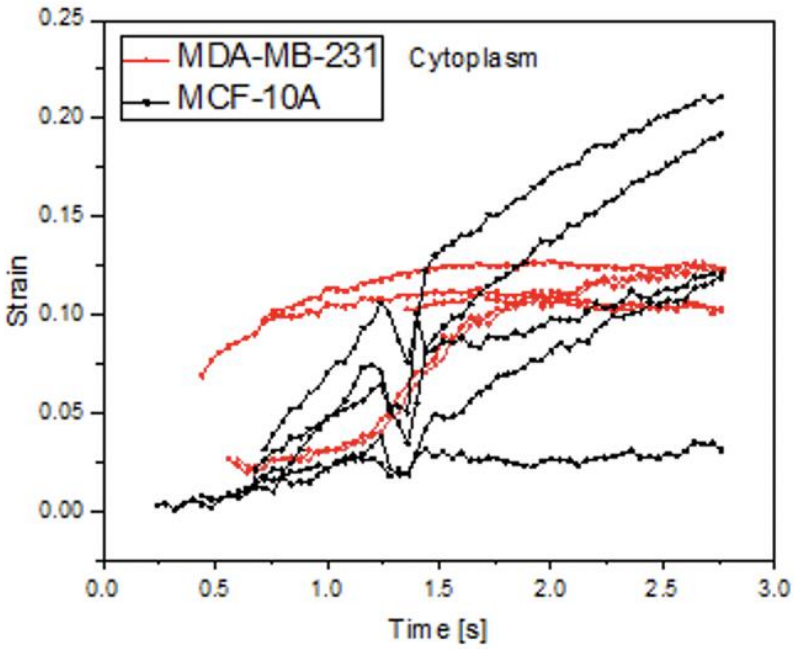

Figure 16: A five-data plot representative of (a) Single-cell strain evolution for the nucleus of the cells at the primary (elastic) creep stage. (b) Single-cell strain evolution for the cytoplasm of the cells at the primary (elastic) creep stage. (c) Single cell

The frequency distributions for the nucleus and cytoplasm for the normal MCF-10A and the tumorigenic MDA-MB-231 cells at the primary creep stage are shown in figures 5a-d, while figures 6a-d show the frequency distributions for the nucleus and cytoplasm for the normal MCF-10A and the tumorigenic MDA-MB-231 cells at the secondary creep regimes and the final stages of deformation. The shear strain data from the experiment was well characterized by lognormal distributions. The frequency distributions also revealed that the normal cells had a higher incidence of lower strain values, while the cancer cells had a higher incidence of larger strains. This was evident for both the nucleus and cytoplasm in the primary and secondary stages of creep in both the nucleus and cytoplasm of the normal (MCF-10A) and breast cancer (MDA-MB-231) cells

(a) (b)

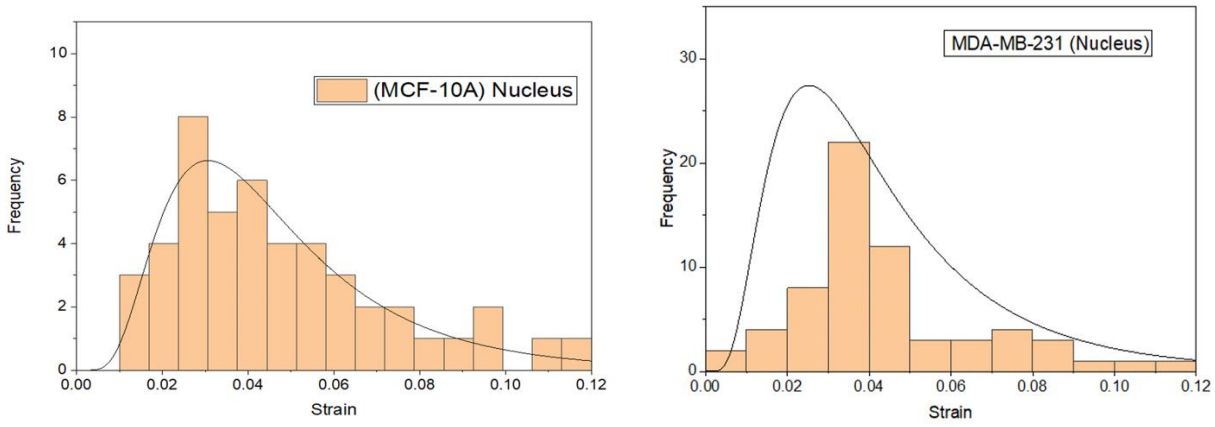

(c) (d)

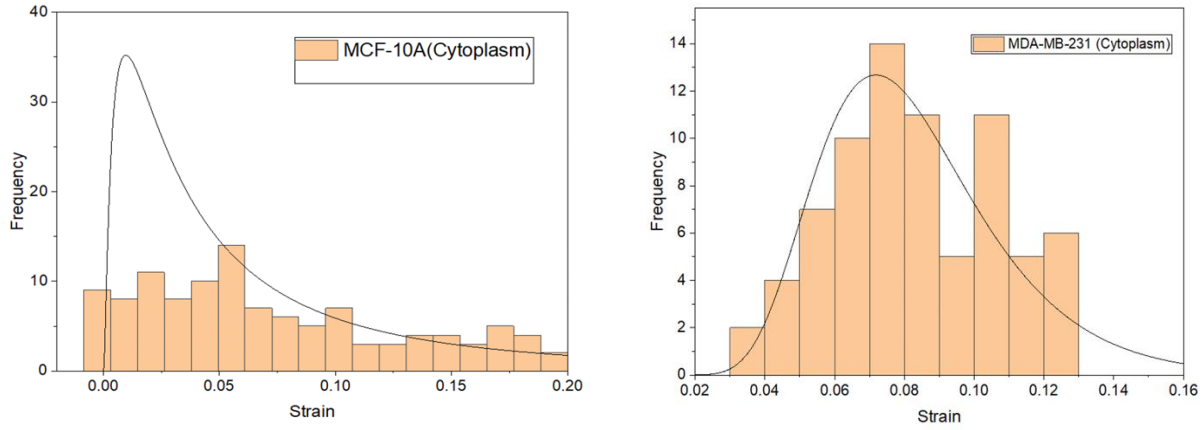

Figure 17:Frequency distribution at the onset of creep (Primary creep), for (a) the nucleus of the MCF-10A cell (b) the nucleus of the MDA-MB-231(c) cytoplasm of the MCF-10A, and (d) the cytoplasm of the MDA-MB-231.

(a) (b)

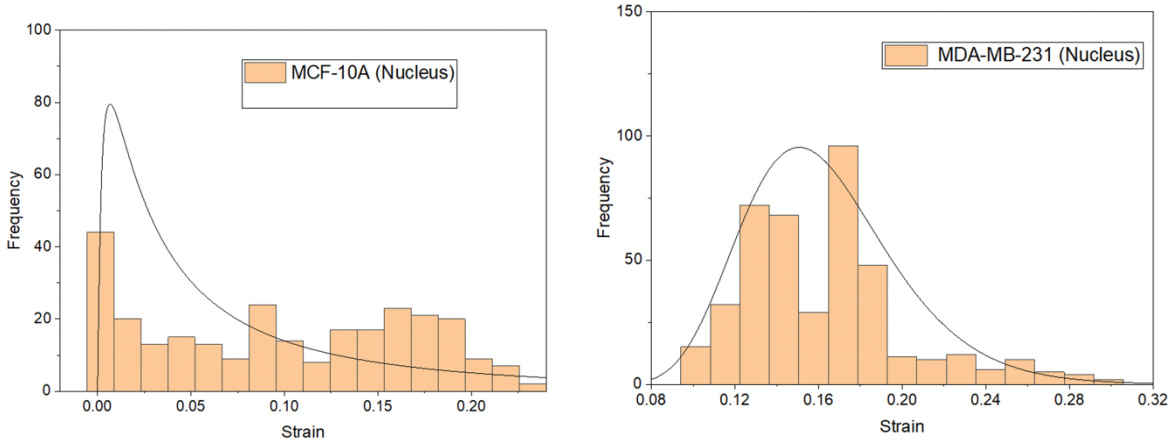

(c) (d)

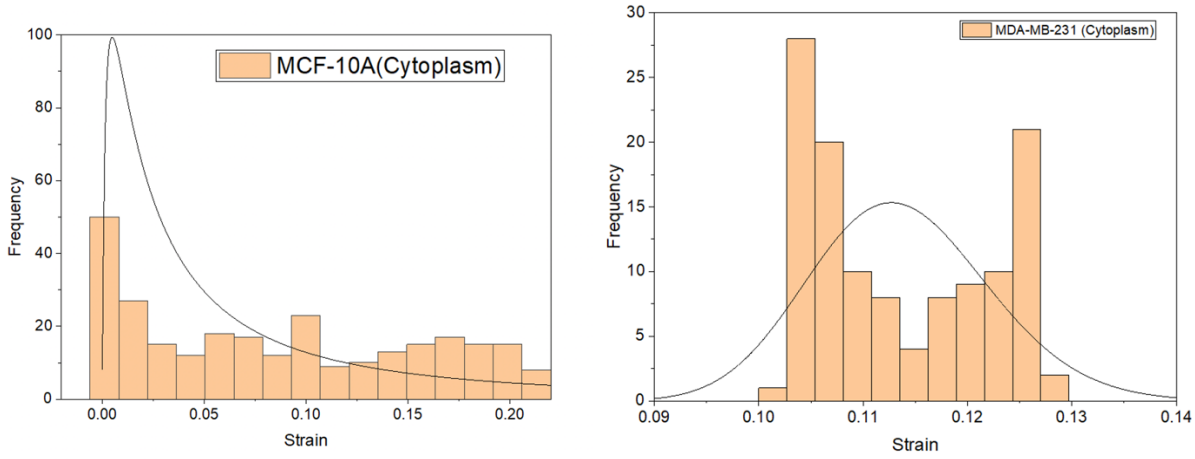

Figure 18: Frequency distribution at the onset of creep (Primary creep), for (a) the nucleus of the MCF-10A cell (b) the nucleus of the MDA-MB-231(c) cytoplasm of the MCF-10A, and (d) the cytoplasm of the MDA-MB-231.

Table 4: Statistical analysis for strain evolution of the cells at the onset of deformation (Primary creep regime)

Cells	***Av. Strain [Nucleus]***	***Av. Strain [Cytoplasm]***	***Tukey's sig value***	***FPC mean Grouping [Nucleus]***	***FPC mean Grouping [Cytoplasm]***
MCF-10A	0.08406	0.12409	1	A	B
MDA-MB-231	0.01977	0.03425	1	B	A

*Means that do not share a letter are significantly different (FPC)

**Means with Tukey's sig value =1, is significantly different

Table 4b: Statistical analysis for strain evolution of the cells at complete deformation

Cells	***Av. Strain [Nucleus]***	***Av. Strain [Cytoplasm]***	***Tukey's sig value***	***FPC mean Grouping [Nucleus]***	***FPC mean Grouping [Cytoplasm]***
MCF-10A	0.13634	0.20844	1	A	A
MDA-MB-231	0.03613	0.07377	1	B	B

**Means that do not share a letter are significantly different (FPC)

**Means with Tukey's sig value =1, is significantly different

4.3.2. Cell Viscoelastic Properties

The viscoelastic properties of the non-tumorigenic and TNBC cells as described in our previous study [25], were obtained using the three-element generalized Maxwell model (described in section 2.6 of this paper and shown schematically in Fig 3. From the strain-time analysis, the Maxwell model for viscoelastic materials was fitted to obtain young's moduli, viscosities, and relaxation times for the different cell types. Hence, in this way, the spatial variations in the cell viscoelastic properties were characterized. The viscoelastic properties of the different cells, the non-tumorigenic breast, and tumorigenic cancer cells are presented in Table 2. It shows clear differences between the viscoelastic properties of the non-tumorigenic and TNBC cells. These variations in the cell viscoelastic properties could be due to the spatial variations in the cell cytoskeletal structures. Further investigations are therefore necessary for the validation of this claim. It is however seen from table 2 that for the normal cells, the mechanical properties (Young's moduli and viscosities) were higher compared to the cancer cells. This variation in mechanical properties according to literature can be attributed to the role of the cytoskeleton on the cells[25], [37], [43], [46], [47], [81], [96], [101], [102]

Table 5:Viscoelastic properties of normal and cancerous TNBC cells [25]

Cell Type	***Av. Modulus, E, [Pa]***	***Av. Modulus, E [Pa]***	***Av. Viscosity, η [Pa*s]***	***Av. Viscosity, η [Pa*s]***	***Av. Relaxation Time, τ [s]***

	Nucleus	*Cytoplasm*	*Nucleus*	*Cytoplasm*	*Nucleus*
MCF-10A	7966 ± 2536	3598 ± 1511	6868 ± 3095	3132 ± 1745	0.514 ± 0.290
MDA-MB-231	622 ± 399	261 ± 148	325 ± 234	215 ± 135	0.309 ± 0.353

4.3.3. Relative volume density distributions of the different proteins

The relative volume densities of the different cytoskeletal proteins were calculated by quantifying the average fluorescence intensities per unit area of a given protein and determining its relative volume densities as a function of the cell cytoskeletal proteins as seen in equation 3.

$$\text{Relative volume density of A} = \frac{I_A}{I_n + I_A + I_B + I_C + \ldots + I_N} \quad (3)$$

Where I represent the average intensity/area of a given protein (volume of protein), n represents the nucleus of the cell, and A, B, C, N represent the different proteins of the cell. For each Z stack image, the fluorescent intensity/area per Z-stack position/height was analyzed and their averages were computed. However, the expression of a certain amount of fluorescent intensity for a given protein represents the volume amount of that protein present in a particular cell per given area. After staining the cell with the required antibody reagent to reveal the amount of a particular protein, the cell was imaged under the confocal microscope to reveal the fluorescent intensities (volume amount of the protein) expressed by the cell. These intensities are then quantified using the Leica software, to determine the grayscale values per unit area.

The fluorescence intensities of the different cell proteins, the intermediate filaments (K7, K8, K18, K19, and Vimentin), the microtubule (Tubulin), and the actin were analyzed, and their

relative volume densities were determined. Figure 7 shows the average intensity per area of the different cytoskeletal proteins for the two types of cells (MCF-10A, and MDA-MB-231). Numerically, for the fluorescence intensities, actin, keratin18, keratin8, and keratin7 had higher intensities in the normal cells (MCF-10A) compared to the metastatic cells (MDA-MB-231). However, in the case of the metastatic cell line (MDA-MB-231), keratin19, vimentin, and tubulin had higher fluorescence intensities, compared to that in the non-tumorigenic cells (MCF-10A). With a P-value of <0.05, there were significant differences in the expression of keratin 19, keratin 18, vimentin, tubulin 8, and actin. There was no recorded statistical difference in the expression of keratin 7 and keratin 8 between the normal and the cancer cells.

The frequency distribution curves in figure 8 represents the probability density function for the expression of the different proteins. Most of the proteins were well characterized by a lognormal distribution, with a left skew in the distribution. Keratin 18, tubulin, and actin showed a more pronounced difference in distribution frequency and as such could be analyzed to give more insights as to how their cytoskeletal properties affect the mechanical strength of biological cells.

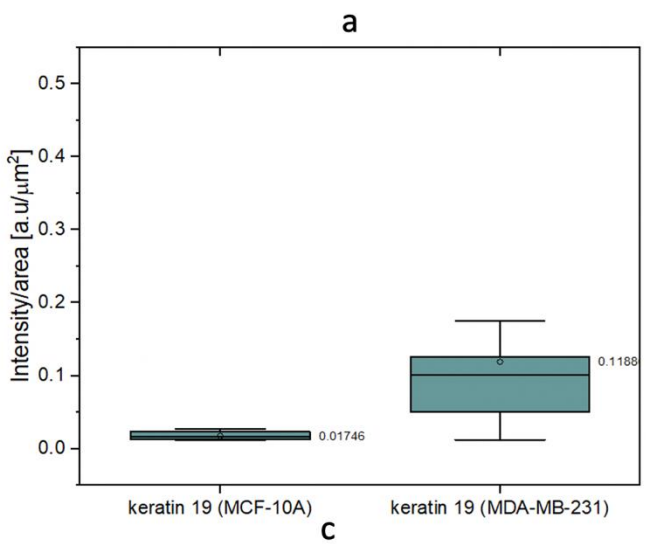
a
Intensity/area [a.u/µm²]
0.5
0.4
0.3
0.2
0.1
0.0
0.01746
0.1188
keratin 19 (MCF-10A)
keratin 19 (MDA-MB-231)

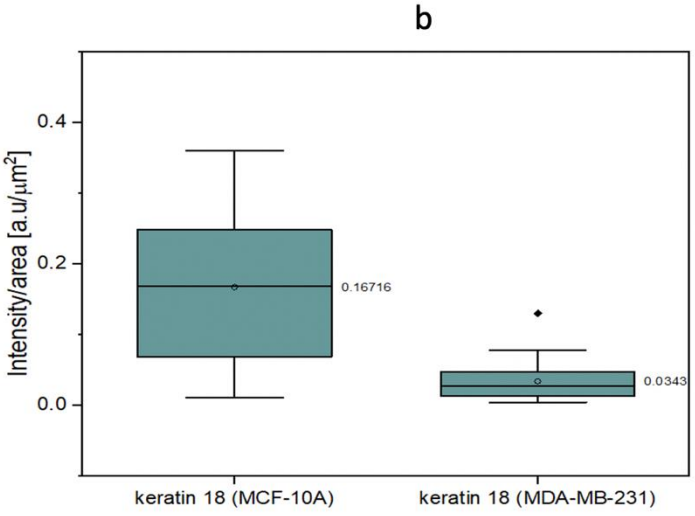
b
Intensity/area [a.u/µm²]
0.4
0.2
0.0
0.16716
0.0343
keratin 18 (MCF-10A)
keratin 18 (MDA-MB-231)

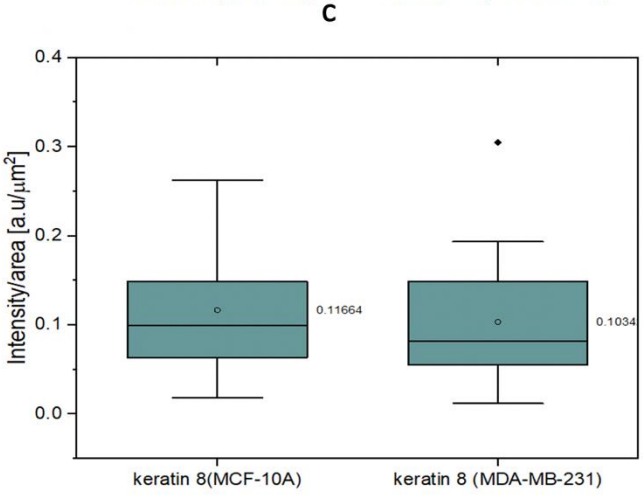
c
Intensity/area [a.u/µm²]
0.4
0.3
0.2
0.1
0.0
0.11664
0.1034
keratin 8(MCF-10A)
keratin 8 (MDA-MB-231)

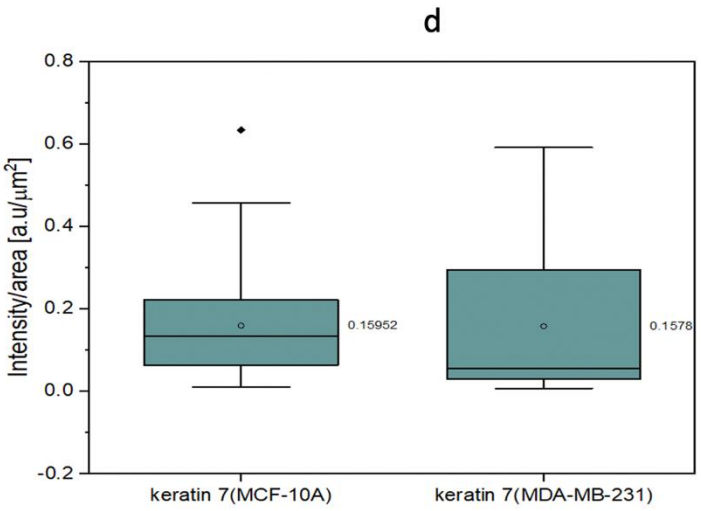
d
Intensity/area [a.u/µm²]
0.8
0.6
0.4
0.2
0.0
-0.2
0.15952
0.1578
keratin 7(MCF-10A)
keratin 7(MDA-MB-231)

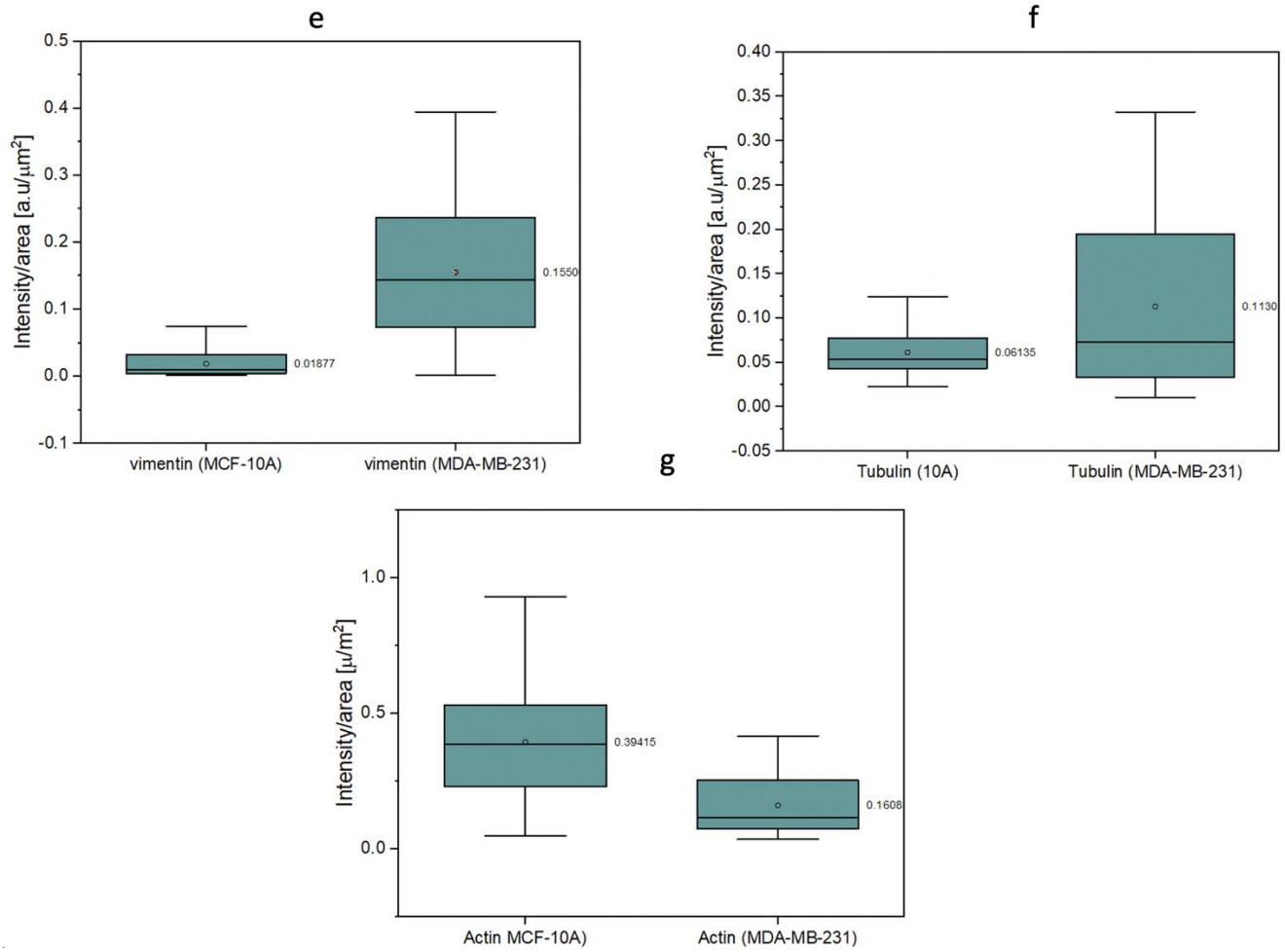

Figure 19:The fluorescence intensities/ area for the normal MCF-10A and cancerous MDA-MB-231 for the different proteins (a) Keratin 19 (b) keratin 18 (c) keratin 8 (d) keratin 7 (e) vimentin (f) tubulin (g) actin

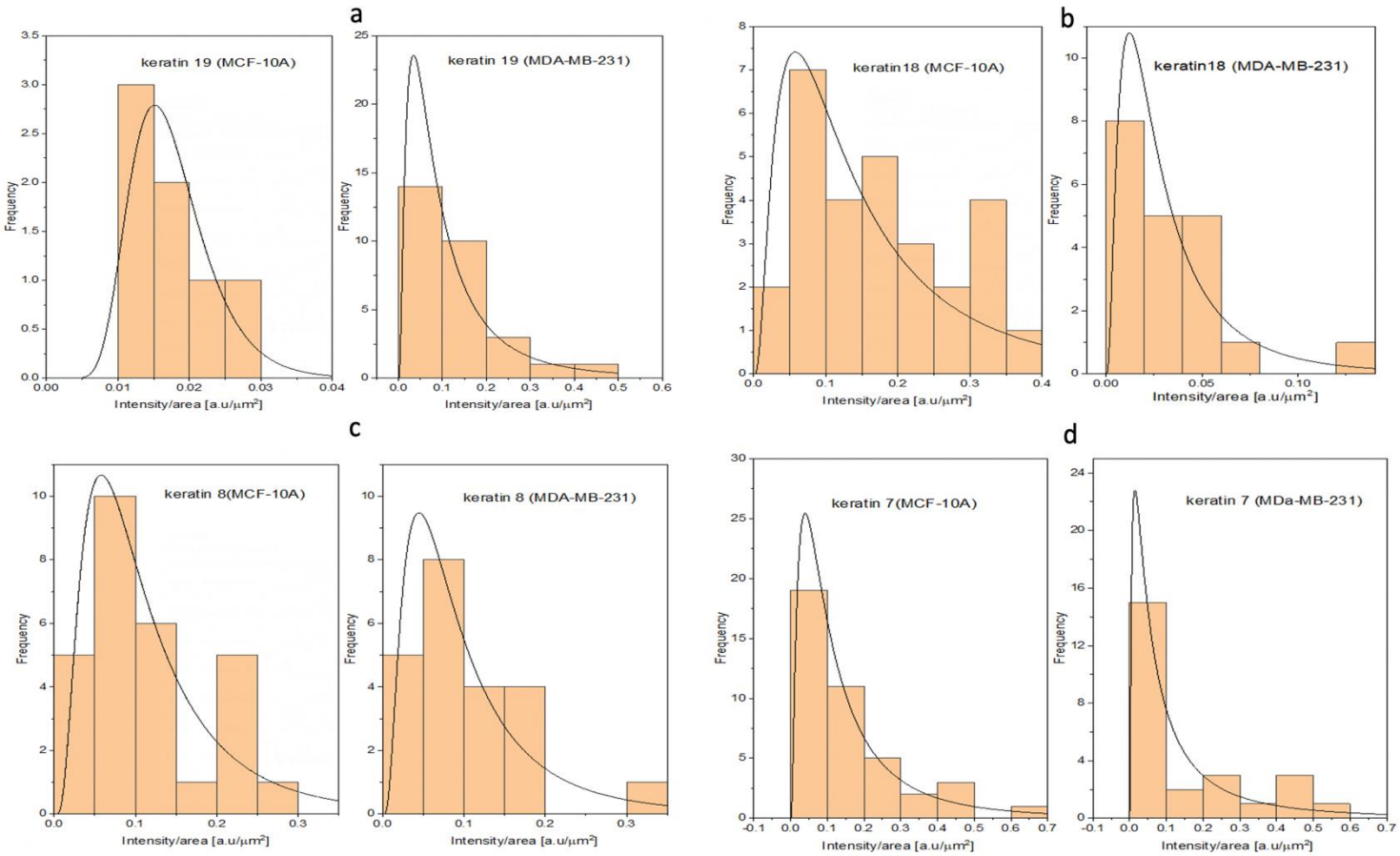
a
keratin 19 (MCF-10A)
keratin 19 (MDA-MB-231)
Frequency
Intensity/area [a.u/μm²]
b
keratin18 (MCF-10A)
keratin18 (MDA-MB-231)
c
keratin 8(MCF-10A)
keratin 8 (MDA-MB-231)
d
keratin 7(MCF-10A)
keratin 7 (MDa-MB-231)

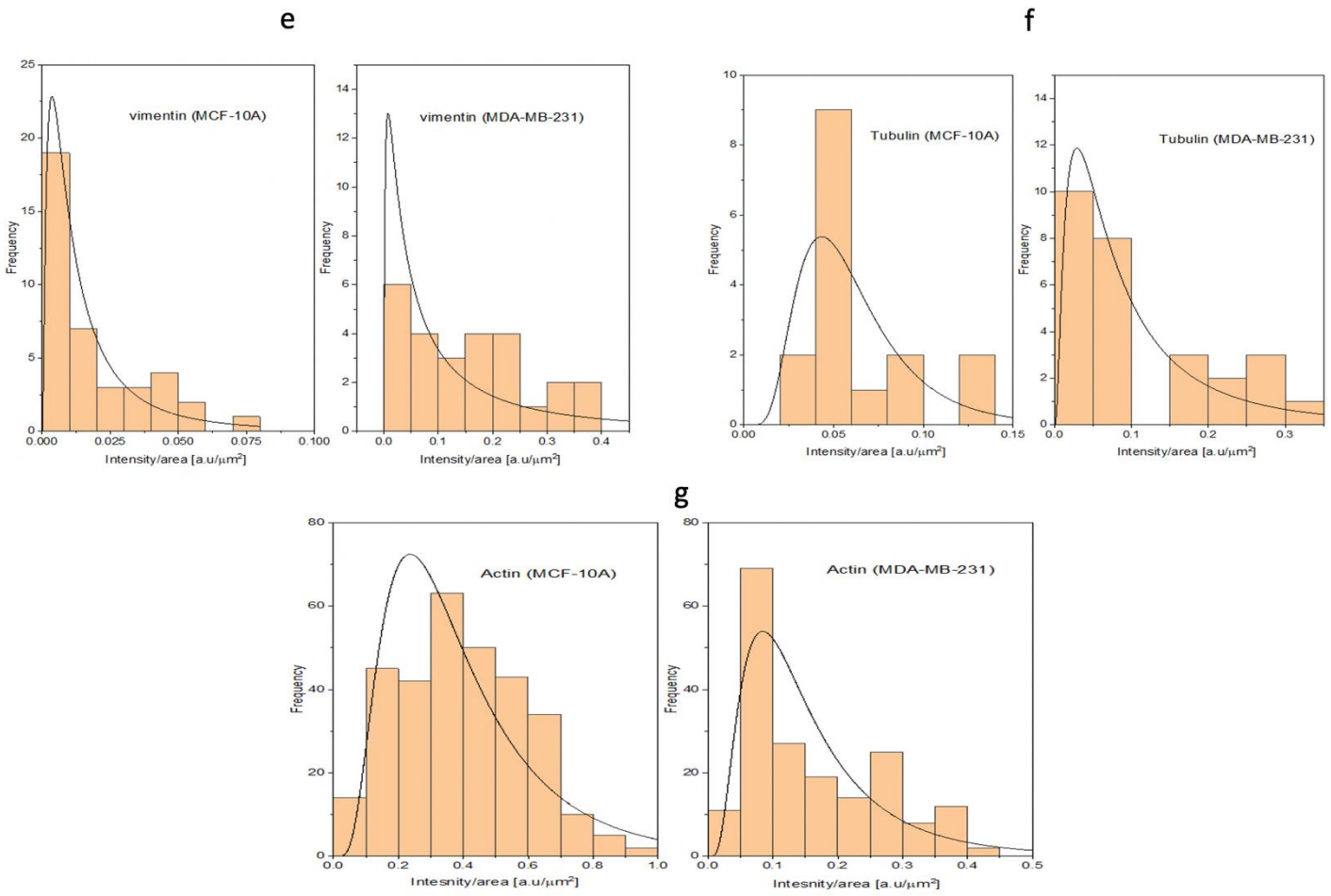

Figure 20: Frequency distribution of the different cytoskeleton proteins for the MCF-10A and MDA-MB-231 cells: (a) Keratin 19 (b) Keratin 18 (c) Keratin 8 (d) Keratin 7 (e) Vimentin (f) Tubulin (g) Actin

Figures 9 and 10 present the confocal images of the cell cytoskeletal proteins and the cell nucleus. These images show the variation in the volume of the proteins relative to one another across the two cell lines (MCF-10A) and (MDA-MB-231). The relative volume densities of each component of the cytoskeleton are calculated relative to the rest of the proteins and the nucleus. The nucleus and actin in both the non-tumorigenic MCF-10A cells and the cancerous MDA-MB-231 cells constitute the highest volumes relative to the rest of the cell constituents.

From the study, it was found that the nucleus and actin contain about 53 percent and 20 percent, respectively, of the total volume of the structure of the cell in the MCF-10A cell, and about 40 percent and 11 percent, respectively, of the total volume of the cell structure in the MDA-MB-231 cells, contributing largely to cell physiological and structural properties. Amongst the other cell proteins (IF and microtubulin), keratin 19, vimentin, and tubulin had the least volume densities relative to the other cell proteins in the MCF-10A cells. For the MDA-MB-231 cells, keratin 18 had the least volume percentages, with about 2 percent of the total volume. Keratin 19, keratin 8, and tubulin had 8.4, 7.3, and 8 percentages, respectively, of the total protein volumes, while other IF proteins, such as vimentin and keratin 7, each had volume percentages of about 11 percent. While these percentages can be slightly different from one study to another, it gives a near approximation to the relative of amount of the different proteins in the cells as

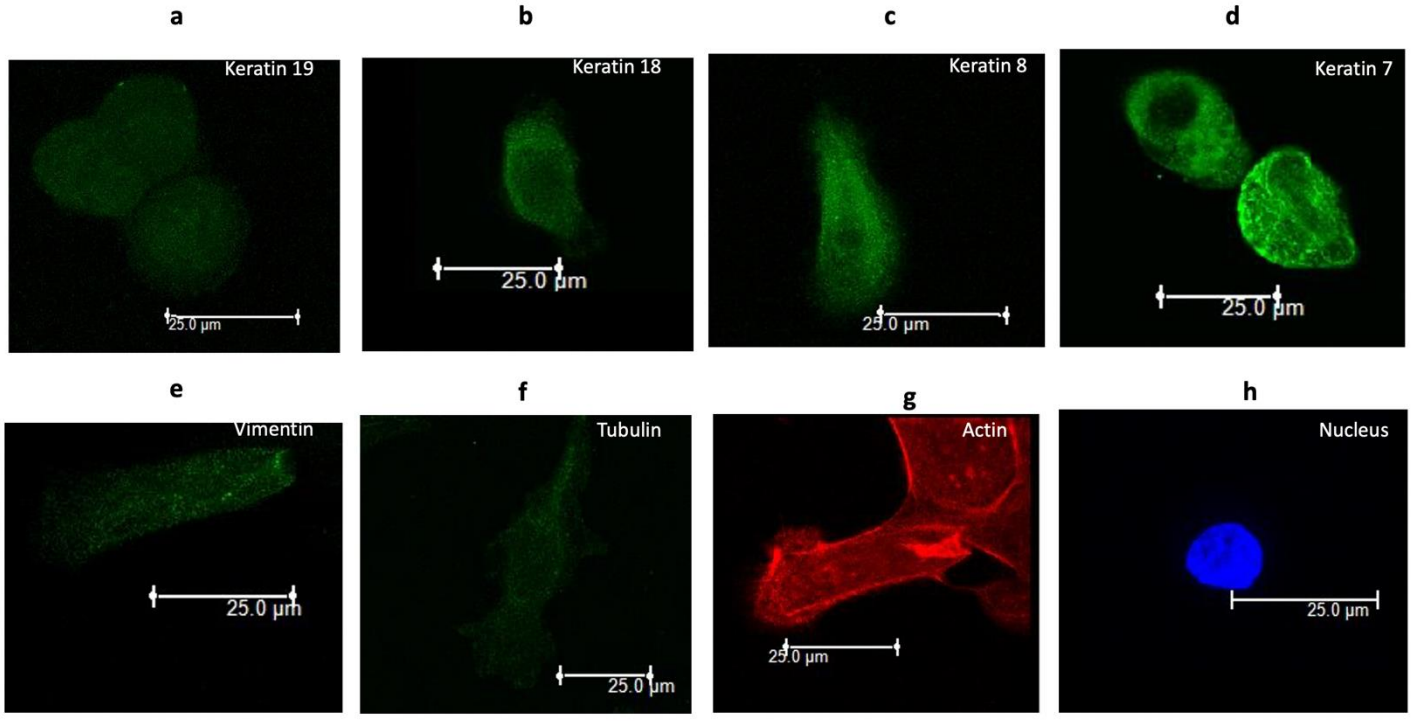

cancer progresses.

Figure 21:Confocal images of the cell cytoskeletal proteins and the nucleus for MCF-10A

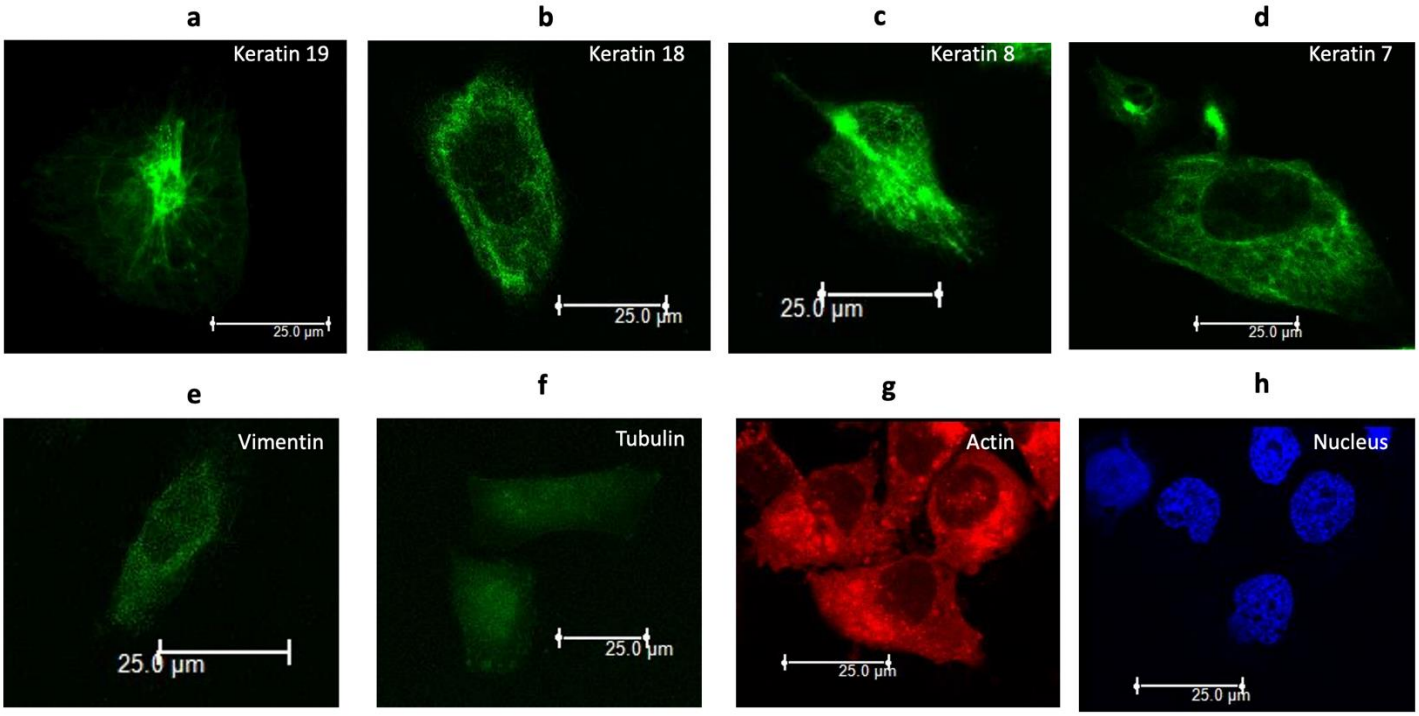

Figure 22:Confocal images of the cell cytoskeletal proteins and the nucleus for MDA-MB-231.

Figures 11aand 11b show further stained images of the actin sub-structures, the globular actin (G-actin), and the filamentous actin (F-actin. The F-actin stain reveals both the volume densities of both the filamentous, while the globular actin stain was stained using Alexa-594 DnaSe, and thus shows the individual structure for the G-actin.

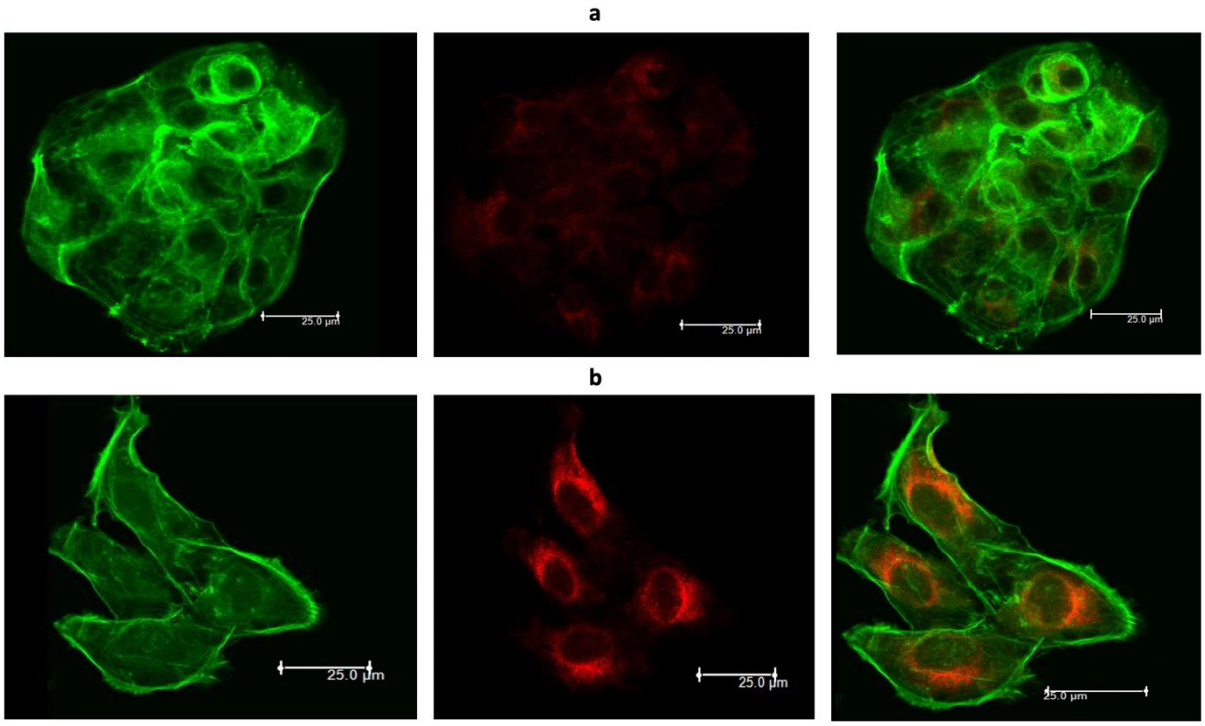

Figure 23: (a) Confocal images of the F-actin and G -actin structures for MCF-10A. (b) Confocal images of the F-actin and G -actin structures for MDA-MB-231.

The F-actin structure is found to express more at the base of the cell, away from the nucleus, and mostly at the boundaries between cells and between the surrounding cell environments. Its structures contain fibrous-like filaments which have been found to create mechanical support to the cell. On the other hand, the globular actin is found to be more localized towards the nucleus of the cell and does not possess fibrous strands as the F-actin, but over time polymerizes to such filamentous actin structures. The filamentous actin structures in the normal cells are however seen mostly as bundles and are not expressed distinctly as single strands of filaments as in the MDA-MB-231 cells. Furthermore, the G-actin is seen to be expressed more in the cancerous cell than in normal cells. Table 3 shows the statistical variations of the relative volume densities of the cell cytoskeleton. It shows that statistically, keratin 19, keratin 18, vimentin, tubulin, actin, and cell nucleus are significantly different and thus their expression at different stages of tumor progression can be indicators of variabilities in cell states.

Table 6: The relative volume densities of the cell cytoskeleton

Protein	Relative volume density [MCF-10A]	Relative volume density [MDA-MB-231]	Tukey's sig value	FPC mean Grouping [MCF-10A]	FPC mean Grouping [MDA-MB-231]	P-value
Keratin19	0.009	0.084	1	B	A	0.021
Keratin18	0.087	0.024	1	A	B	0.000
Keratin8	0.061	0.073	0	A	A	0.507
Keratin7	0.083	0.111	0	A	A	0.965
Vimentin	0.010	0.110	1	B	A	0.000
Tubulin	0.016	0.080	1	B	A	0.049
Actin	**0.205**	**0.114**	**1**	**A**	**B**	**0.000**
Nucleus	**0.530**	**0.403**	**1**	**A**	**B**	**0.000**

*Means that do not share a letter are significantly different (FPC);

**Means with Tukey's sig value =1, is significantly different,

***Means with P-value <0.05 are significantly different.

4.3.4. Strain evolution analysis, the relative volume density of cell cytoskeletal structure, and correlation with cell mechanics.

The relative volume density analyses of the cell cytoskeleton show that certain cell proteins are denser than others at different cell states, and hence have a large role to play in the physical and mechanical structure of the cell. This attribute, however, contributes to the variation in the strain evolution of the cell during the deformation process. In the normal cell, there were more discrete-sized magnitudes of strain, resulting from short displacement spans. This, however, can be attributed to the denser actin structure of the normal cell, which provides mechanical structure and resists deformation, causing more discrete displacement of the structure and thus smaller strain values. This is, however, in line with results from several authors, where actin filaments were seen to provide robust mechanical structures and, degradation of actin caused a reduction in mechanical properties of the cell[84], [96], [101], [102]

In the cell cytoplasm and nucleus, the degree of strain was different. There was considerably more strain in the cell cytoplasm than there are in the cell nucleus during the initial stages of creep, but with constant stress, the nucleus experienced considerable higher strain than the cytoplasm, where the proteins in the cytoplasm re-organize to withstand stress, thereby causing lesser deformation and strain. This, however, could be attributed to the internal structure of the cell, whereby the cell nucleus is a homogeneous structure, with relatively lesser structural ability to withstand stress than the layered cytoplasm, which consists of heterogeneously different components that can reduce the ability of the cell to undergo deformation.

The microstructure of the cell shows a higher density of actin and keratin 18 in the normal MCF-10A cells, and a higher density of the other proteins (Keratin 19, keratin 7, keratin 8, vimentin, and tubulin) in the cancerous MDA-MB-231 cells. This variation in the expression of the proteins is interesting in the understanding of the specific role of some of the proteins in cancer progression. The relative volume density of the actin microfilament and keratin 18 suggests that

for the normal cells, these proteins help to provide considerable resistance to applied stress. The denser these proteins, the more mechanical strength it possesses to withstand stress.

In this study, it was observed that the actin filament contributes largely to the total volume of the cell structure, with the total cell cytoskeletal microstructure made up of about 20% actin in the normal cell and about 11% in the cancerous cells, and as such plays, a key role in cell shape and movement, providing mechanical structure and motility [39]. Therefore, the density of the actin filament can be said to largely contribute to the variation in the mechanical structure of the cell. Over expression of other proteins such as Vimentin, tubulin, keratin 19, keratin 7, and keratin 8 can be correlated to the decreased mechanical properties of the cancerous MDA-MB-231. Most IF proteins such as keratins have been linked to low bending stiffness and decreased mechanical properties of cells[103].

4.4. Discussion

The results of the current study are useful in the characterization of the structure and properties of the normal breast cells (MCF-10A) and the metastatic triple-negative breast cancer cells. First, the results show that the fluorescence images with the mechanical properties of the cells provide important information that can be used to describe the cell structure in ways that can discriminate between non-tumorigenic cells and tumorigenic cells. Such digital imaging could enable the identification of triple-negative breast cancer cells in future biopsies. However, further work is needed to determine the extent to which fluorescence imaging techniques can be used to discriminate between cancer cells at different stages of tumor progression.

The current work also identifies significant differences between the components of the cytoskeletal structures in non-tumorigenic cells and tumorigenic cells. Hence, beyond the decrease in the actin cytoskeletal structural components that occur with cancer progression, the current work suggests that variations in micro-tubulin and keratin components can also occur in ways that can be used to distinguish between non-tumorigenic and tumorigenic states and correlate them with the individual mechanical properties of the cell. Further work is needed to establish the extent to which the identification of these structural components can be used to diagnose the onset and progression of breast cancer under clinical scenarios.

Finally, it is of interest to note that the above changes in the cytoskeletal structures can be correlated to the creep strain rates and viscoelastic properties, which we have shown to change significantly, as the cells evolve from non-tumorigenic to tumorigenic states [13]. In particular, the dependence of the stiffness and viscosity (of the nuclei and cytoplasm) appear to provide strong indications of the presence of TNBC. The trends in the cell viscoelastic properties can also be correlated with changes in cell cytoskeletal proteins in ways that could inform future analyses of cell biopsies and the use of shear assay techniques for the determination of mechanical biomarkers for the detection of TNBC in biopsies. Future work is, therefore, needed in the clear-cut understanding of how the expression of these proteins affects cell mechanics and promotes tumor progression. Cytoskeletal inhibitors can, also, be used for further studies of their individual effects on the cell. Finally, shear assay techniques can be used to m study of the physiological responses of cells under controlled shear/laminar flow conditions. These are clearly opportunities for future work.

Chapter 5

A Shear Assay Study of the Viscoelastic Deformation and Interfacial Fracture Behavior of Non-tumorigenic and Triple-Negative Breast Cancer Cells

5.1 Introduction

In recent years, several materials and mechanics approaches have been developed for the detection of diseases [1]–[3]. In the case of complex diseases such as cancer, the detection can also depend on cell genetics, protein/cell interactions, and cell mechanical[4]. Cell mechanical

properties have also been explored as biomarkers for the detection of cell states, malignancy, and metastasis[5]–[15]

The stiffnesses and viscosities of cancer cells have also been observed to decrease with increasing metastases[13], [14], [16]. These trends have been attributed to variations in the cell cytoskeleton, adhesion proteins, and cell detachment conditions for different cells[6], [9], [13], [17]–[20]. Depending on the state of the cell (normal or cancerous), these properties can differ, and thus provide estimates of the states as cancer progresses.

The role of cells in cancer metastases involves the rapid migration of cancer cells to induce tumors at target sites in other organs. The changes in cell mechanical properties can also induce changes in the tumor microenvironment[5], [21], [22]. Furthermore, changes in the cell's mechanical/viscoelastic properties can also affect their ability to squeeze through capillaries and blood vessels on their way to target organs. The induction of tumors in the metastatic organs can also result in the formation of receptors for the targeting of the metastatic organs [23]

In our earlier work [20], [25], a shear assay technique was developed for the measurement of the shear stresses associated with the detachment of cancer cells from substrates in a laminar flow chamber. This was followed by subsequent work in which lift and drag forces were computed for cell detachment conditions under laminar shear flow conditions [26]. Most recently, we used the interfacial fracture mechanics approach to compute the crack driving forces associated with cell detachment under laminar shear flow[13].

However, prior work did not link the mechanics of interfacial fracture (associated with the detachment of biological cells during shear assay experiments) to the different types of detachment that can occur during the deformation of cells associated with such experiments.

Hence, in this work a cohesive zone approach is linked to the different stages of cell deformation and detachment in ways that provide us with some insights into the crack driving forces and the crack-tip shielding phenomenon that are associated with the cell detachment process.

In this work, a combination of cohesive zone models and *in-situ* observation of cell deformation and detachment is used to study the viscoelastic/creep deformation of non-tumorigenic and triple -negative breast cancer cells. These are used to determine the cohesive zone parameters and critical energy release rates associated with the detachment of non-tumorigenic and triple negative breast cancer cells. The implications of the results are also discussed for the development of potential mechanical biomarkers for the detection of triple negative breast cancer.

(a)

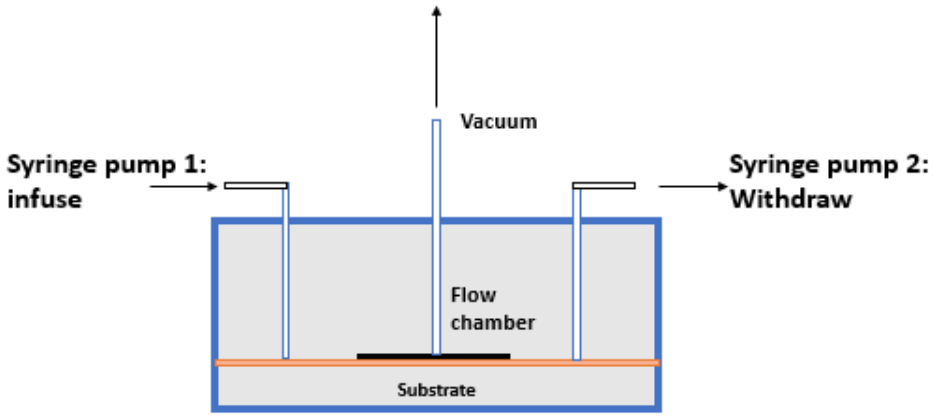

(b)

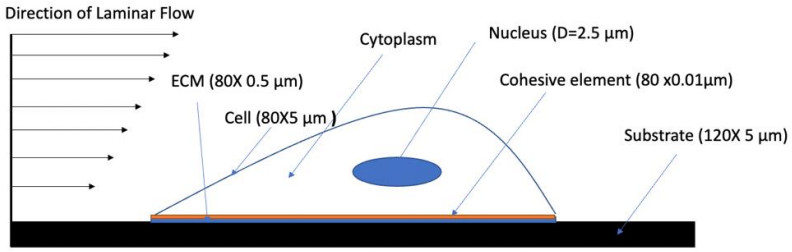

Figure 24: (a) Shear assay set-up (b) Schematic of a cell under laminar flow

5.2. Materials and Methods

5.2.1 Cell Culture Experiments

The normal MCF-10 cells and the metastatic MDA-MB-231 cells were cultured in 35 X 10 mm falcon Petri dishes (Thermofisher, USA). Both cell lines MCF-10A (Cat # HTB-132) and MDA-MB-231 (Cat # HTB-26) was obtained from the American Type Culture Collection (ATCC). The normal MCF-10A cells were cultured in a mixture of DMEM medium (Invitrogen, Carlsbad,

CA, USA), supplemented with 100 ng/ml cholera toxin (Sigma-Aldrich, St. Louis, MO, USA), 10 μg/ml insulin (Sigma-Aldrich, St. Louis, MO, USA), 1% Penicillin-Streptomycin (Invitrogen, Carlsbad, CA, USA), 5% horse serum (Invitrogen, Carlsbad, CA, USA), 30ng/ml murine epidermal growth factor (PeproTech, Rocky Hill, NJ, USA), 0.5.5 μg/ml hydrocortisone (Sigma-Aldrich, St. Louis, MO, USA), and 0.2% amphotericin (Gemini Bio-Products, West Sacramento, CA, USA). The cultured cells were incubated for 48 hours at 37 °C in a 5% CO_2 atmosphere, to enable the growth of the cancer cells

The metastatic MDA-MB-231 cells were cultured in a mixture of L-15 medium, supplemented with 100 I.U./ml penicillin/100 μg/ml streptomycin and 10% FBS. These were all obtained from the American Type Culture Collection (ATCC), Manassas, VA, USA. The cultured cells were incubated for 48 hours at 37°C under normal atmospheric pressure.

The cells were dispersedly seeded on the Petri dishes to ensure non-confluence growth of the cells to enable individual cell growth for further single-cell studies and analysis.

5.2.2. Shear Assay Experiments

Before the shear assay experiments, the cultured cells were aspirated from the culture medium. The shear assay setup is presented in fig 1. It has been used by our group [28] to determine the adhesion of biological cells to different substrates. It consists of a microfluidic parallel plate flow chamber (Glycotech Corporation, Gaithersburg, MD, the USA that has an inlet and outlet to support fluid flow. The microfluidic device is connected to a programmable Harvard syringe pump (Harvard Apparatus, Holliston, MA, USA) that uses 50ml syringes and fluid hose tubing.

The pump introduces the fluid into the microfluidic device by injecting the fluid in the syringe through the hose and withdrawing fluid from the outlet of the device through a hose. A steady-state flow of fluid is obtained by maintaining respective flow rates of 3ml/min and 5ml/min for the MDA-MB-231 and MCF-10A. The parallel plate microfluidic device was designed to fit 35 mm Petri dishes. A rubber gasket was also attached between the microfluidic device and the Petri dish, to ensure controlled flow during the shear assay experiment. The rubber gasket had a length of 20.5 mm, a width of 2.5 mm, and a height of 0.254 mm, with a vacuum suction around its perimeter. Before shear assay experiments, the viscosity of fluid was measured with a rheometer (Anton Paar, Ashland, VA, USA)

This was carried out on mixtures of non-toxic methylcellulose and cell culture media, with concentrations of 3.5wt% of methylcellulose. However, in the case of the metastatic MDA-MB-231 cells, no extra cellulose was added, and the viscosity of the medium was 0.001Pa.s. Thus, small shear stress was needed to deform and detach the MDA-MB-231 cells enough to determine their properties.

However, the shear rates were kept identical at a rate of 2500s $^{-1}$. The wall shear stress was calculated from:

$$\frac{6\mu Q}{wh^2} \qquad (1)$$

The shear assay experiments were carried out for 5 minutes to enable that the deformation and/or detachment were observed under an optical microscope with a 40X objective lens. An *in-situ* Nikon video camera was also used to study the real-time, shear deformation of the cells which were then analyzed using digital image correlation analysis.

5.2.3. Strain Mapping

Strain mapping was carried out using a Digital Image Correlation (DIC) technique[13], [14], [20], [25]. This was done using Davis software (LA Vision, Gottingen, Germany). The videos of the shear deformation of cells were obtained from the shear assay experiment and are converted to image frames, to enable deformation correlation using the DIC. A region of interest is chosen, by highlighting the perimeter of the single cell under consideration and choosing suitable seeding points on the cell to capture areas of possible deformation on the cell (The number of seeding areas is dependent on the size of each cell). The seeding points/seeding areas (31 X 31 pixel) was used as a reference point/ area that tracks the change in the position of a given point/area in the subsequent images for the seeding area in the first image. For each seeding area chosen on the cell, there were accompanying changes in the distance between the seeding area of the first image frame and the last image frame. These changes in distance between these seeding areas, which corresponds to the displacement of that given within the cell, are computed by the DIC, for the numerous seeding areas chosen on the cell. The DIC also uses the same technique, to provide the accompanying strain components associated with the change in distance/displacement within the cell. The DIC also provides strain and displacement maps that show the varying magnitudes of displacement/ strain witnessed by each cell during deformation.

During deformation, the cell witnesses the effect of external forces in the form of fluid flow, the fluid either penetrates between the layer between the cell and the ECM, causing the cells to flip or shear, or it causes micro buckles within the cells. Most MDA-MB-231 cells witness the flip and shear deformation process, while the normal MCF-10A cells witness micro buckling.

5.2.4. Immunofluorescence Staining of the ECM

In most cases during shearing and cell detachment, the detaching cells leave behind focal adhesion proteins and adhesive extracellular matrix (ECM) materials. behind on the ECM as shown in Fig 6. However, the residual ECM also contains adhesion proteins such as vinculin and actin that were left behind on the residual ECM, following the detachment of the cells by the shear assay process. This suggests that the transmembrane vinculin and actin were attached to the ECM during the shearing-off of the cell membrane from the ECM. The interfacial cracks were, therefore "bridged" by the attached vinculin and actin fibers before the fracture of the actin fibers or actin/vinculin interfaces or vinculin that remained attached to the ECM. The staining of ECM was done after fixing with paraformaldehyde. This was followed by rinsing with 10%PBS and 90 % distilled water. The residual materials were then permeabilized with 0.1% Triton X-100 and blocked with 1% bovine serum albumin solution (BSA) for 1 hour at room temperature. The treated ECM was then again rinsed three times with 10% PBS and 90% distilled water. Vinculin mouse monoclonal antibody (Thermofisher, Massachusetts USA) was prepared in 0.1%

BSA and incubated. It was then added to the treated ECM at a concentration of 2µg/ml and incubated for 3 hours at room temperature. The resulting sample was rinsed again with 10% PBS and 90% distilled water after 1 hour after which F-actin stain was added. The goat anti-mouse super clonal conjugated Alexa 488 flour rhodamine-phalloidin (Thermofisher, Massachusetts) antibody was used to label the cells for the f-actin stains. The nucleus was stained as well using DAPI, and then the Gold antifade was used as an antifading agent. The Leica SP5 point scanning confocal microscopy (Leica Microsystems, Heidelberg, Germany) with an APO CS 40X 1.25 oil objective w used to image the cells.

5.2.5. Finite Element Analysis

A cohesive zone model was used to study the interfacial cell detachment fracture process. The cells (non-tumorigenic and tumorigenic) were modeled as semi-ellipses on a flat substrate. A two-dimensional axisymmetric plane model was implemented using the ABAQUS software package (ABAQUS, Simulia, Pawtucket, Rhode Island, USA). A 4-node two-dimensional cohesive element was introduced at the interface between the cell and the ECM. The cohesive zone was meshed using under the assembly module. This was done with a standard linear geometric order from the cohesive family. A structured quad-mesh-type was used along with curvature control of 0.1 and typical element sizes of ~0.01. All other parts of the model were implemented using a plane strain approach with an approximate element size of 0.1. A total of 403 elements was generated for the cell geometry along with 80 elements for the cohesive element, 80 elements for the ECM, and 600 elements for the PDMS. The material properties for the cell were obtained from a previous experiment from our group[14].

5.3. Results and Discussion

5.3.1. Cell Detachment Behaviors and Characteristic Creep Profiles

The deformation characteristics of the cells under applied stress are generally a factor of their internal structure (cytoskeletal structure), growth orientation, cell adhesion, and cell mechanical properties (the cytoplasm and nucleus). In this study, we observed that the deformation of single cells was subjected to constant shear stress for 240 seconds. The deformation behaviors observed within the cells were classified as either peel (Mode I, tensile crack opening mode), shear (in-plane shear by mode II cracking), and/or induced changes in internal structure (micro-buckling). The peel-off deformation mode I type was mostly observed in the cancerous MDA-MB-231 cells as shown in Figs. 2a and 2b. This was associated with initial delamination of some parts of the cells followed by stress concentration at the crack-tip and mode I cell detachment. In contrast, some cancer cells also exhibited interfacial failure by in-plane shear, which resulted in *in-plane* shear detachment by mode II fracture. Lastly, Figs 2c and 2d show evidence of transmembrane deformation before the formation of circular “micro-buckles” before the onset of cell detachment. However, in most cases, the onset of micro-buckling was followed by about 5 minutes of shear flow before the detachment of the cells from the ECM/substrate.

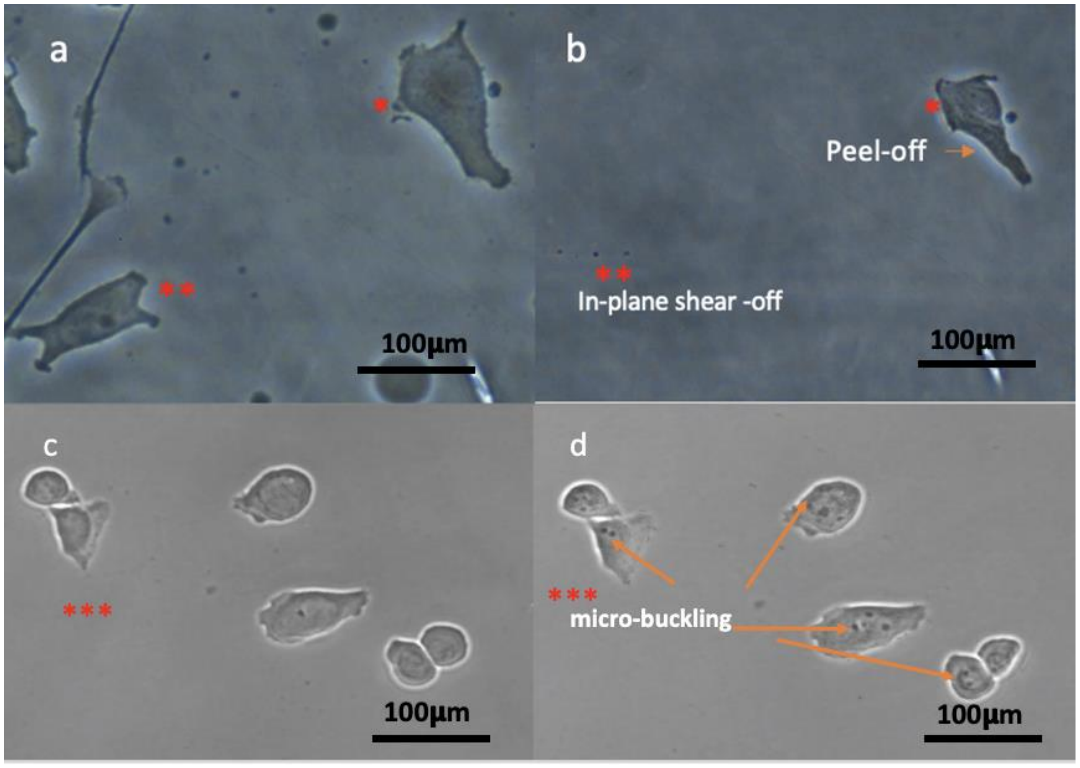

Figure 25: Deformation mechanisms for different cells: (a) Before the deformation of cancerous MD-MB-231 cells (b) Peel-off (tensile failure) and in-plane shear-off (shear failure) of cancerous MD-MB-231 cells (c) Before the deformation of normal MCF-10A cells and (d) Micro-buckling of the internal structure of the Normal MCF-10A cells

5.3.2. Detachment of Cells from the Extra Cellular Matrix

The extracellular matrix of the cell acts as a mechanical support for the cells and helps the cells bind together and to their substrates where applicable [31], [32]. During the shear process, the cells are subjected to constant shear stress of 10 Pa for the cancerous MDA-MB-231 and 410 Pa

for the non-tumorigenic MCF-10A cells. When critical driving forces were reached, the cells sheared off from the substrate leaving behind the ECM, and other adhesive proteins as shown in figure 3. At the onset of detachment, the cell was aligned in the direction of the shear stress, thus exposing the ECM and other adhesive proteins. Residual adhesion proteins are also left behind in the ECM following the shear detachment of the cells from the ECM. This is shown in figure 6 in which evidence of residual actin and residual vinculin is present in the ECM that is left behind after the shearing off the non-tumorigenic MCF-10A cells (Fig 6a) and the triple-negative MDA-MB-231 cancer cells (Fig. 6b) and materials depicting a snap-off between the cells and the ECM. This is seen in figure 3 and the vinculin and actin staining of the ECM in figure 6. The ECM is further analyzed in section 3.3 to depict the difference in its interaction between the cancerous MDA-MB-231 and normal MCF-10A cells.

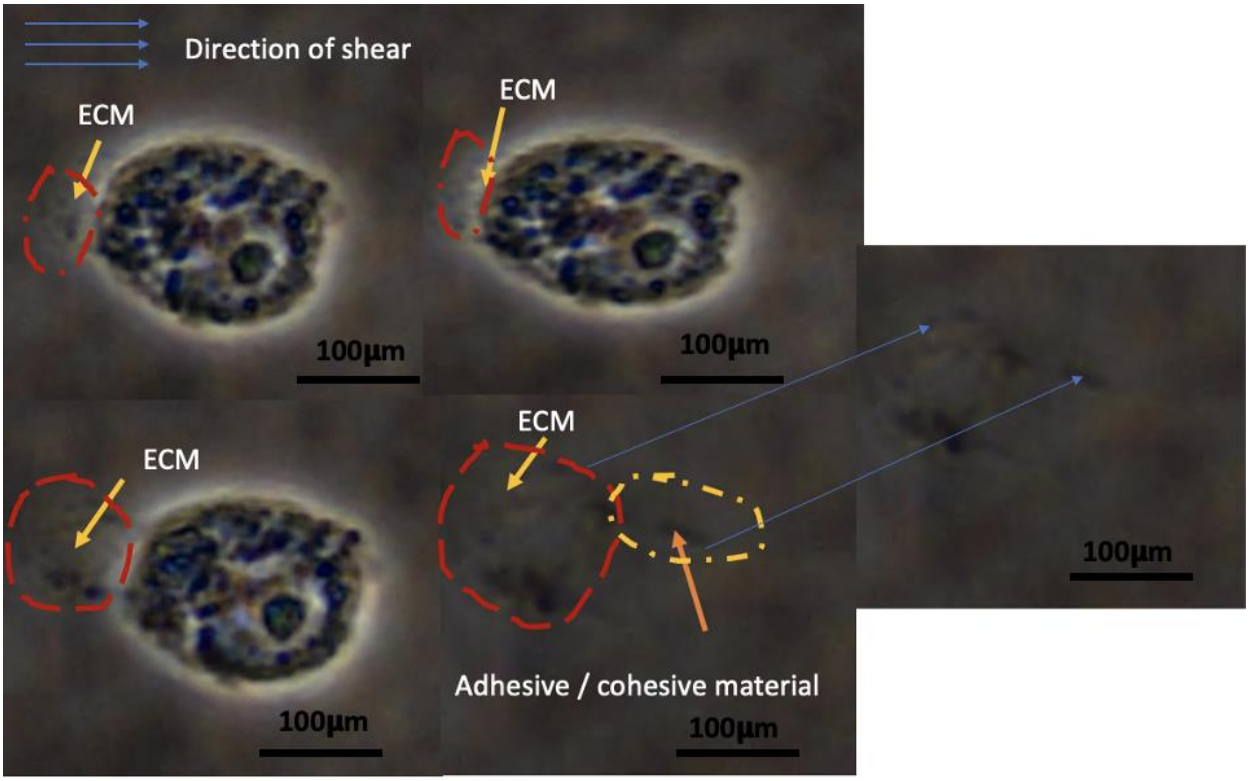

Figure 26: Description of Cell-ECM detachment revealing the ECM and cohesive material post - shear

5.3.3. Effects of strain Evolution on Cell Orientation and Viscoelastic/Creep Behavior

Figures 4a and 4b, show the various displacements and strains associated with cell deformation. Fig. 4a shows the displacements and strains experienced by the normal cells during the deformation process. A gradual build-up of strain was observed within the cell, where the nucleus experienced lower displacements and strains compared to regions in the cytoplasm. The strain distributions observed with the MCF-10A were associated mostly with micro buckling

within the cell. However, in the case of the cancerous MDA-MB-231 cells, they experienced lower magnitudes of displacements and strain, but with faster creep. Also, non-uniform and increasingly higher displacements and strains were observed in the cell cytoplasm and boundaries of the cells/cell membrane during the deformation, suggesting weaker cell adhesion and preceding early failure of the cancer cell. The strain distributions were also associated with the peel-off and shear-off of the cell. Figures 5a and 5b present plots of the time-dependent strains experienced by the cell. The plots show that the cancerous MDA-MB-231 cells experienced faster creep and earlier failure/detachment compared to the normal MCF-10A cells. There were more strain and deformation in the cytoplasm for both the normal and cancerous cells compared to the nucleus [13]

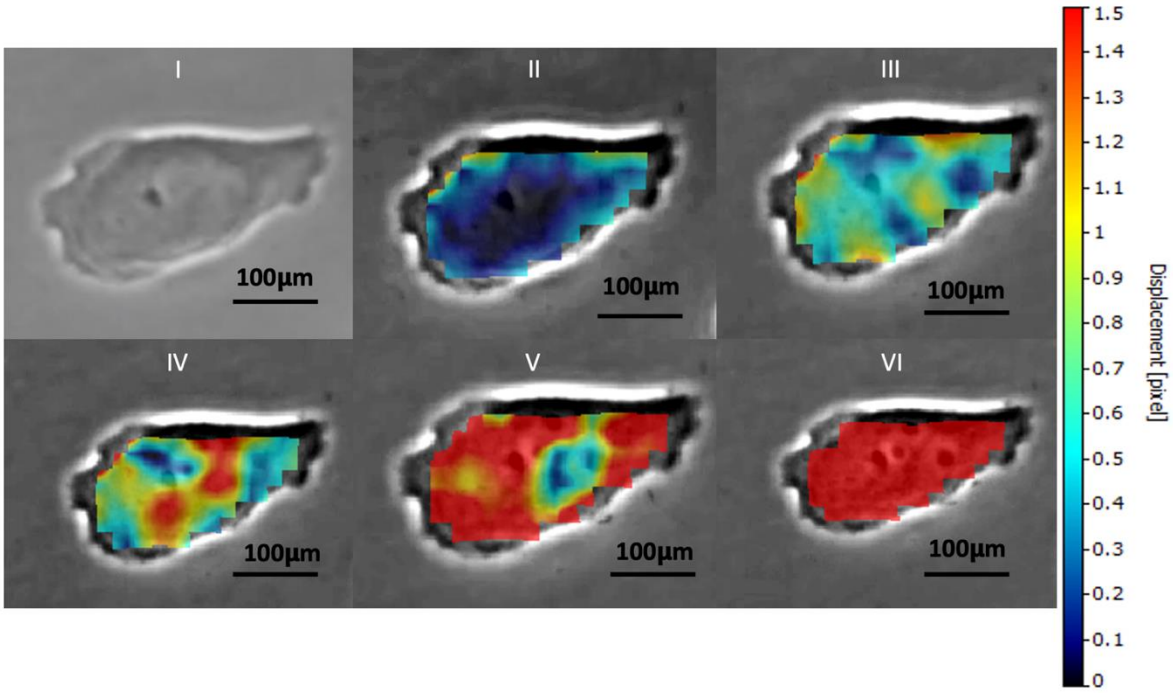

(a)

(b)

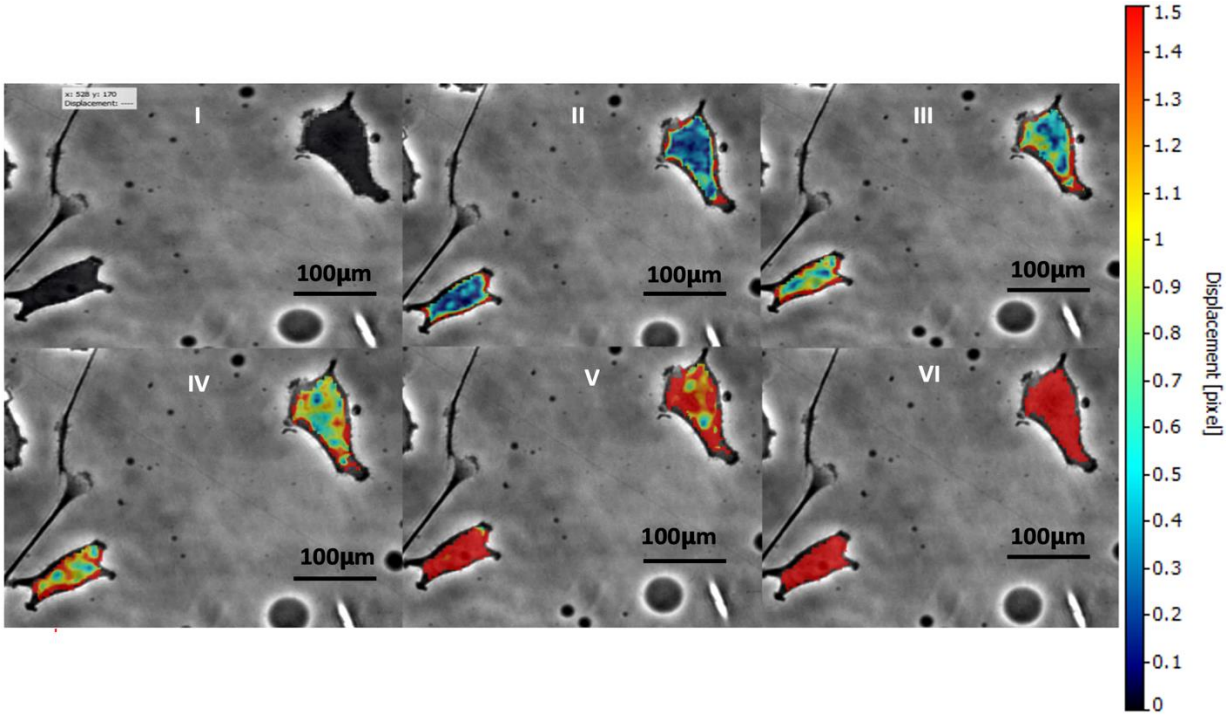

Figure 27: (a) Displacement evolution and mapping for the Normal MCF-10A cells (I) Cell structure at t=0, and without deformation (II) A gradual buildup of stress around the cell cytoplasm and nucleus (III) Uniform stress distribution within the cytoplasm and nucleus (IV) The onset of micro buckling within the cell structure and onset of tertiary creep (V) Increased failure progression (VI) Final failure/Detachment of the cell.

Figure 28: (b)Displacement evolution and mapping for cancerous MDA-MB-231 cells (I) Cell structure at t=0, and without deformation (II) Larger displacements within the cell membrane than in the cell cytoplasm and nucleus, preceding the early peel-off/shear-off of cells (III) Increased stress and displacement within the cell structure (IV) Onset of failure (V) Failure progression within the structure of the cell (VI) Final failure by shearing off and peeling-off of cell

(a)

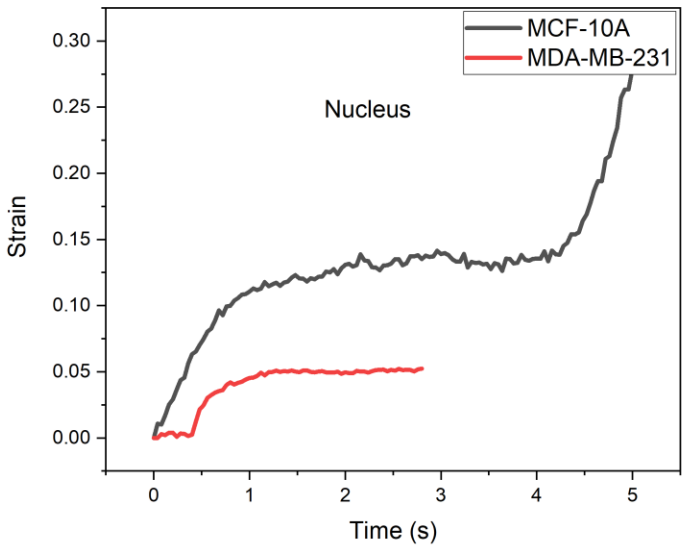

(b)

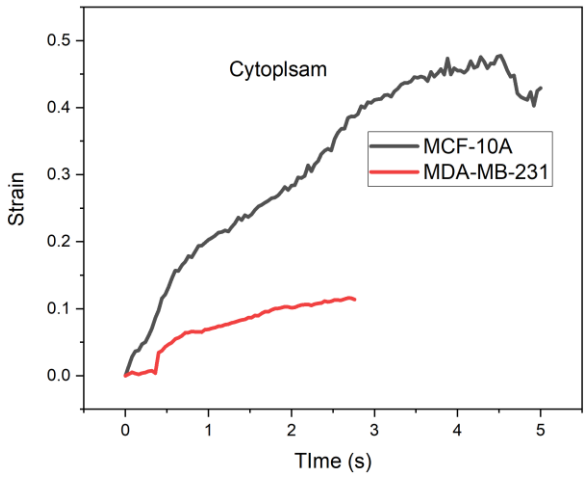

Figure 29:Creep curve for the deformation of the Cell nucleus for the normal and cancerous cell (b) Creep curve for the deformation of the cell cytoplasm for the normal and cancerous cell

5.3.4. Focal Adhesion/ Cytoskeletal Protein Staining of the ECM

Figures 6a and 6b show the distribution of cell adhesion proteins in the ECM that is left behind after shearing off the cells. The green stains correspond to the presence of actin, which supports cell growth, migration, deformation, and survival [33]–[35], while the red stains correspond to vinculin from the cells. These have been left behind on the residual ECM, following the detachment of the cells from the ECM between the cells and the substrates. Cells devoid of these focal adhesion structures such as vinculin are found to have fewer and fewer adhesions[35], [36]. The results suggest that these residual proteins bridged the interfacial cracks that were formed during the detachment of the cells from the substrates. Thus, we conclude that these proteins

bridged the interfacial cracks during the detachment of the cells from the ECM. However, they were left behind on the ECM, after their fracture during the detachment process.

(a)

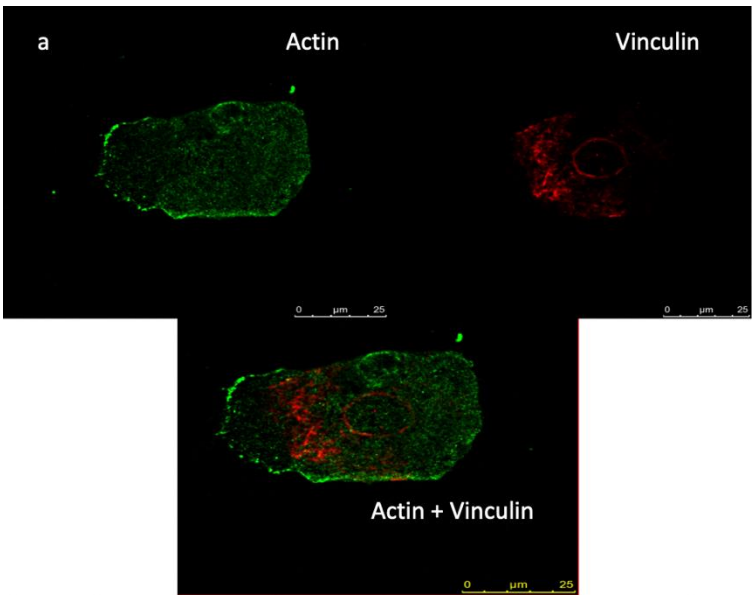

(b)

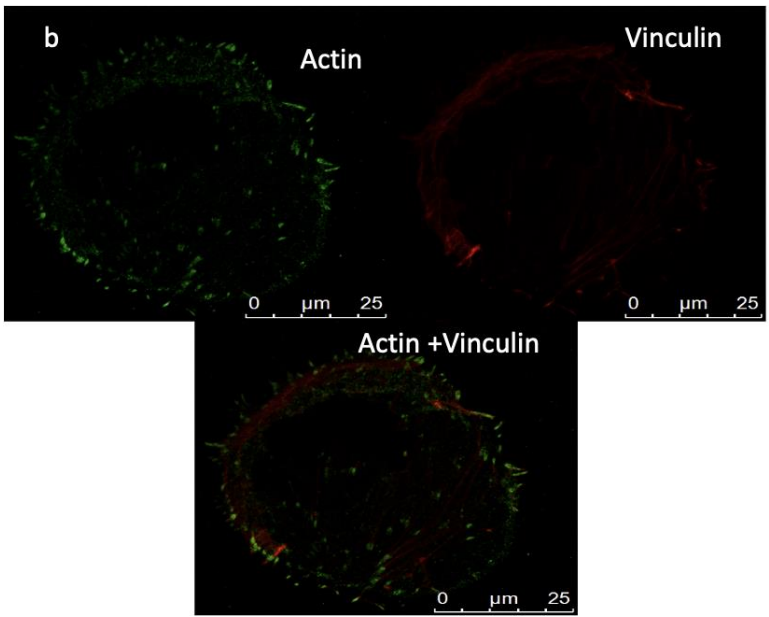

Figure 30: Fluorescence imaging of the vinculin and actin structures of the (a) Normal MCF-10A cell (b) Cancerous MDA-MB-231 cell

5.3.5. Contribution of the cell Cytoskeleton to strengthening and Cell Deformation

Fig 7 shows the role of the cell cytoskelton in deformation and detachment of cells in response to external influences (stress, applied force). The cell cytoskeleton which consists of fibrous proteins plays a very crucial role in the structural integrity of cells. They largely determine the movement and migration of cells, their mechanical abilities and interaction with the environment. Under an applied stress, the behavior of cells to induced deformation largely depend on the presence or absence of most of the proteins such as vimentin and actin. From figures 6a and 6b, staining the ECM for the adhesion proteins, showed the expression some of the proteins (actin and vimentin) which, however, demonstrates deflection and bridging of cracks via the protein fibers prior to failure. Hence for a cell with an abundance of these fibers, there will be considerable resistance to deformation, and strengthening prior to final failure. More fibrous cells such as in the normal MCF-10A breast cells, experience micro void effect that causes local buckling and proceeds final failure.

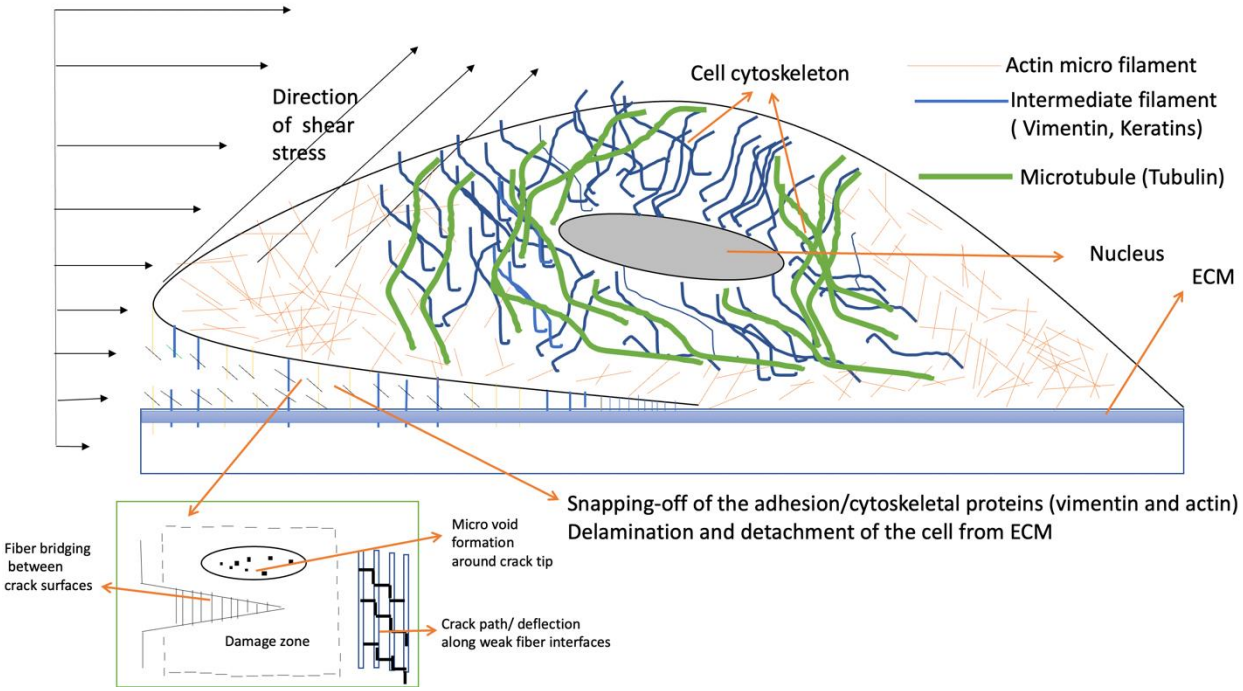

Figure 31: Schematic of the contribution of cell cytoskeleton in the strengthening and deformation/detachment of the cell

5.3.6. Finite Element Modeling

A typical finite element model of the non-tumorigenic and triple-negative breast cancer cells is presented in Figures 9a and 9b respectively. This was modeled using the ABAQUS software package (ABAQUS, Pawtucket, RI, USA). The delamination was modeled using a displacement-controlled approach. This was done by introducing a cohesive element between the cell and the extracellular matrix (ECM). The cohesive element (figure 3) represents the binding adhesive proteins that connect the cell membrane to the ECM. The cohesive thickness was assumed to have a thickness of 0.001□m, and the same length as the cell

Figure 8 shows the different constitutive laws that were used for the force-traction functions in the cohesive zone model. These were adopted from a previous publication on the constitutive

forms for force-traction laws [40]. The properties of the cell, the ECM, and the PDMS substrate were obtained from previous works [14], [41], [42]. These are summarized in table 2.

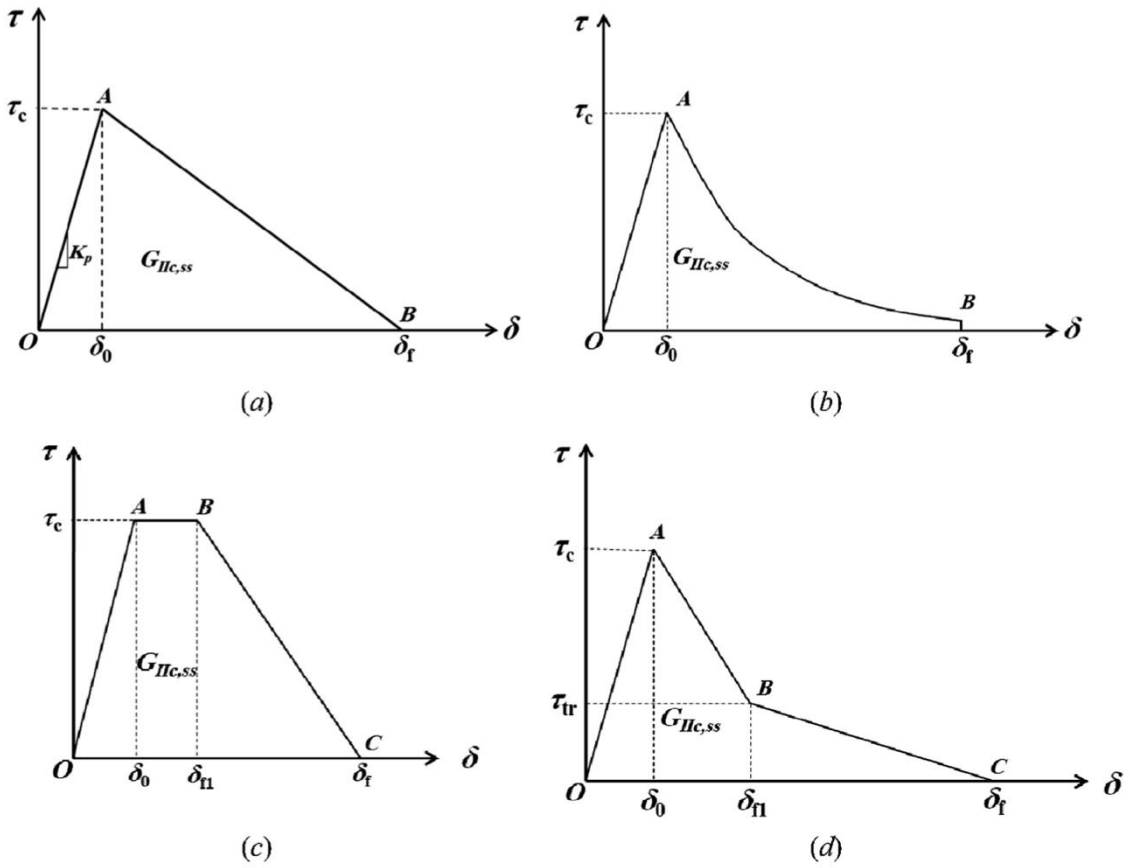

Figure 32: Different traction-separation laws: (a) Bilinear form (b) linear-exponential form (c) trapezoidal form (d) trilinear form

In this study, the following assumptions were made in the simulation of cell detachment:

I. the cells are elliptical with a flat base in contact with the substrate.

II. The deformation of cells is primarily a mode I failure problem, where the cells detach by opening (tensile mode) before complete failure.

III. The stress witnessed at the interface between the cell and the extracellular matrix is closely the same as the applied shear stress acting on the body of the cell.

IV. The nominal stress in the normal mode is the same in both directions of shear (first and second).

All the material properties that are needed to define the cohesive elements in finite element analysis are summarized in Table 2

Table 7a: Viscoelastic properties of the cell (cytoplasm and Nucleus)

Viscoelastic Property	**MCF-10A (Nucleus) (Pa)**	**MCF-10A (Cytoplasm) (PA)**	**MDA-MB-231 (Nucleus) (Pa)**	**MDA-MB-231 (Cytoplasm) (Pa)**
Modulus of elasticity(E)	7966	3598	622	261
Viscosity	6868	3132	325	215
Relaxation time	0.5	0.6	0.3	0.4

Table 7b: Typical Cell Dimensions and Cell Poisson's ratios

Property	MCF-10A	MDA-MB-231	ECM
Length (µm)	80	80	80
Height (µm)	5	5	5
Thickness(µm)	5	5	5
Poisson's ratio	0.49	0.49	0.4

Table 7: Properties of the cohesive zone

Property	MCF-10A Cells	MDA-MB-231 Cells
$E_{nn}=E_{ss}=E_{tt}$	210	5
Nominal stress (Normal-only mode)	410	10
Nominal stress (First direction)	410	10
Nominal stress (second direction)	410	10
Displacement at failure (µm)	0.25	0.004
Viscosity coefficient	0.001	0.001
Length (µm)	80	80
Thickness (µm)	0.01	0.01

The induced Mises stress distributions associated with the laminar flow processes are presented in figures 9a and 9b for the normal cell (fig 9a), and the triple-negative breast cancer cells (Fig 9b). In the case of the normal MCF-10A cells, there was a gradual fracture process that induced

crack initiation and crack growth before a complete interfacial failure. However, in the case of the cancerous MDA-MB-231 cells, there was a more rapid fracture process, where there was no distinct crack propagation phase before final failure. Thus, the current results suggest that the cancerous cells have a much lower resistance to crack growth than the non-tumorigenic cells.

The normal MCF-10A cells in figure 8a, at t=121.9s, show the gradual delamination and breakage of the cohesive element/adhesive materials binding the cell to the ECM. This is also demonstrated in figure 3, depicting the shear-off of cells from the ECM.

Figure 10 shows the characteristic force-traction profiles and the corresponding critical energy release rate associated with the non-tumorigenic and triple-negative breast cancer cells. The critical energy release rates for the normal cell at degrees of freedom/displacement magnitude of 3 and 5 was $9.28x10^{-7}J/m^2$ and $5.65x10^{-7}J/m^2$. However, for the cancerous (MDA-MB-231) cells, the critical energy release rates at degrees of freedom/displacement magnitude of 3 and 5 was $2.592\ x10^{-8}J/m^2$ and $2.095\ x10^{-8}J/m^2$.

The force-traction profile for the MCF-10A at a displacement magnitude of 3 and 5 were bi-linear and tri-linear, respectively, while for the MDA-MB-231 cells, they have a bilinear force-traction curve for different displacement magnitudes (U=3, U=5). The bi-linear cohesive zone model for the MDA-MB-231 cell experienced a short critical opening displacement that compared to the longer critical opening displacements experienced by the MCF-10A cells. [40]. The tri-linear force-traction curve of the cohesive zone model consists of an initial linear elastic undamaged region and a bi-linear softening. It simulates plasticity, microcracking, and fiber bridging. This suggests that, for cracking at higher stress and increased displacement in the MCF-10A up to a displacement magnitude of 5, a combination of plastic deformation and

subsequent deformation by microcracking and fiber bridging is associated with crack-tip shielding by the adhesion proteins and the cell cytoskeletal proteins.

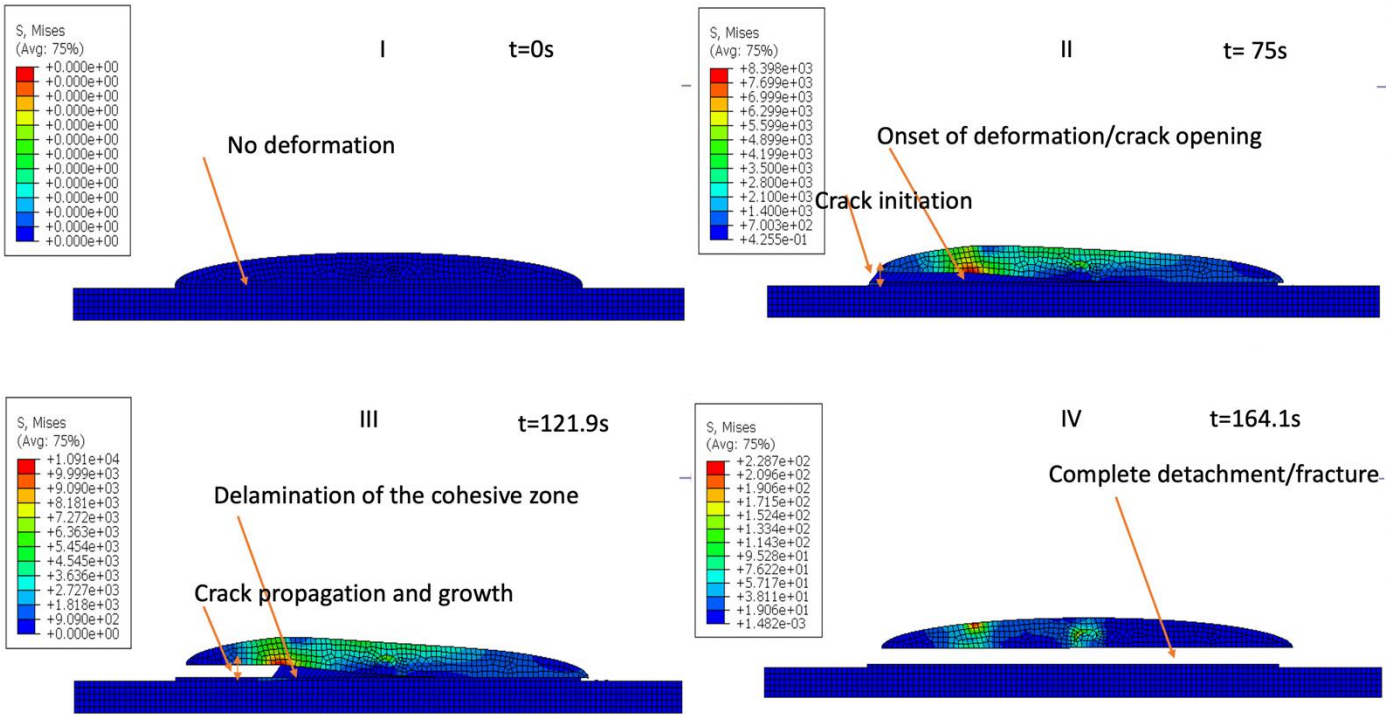

(a)

(b)

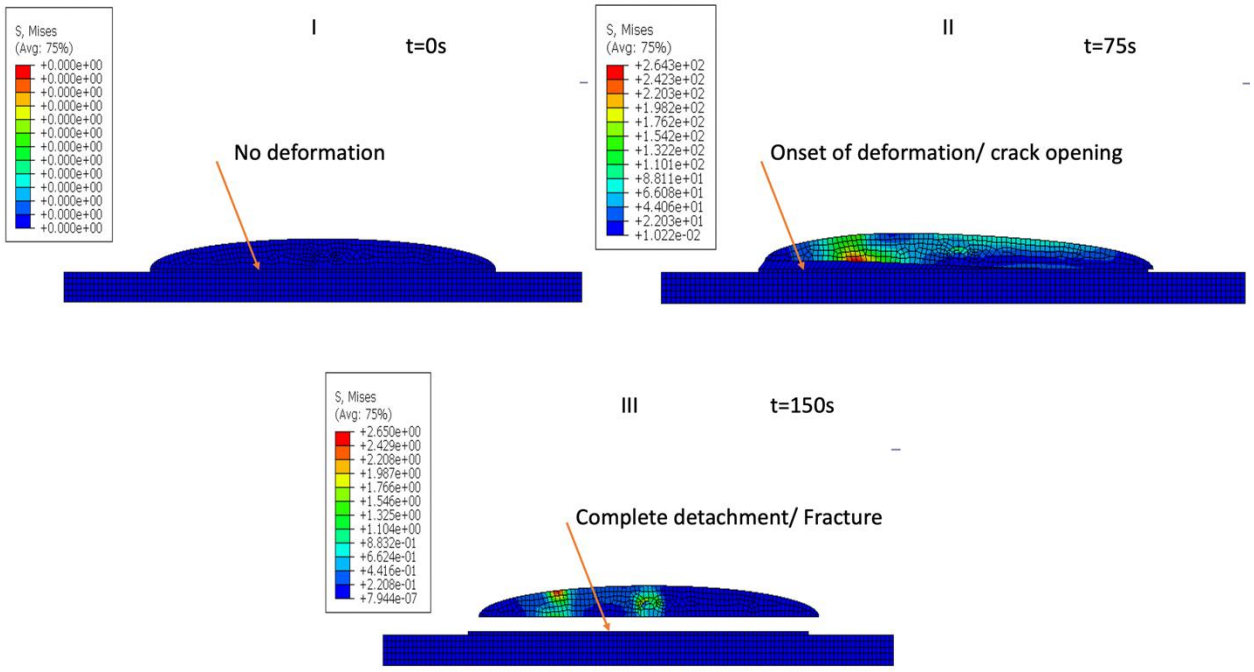

Figure 33: Finite element modelling of (a) MCF-10A (b) MDA-MB-231

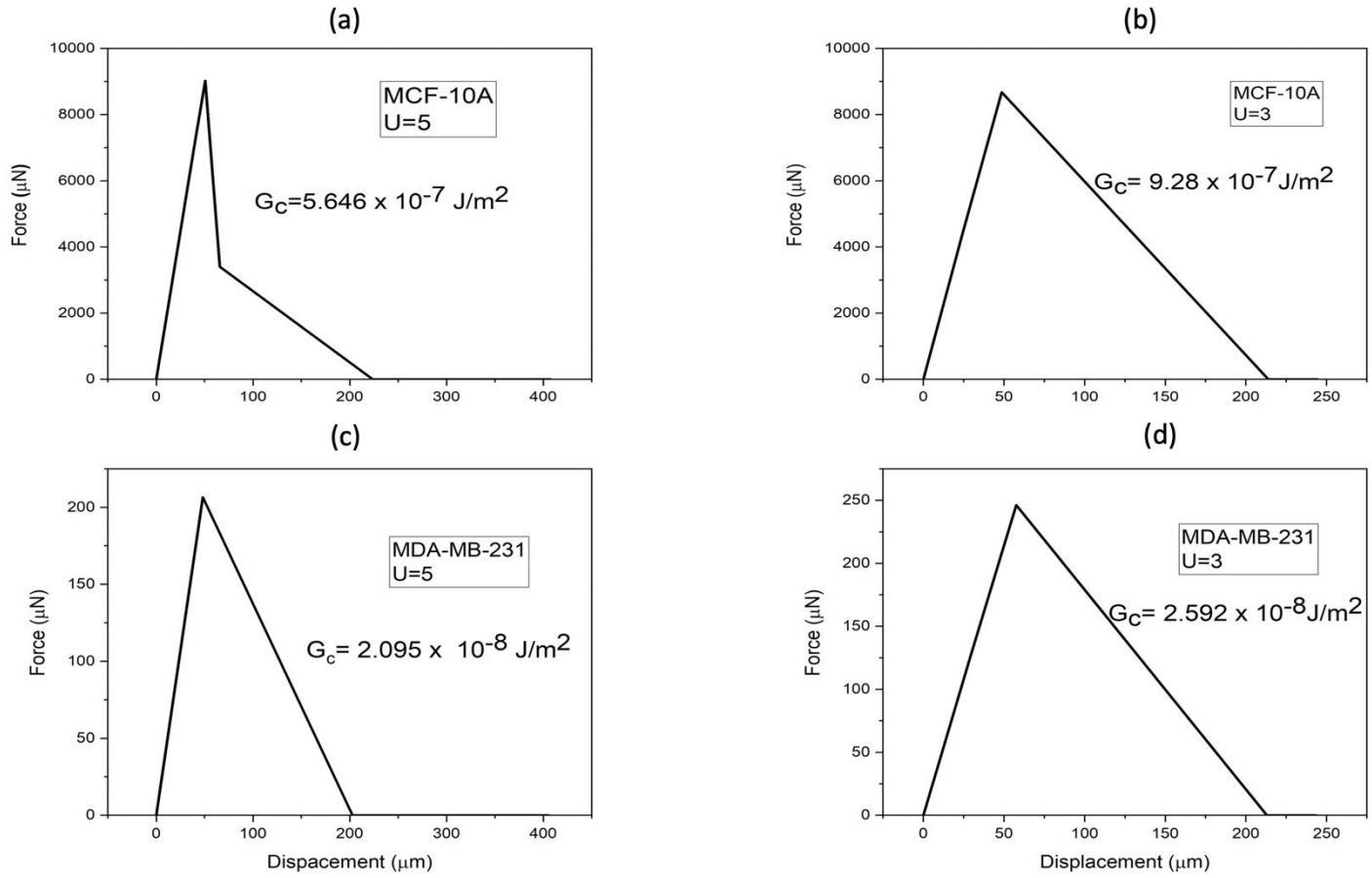

The computed critical energy release rate obtained for the non-tumorigenic breast cells and the tumorigenic triple-negative breast cancer cells are shown in table 3.

Figure 34: Force- traction curve and energy release rate for (a) MCF-10A cell at a displacement magnitude of 3 (U=3) (b) MCF-10A cell at a displacement magnitude of 5 (U=5) (c) MDA-MB-231 cell at a displacement magnitude of (U=3) (d) MDA-MB-231 cell at a displace displacement magnitude of 5 (U=5)

Table 8: Fracture toughness of the cells computed experimentally and theoretically

Cell type	Critical energy release rate (J/m^2)
MCF-10A (experimental)	$4.96 \times 10^{-5} \pm 1.65 \times 10^{-5}$
MCF-10A (theoretical)	$7.460 \times 10^{-7} \pm 2.570 \times 10^{-7}$
MDA-MB-231 (experimental)	$1.009 \times 10^{-6} \pm 5.055 \times 10^{-7}$
MDA-MB-231 (theoretical)	$2.343 \times 10^{-8} \pm 0.351 \times 10^{-8}$

The experimental critical energy release rates of the cells greater than those predicted by the cohesive zone model. Also, the critical energy release rates obtained for the cancerous MDA-MB-231 cells were lower than those of the normal MCF-10A cells. The theoretically computed critical energy release rates obtained for the cancerous MDA-MB-231 were lower than those of the normal MCF-10A cells. The significant differences between the theoretical critical energy release rates and the experimental critical energy release rates are attributed largely to the effects of crack-tip shielding via crack bridging by the initial crack bridging provided by the uncracked focal adhesion/ vinculin/actin structures that remain attached to the ECM after the cell detachment process.

5.4. Implications

The result of the current study provides insight into the failure mechanisms and fracture in non-tumorigenic breast cells and tumorigenic triple-negative breast cancer cells. The normal breast cell demonstrated higher resistance to applied forces and exhibited crack-tip shielding by crack bridging which was enabled by focal adhesions attached to vinculin or actin fibers. This is consistent with a higher incidence of cytoskeletal proteins such as actin and vinculin in normal cells. Such fiber bundles shield the crack-tips prior to the detachment of the cells from the ECM. However, crack propagation in cancer cells is associated with reduced volume fractions of fibrous actin networks and cytoskeletal structures. Thus, the extent of crack-tip shielding via crack bridging is much lower. This results in lower critical energy release rates for fracture between the cell membrane and the ECM. Thus, the interfacial fracture toughness of the cancer cells is lower than that of the non-tumorigenic cells. This suggests that the interfacial critical energy release rates may be used as mechanical biomarkers for the detection of non-tumorigenic breast cells and triple-negative breast cancer cells

6.0 Chapter Conclusion

1. Shear assay measurements of cell viscoelastic properties (Young's moduli, viscosities, and relaxation times), and their statistical distributions, can be used as mechanical biomarkers for the detection and classification of non-tumorigenic and tumorigenic TNBC cells/biopsies at different stages of cancer progression. They may also be correlated with quantitative fluorescence intensities obtained using confocal microscopy imaging techniques. The current work shows that statistical variations in the fluorescence intensities and the average fluorescence intensities (of the actin cytoskeleton structures)
2. The average young's moduli are highest in non-tumorigenic cells and lowest in the highly metastatic (MDA-MB-231) cells. Intermediate Young's moduli are also observed in the less metastatic cells (MDA-MB-468 cells). No clear trends are observed in the viscosities and relaxation times of the non-tumorigenic cells (MCF-10A) and the tumorigenic TNBC cells (MDA-MB-468 and MDA-MB-468 cells). However, the relaxation times of the cytoplasm are greater than those of the nuclei.
3. The fluorescence intensities of the actin cytoskeletal structure are highest in the non-tumorigenic cells (MCF-10A) and lower in tumorigenic TNBC cells (MDA-MB-468 and MDA-MB-468 cells). The fluorescence intensities and the incidence of the actin cytoskeletal structure also decrease with increasing metastatic states. Consequently, the less metastatic MDA-MB-468 cells have higher actin cytoskeletal fluorescence intensities than more metastatic MDA-MB-231 TNBC cells. The statistical variations in the fluorescence intensities are well characterized by normal distributions.

4. The fluorescence intensities of the different components of the cell cytoskeletal structure (Actin microfilaments, microtubules, and intermediate filaments) can be used to determine the relative volume densities of the individual components of the cell cytoskeletal structure, and hence can be used to distinguish between the structures of non-tumorigenic MCF-10A and tumorigenic MDA-MB-231 TNBC cells. The relative volume density of the intermediate filaments (Keratin 19, keratin18, keratin8, keratin 7, and vimentin), and microtubules (tubulin) are different in non-tumorigenic breast cells and tumorigenic TNBC cells. Also, the relative volume densities of the intermediate filaments are higher in the metastatic MDA-MB-231 TNBC cells. For keratin 18 and actin, their relative volume densities were greater in the non-tumorigenic (MCF-10A cells) than in the metastatic MDA-MB-231 cells. Similar trends are observed for the microtubules, for which the expression of the tubulin is greater in the metastatic MDA-MB-231 cells than in non-tumorigenic MCF-10A cells.
5. The average Young's moduli of the non-tumorigenic and tumorigenic breast cells increase with the increasing fluorescence intensity (volume fraction of actin cytoskeletal structure). The statistical variations in the fluorescence intensities are also associated with the statistical variations in young's moduli of the non-tumorigenic and tumorigenic cells. However, no clear continuous trends are observed in the viscosities and relaxation times of the nuclei and cytoplasms of non-tumorigenic and tumorigenic TNBC cells.
6. The measured young's moduli, viscosities, and relaxation times are well-characterized by normal distributions. These can be used for the estimation of the probabilities of occurrence or non-occurrence. They can also be integrated into PDFs and CDFs for the estimation of occurrence or non-occurrence under shear flow conditions that mimic the

conditions of blood flow in the body. Hence, the parameters of the normal distributions presented in this study can be used to model the probability of occurrence/non-occurrence of the corresponding cell viscoelastic properties under laminar shear flow conditions.

7. A combination of the relative volume densities and shear assay measurements can be used to provide diagnostic insights for the characterization of non-tumorigenic and tumorigenic TNBC cells. Such approach can be enabled by fluorescence microscopy imaging (to reveal the incidence and relative volume densities of the cytoskeletal proteins, especially actin) and shear assay measurements of creep strain rates/cell viscoelastic properties (Young's moduli/viscosities of the nuclei and cytoplasm). These can be used, respectively, as fluorescence and mechanical biomarkers, for the classification of breast cells into non-tumorigenic breast cells and tumorigenic TNBC cells.

8. The viscoelastic deformation of cells (induced b in the shear assay chamber) has been elucidated for non-tumorigenic breast cells and triple-negative breast cancer cells. The studies reveal that the cancer cells are more compliant and less viscous than non-tumorigenic cells.

9. The detachment of the triple-negative breast cells (MDA-MB-231 cells) occurs by either mode I (peeling/crack opening) or mode II (shear) mechanisms. However, in the case of non-tumorigenic breast cells (MCF-10A cells), local micro-buckling can occur within the cell membrane before the interfacial cracking that gives rise to cell detachment.

10. The critical energy release rates for cell detachment from ECM layers on substrates are lower for triple-negative breast cancer cells (MDA-MB-231 cells) than for normal breast cells (MCF-10A). The lower critical crack driving forces obtained for cancer cells are also associated with a much higher incidence of transmembrane vinculin that is attached to the ECM in ways that promote crack-tip shielding by crack bridging.

11. The differences between the predicted critical energy release rates obtained from the cohesive zone model (for the detachment of the cell membrane) are attributed to the shield differences in the crack tip shielding provided by the actin/vinculin/focal adhesion complexes in the non-tumorigenic and triple negative breast cancer cells. More so, the experimental approach factored the work of fracture, considering the molecular contribution of the fibrous networks of the adhesion proteins and the cell cytoskeleton, while the predicted approach, considered majorly the surface interactions between the cell and the ECM.

12. The significant differences between the critical energy release rates and cohesive zone parameters obtained for the non-tumorigenic and triple-negative breast cancer cells may serve as mechanical biomarkers for the respective detection of non-tumorigenic and tumorigenic triple-negative breast cancer cells. Further work is needed to determine the extent to which other breast cancer cell types exhibit similar trends during cell detachment via shear assay techniques.

General Conclusion and Recommendation for Future Work.

This thesis has explored the basic science of mechanics and structural components of biological materials. We utilized a shear stress-dependent system to study the mechanical properties (Stiffness, viscosity, and relaxation time) of biological cells. The shear assay technique utilized the fluid shear stresses to deform attached cells, and their correspondent response to mechanical stress and deformation was analyzed and their correspondent mechanical properties were determined. The cytoskeletal structures of the cells were also analyzed and correlated its effect on the mechanical properties of the cell. At different stages of cancer progression, different cytoskeletal proteins of the cells behaved differently from the rest, and hence indicated cell states and their expressions with cancer progression. The behavior of cells during deformation and their mode of deformation and detachment was also analyzed, to give insights to their interfacial fracture properties (critical energy release rate) and fracture toughness of the cell as cancer progresses. The mechanical properties and the fracture properties of the cells decreased with increasing metastasis. This was largely dependent on the structural composition of the cells (Cytoskeleton) and could be correlated to the mechanical properties and fracture behavior of the cells with increasing tumorigenesis. A combination of the mechanical properties, fracture properties and volume density of certain cytoskeletal proteins can be indicators for cell states and are potential biomarkers for the detection and detection of triple negative breast cancer.

Reference:

[1] M. H. Al-Azri, "Delay in cancer diagnosis: Causes and possible solutions," *Oman Medical Journal*, vol. 31, no. 5. pp. 325–326, 2016. doi: 10.5001/omj.2016.65.

[2] S. Chakraborty and T. Rahman, "The difficulties in cancer treatment.," *Ecancermedicalscience*, vol. 6, p. ed16, 2012, doi: 10.3332/ecancer.2012.ed16.

[3] N. Azamjah, Y. Soltan-Zadeh, and F. Zayeri, "Global trend of breast cancer mortality rate: A 25-year study," *Asian Pacific Journal of Cancer Prevention*, vol. 20, no. 7, pp. 2015–2020, 2019, doi: 10.31557/APJCP.2019.20.7.2015.

[4] J. Collignon, L. Lousberg, H. Schroeder, and G. Jerusalem, "Triple-negative breast cancer: Treatment challenges and solutions," *Breast Cancer: Targets and Therapy*, vol. 8, pp. 93–107, 2016, doi: 10.2147/BCTT.S69488.

[5] C. Melzer, J. von der Ohe, and R. Hass, "Breast Carcinoma: From Initial Tumor Cell Detachment to Settlement at Secondary Sites," *BioMed Research International*, vol. 2017, 2017, doi: 10.1155/2017/8534371.

[6] Hyuna Sung, Jacques Ferlay, Rebecca L. Siegel, Mathieu Laversanne, Isabelle Soerjomataram, Ahmedin Jemal, and Freddie Bray, "Global Cancer Statistics 2020: GLOBOCAN Estimates of Incidence and Mortality Worldwide for 36 Cancers in 185 Countries," *CA: A Cancer Journal for Clinicians*, vol. 71, no. 3, pp. 209–249, 2021, doi: 10.3322/caac.21660.

[7] L. Caplan, "Delay in breast cancer: Implications for stage at diagnosis and survival," *Frontiers in Public Health*, vol. 2, no. JUL, pp. 1–5, 2014, doi: 10.3389/fpubh.2014.00087.

[8] S. M. Reddy C H Barcenas, A K Sinha, L Hsu, S L Moulder, D Tripathy, D Tripathy, G N Hortobagy, and V Valero. "Long-term survival outcomes of triple-receptor negative breast cancer survivors who are disease free at 5 years and relationship with low hormone receptor positivity," *British Journal of Cancer*, vol. 118, no. 1, pp. 17–23, 2018, doi: 10.1038/bjc.2017.379.

[9] H. Gonçalves, M. R. Guerra, J. R. Duarte Cintra, V. A. Fayer, I. V. Brum, and M. T. Bustamante Teixeira, "Survival Study of Triple-Negative and Non–Triple-Negative Breast Cancer in a Brazilian Cohort," *Clinical Medicine Insights: Oncology*, vol. 12, 2018, doi: 10.1177/1179554918790563.

[10] O. Abulkhair, J. S. Moghraby, M. Badri, and A. Alkushi, "Clinicopathologic features and prognosis of triple-negative breast cancer in patients 40 years of age and younger in Saudi

Arabia," *Hematology/ Oncology and Stem Cell Therapy*, vol. 5, no. 2, pp. 101–106, 2012, doi: 10.5144/1658-3876.2012.101.

[11] E. S. Stovgaard, D. Nielsen, E. Hogdall, and E. Balslev, "Triple negative breast cancer–prognostic role of immune-related factors: a systematic review," *Acta Oncologica*, vol. 57, no. 1, pp. 74–82, 2018, doi: 10.1080/0284186X.2017.1400180.

[12] T. Ovcaricek, S. G. Frkovic, E. Matos, B. Mozina, and S. Borstnar, "Triple negative breast cancer - Prognostic factors and survival," *Radiology and Oncology*, vol. 45, no. 1, pp. 46–52, 2011, doi: 10.2478/v10019-010-0054-4.

[13] L. Yin, J. J. Duan, X. W. Bian, and S. C. Yu, "Triple-negative breast cancer molecular subtyping and treatment progress," *Breast Cancer Research*, vol. 22, no. 1, pp. 1–13, 2020, doi: 10.1186/s13058-020-01296-5.

[14] H. A. Wahba and H. A. El-Hadaad, "Current approaches in treatment of triple-negative breast cancer," *Cancer Biology and Medicine*, vol. 12, no. 2, pp. 106–116, 2015, doi: 10.7497/j.issn.2095-3941.2015.0030.

[15] H. Yagata, Y. Kajiura, and H. Yamauchi, "Current strategy for triple-negative breast cancer: Appropriate combination of surgery, radiation, and chemotherapy," *Breast Cancer*, vol. 18, no. 3, pp. 165–173, 2011, doi: 10.1007/s12282-011-0254-9.

[16] Sylvia Annabel Dass, Kim Liu Tan, Rehasri Selva Rajan, Noor Fatmawati Mokhtar, Elis Rosliza Mohd Adzmi, Wan Faiziah Wan Abdul Rahman, Elis Rosliza Mohd Adzm, Wan Faiziah Wan Abdul Rahman, Tengku Ahmad Damitri Al-Astani Tengku Din, and Venugopal Balakrishna. "Triple negative breast cancer: A review of present and future diagnostic modalities," *Medicina (Lithuania)*, vol. 57, no. 1, pp. 1–18, 2021, doi: 10.3390/medicina57010062.

[17] G. Y. Yoon, J. H. Cha, H. H. Kim, H. J. Shin, E. Y. Chae, and W. J. Choi, "Sonographic features that can be used to differentiate between small triple-negative breast cancer and fibroadenoma," *Ultrasonography*, vol. 37, no. 2, pp. 149–156, 2018, doi: 10.14366/usg.17036.

[18] H. Y. Du, B. R. Lin, and D. P. Huang, "Ultrasonographic findings of triple-negative breast cancer," *International Journal of Clinical and Experimental Medicine*, vol. 8, no. 6, pp. 10040–10043, 2015.

[19] Y. Bu, L. Li, C. Yang, R. Li, and J. Wang, "Measuring Viscoelastic Properties of Living Cells," *Acta Mechanica Solida Sinica*, vol. 32, no. 5, pp. 599–610, 2019, doi: 10.1007/s10338-019-00113-7.

[20] G. U. Unnikrishnan, V. U. Unnikrishnan, and J. N. Reddy, "Contribution of material properties of cellular components on the viscoelastic, stress-relaxation response of a cell during AFM indentation," *International Journal of Computational Methods in Engineering Science and Mechanics*, vol. 17, no. 3, pp. 137–142, 2016, doi: 10.1080/15502287.2015.1082674.

[21] Y. Jamali, M. Azimi, and M. R. K. Mofrad, "A sub-cellular viscoelastic model for cell population mechanics," *PLoS ONE*, vol. 5, no. 8, 2010, doi: 10.1371/journal.pone.0012097.

[22] E. A. Corbin, O. O. Adeniba, R. H. Ewoldt, and R. Bashir, “Dynamic mechanical measurement of the viscoelasticity of single adherent cells,” *Applied Physics Letters*, vol. 108, no. 9, 2016, doi: 10.1063/1.4942364.

[23] Y. Cao, R. Bly, W. Moore, Z. Gao, A. M. Cuitino, and W. Soboyejo, “Investigation of the viscoelasticity of human osteosarcoma cells using a shear assay method,” *Journal of Materials Research*, vol. 21, no. 8, pp. 1922–1930, 2006, doi: 10.1557/jmr.2006.0235.

[24] N. Schierbaum, J. Rheinlaender, and T. E. Schäffer, “Viscoelastic properties of normal and cancerous human breast cells are affected differently by contact to adjacent cells,” *Acta Biomaterialia*, vol. 55, pp. 239–248, 2017, doi: 10.1016/j.actbio.2017.04.006.

[25] J. Hu, Y. Zhou, J. D. Obayemi, J. Du, and W. O. Soboyejo, “An investigation of the viscoelastic properties and the actin cytoskeletal structure of triple negative breast cancer cells,” *Journal of the Mechanical Behavior of Biomedical Materials*, vol. 86, no. May, pp. 1–13, 2018, doi: 10.1016/j.jmbbm.2018.05.038.

[26] R. J. Rowbury, “Temperature effects on biological systems: introduction.,” *Science progress*, vol. 86, no. Pt 1-2, pp. 1–7, 2003, doi: 10.3184/003685003783238734.

[27] P. F. Davies and S. C. Tripathi, “Mechanical stress mechanisms and the cell: An endothelial paradigm,” *Circulation Research*, vol. 72, no. 2, pp. 239–245, 1993, doi: 10.1161/01.res.72.2.239.

[28] V. Hernández-Hernández, D. Rueda, L. Caballero, E. R. Alvarez-Buylla, and M. Benítez, “Mechanical forces as information: An integrated approach to plant and animal development,” *Frontiers in Plant Science*, vol. 5, no. JUN, pp. 1–16, 2014, doi: 10.3389/fpls.2014.00265.

[29] I. Digel, P. Kayser, and G. M. Artmann, “Molecular Processes in Biological Thermosensation,” *Journal of Biophysics*, vol. 2008, pp. 1–9, 2008, doi: 10.1155/2008/602870.

[30] J. R. Lepock and M. J. Borrelli, “How do cells respond to their thermal environment,” *International Journal of Hyperthermia*, vol. 21, no. 8, pp. 681–687, 2005, doi: 10.1080/02656730500307298.

[31] M. B. Al-Fageeh and C. M. Smales, “Control and regulation of the cellular responses to cold shock: The responses in yeast and mammalian systems,” *Biochemical Journal*, vol. 397, no. 2, pp. 247–259, 2006, doi: 10.1042/BJ20060166.

[32] “Forces in cell biology,” *Nature Cell Biology*, vol. 19, no. 6, p. 579, 2017, doi: 10.1038/ncb3552.

[33] C. S. Chen, J. Tan, and J. Tien, “Mechanotransduction at cell-matrix and cell-cell contacts,” *Annual Review of Biomedical Engineering*, vol. 6, pp. 275–302, 2004, doi: 10.1146/annurev.bioeng.6.040803.140040.

[34] M. Klingler-Hoffmann, P. Mittal, and P. Hoffmann, “The Emerging Role of Cytoskeletal Proteins as Reliable Biomarkers,” *Proteomics*, vol. 19, no. 21–22. 2019. doi: 10.1002/pmic.201800483.

[35] C. Metastasis *et al.*, “Movers and Shakers: Cell Cytoskeleton in Cancer Metastasis 1,” pp. 1–50, doi: 10.1111/bph.12704.

[36] B. O. Sun, Y. Fang, Z. Li, Z. Chen, and J. Xiang, “Role of cellular cytoskeleton in epithelial-mesenchymal transition process during cancer progression (Review),” pp. 603–610, 2015, doi: 10.3892/br.2015.494.

[37] D. A. Fletcher and R. D. Mullins, “Cell mechanics and the cytoskeleton,” *Nature*, vol. 463, no. 7280, pp. 485–492, 2010, doi: 10.1038/nature08908.

[38] T. D. Pollard and J. A. Cooper, “Actin, a central player in cell shape and movement,” *Science*, vol. 326, no. 5957, pp. 1208–1212, 2009, doi: 10.1126/science.1175862.

[39] T. D. Pollard and J. A. Cooper, “Actin, a central player in cell shape and movement,” *Science*, vol. 326, no. 5957, pp. 1208–1212, 2009, doi: 10.1126/science.1175862.

[40] H. M. Pallari and J. E. Eriksson, “Intermediate filaments as signaling platforms.,” *Science’s STKE : signal transduction knowledge environment*, vol. 2006, no. 366, pp. 6–10, 2006, doi: 10.1126/stke.3662006pe53.

[41] R. Sanghvi-Shah and G. F. Weber, “Intermediate filaments at the junction of mechanotransduction, migration, and development,” *Frontiers in Cell and Developmental Biology*, vol. 5, no. SEP, pp. 1–19, 2017, doi: 10.3389/fcell.2017.00081.

[42] N. Wang and D. Stamenović, “Contribution of intermediate filaments to cell stiffness, stiffening, and growth,” *American Journal of Physiology - Cell Physiology*, vol. 279, no. 1 48-1, pp. 188–194, 2000, doi: 10.1152/ajpcell.2000.279.1.c188.

[43] S. Kim and P. A. Coulombe, “Intermediate filament scaffolds fulfill mechanical, organizational, and signaling functions in the cytoplasm,” *Genes and Development*, vol. 21, no. 13, pp. 1581–1597, 2007, doi: 10.1101/gad.1552107.

[44] A. L. Parker, M. Kavallaris, and J. A. McCarroll, “Microtubules and their role in cellular stress in cancer,” *Frontiers in Oncology*, vol. 4 JUN, no. June, pp. 1–19, 2014, doi: 10.3389/fonc.2014.00153.

[45] S. Etienne-Manneville, “Actin and microtubules in cell motility: Which one is in control?,” *Traffic*, vol. 5, no. 7, pp. 470–477, 2004, doi: 10.1111/j.1600-0854.2004.00196.x.

[46] A. F. Pegoraro, P. Janmey, and D. A. Weitz, “Mechanical properties of the cytoskeleton and cells,” *Cold Spring Harbor Perspectives in Biology*, vol. 9, no. 11, 2017, doi: 10.1101/cshperspect.a022038.

[47] X. Zhang, Z. Pei, C. Ji, X. Zhang, J. Xu, and J. Wang, “Novel Insights into the Role of the Cytoskeleton in Cancer,” *Cytoskeleton - Structure, Dynamics, Function and Disease*, 2017, doi: 10.5772/66860.

[48] D. E. Ingber, N. Wang, and D. Stamenović, “Tensegrity, cellular biophysics, and the mechanics of living systems,” *Reports on Progress in Physics*, vol. 77, no. 4, pp. 1–42, 2014, doi: 10.1088/0034-4885/77/4/046603.

[49] B. S. Gan, *Computational Modeling of Tensegrity Structures*. 2020. doi: 10.1007/978-3-030-17836-9.

[50] Y. Shimizu, T. Kihara, S. M. A. Haghparast, S. Yuba, and J. Miyake, “Simple display system of mechanical properties of cells and their dispersion,” *PLoS ONE*, vol. 7, no. 3, 2012, doi: 10.1371/journal.pone.0034305.

[51] E. Moeendarbary and A. R. Harris, “Cell mechanics: Principles, practices, and prospects,” *Wiley Interdisciplinary Reviews: Systems Biology and Medicine*, vol. 6, no. 5, pp. 371–388, 2014, doi: 10.1002/wsbm.1275.

[52] N. Bonakdar *et al.*, “Measuring mechanical properties in cells: Three easy methods for biologists,” *Cell Biology International*, vol. 38, no. 10, pp. 1227–1232, 2014, doi: 10.1002/cbin.10303.

[53] A. P. A. J. Shang-You Tee, Andreas Bausch, “The mechanical cell Shang-You,” *Curr Biol.*, vol. 19, no. 17, 2010, doi: 10.1016/j.cub.2009.06.034.The.

[54] Q. S. Li, G. Y. H. Lee, C. N. Ong, and C. T. Lim, “AFM indentation study of breast cancer cells,” *Biochemical and Biophysical Research Communications*, vol. 374, no. 4, pp. 609–613, 2008, doi: 10.1016/j.bbrc.2008.07.078.

[55] X. Cai, X. Xing, J. Cai, Q. Chen, S. Wu, and F. Huang, “Connection between biomechanics and cytoskeleton structure of lymphocyte and Jurkat cells : An AFM study,” *Micron*, vol. 41, no. 3, pp. 257–262, 2010, doi: 10.1016/j.micron.2009.08.011.

[56] T. D. Nguyen and Y. Gu, “Investigation of Cell-Substrate Adhesion Properties of Living Chondrocyte by Measuring Adhesive Shear Force and Detachment Using AFM and Inverse FEA,” *Scientific Reports*, vol. 6, no. May, pp. 1–13, 2016, doi: 10.1038/srep38059.

[57] Y. Wu, G. D. McEwen, S. Harihar, S. M. Baker, D. B. DeWald, and A. Zhou, “BRMS1 expression alters the ultrastructural, biomechanical and biochemical properties of MDA-MB-435 human breast carcinoma cells: An AFM and Raman microspectroscopy study,” *Cancer Letters*, vol. 293, no. 1, pp. 82–91, 2010, doi: 10.1016/j.canlet.2009.12.016.

[58] I. Titushkin and M. Cho, “Distinct membrane mechanical properties of human mesenchymal stem cells determined using laser optical tweezers,” *Biophysical Journal*, vol. 90, no. 7, pp. 2582–2591, 2006, doi: 10.1529/biophysj.105.073775.

[59] M.-T. Wei *et al.*, “A comparative study of living cell micromechanical properties by oscillatory optical tweezers,” *Optics Express*, vol. 16, no. 12, p. 8594, 2008, doi: 10.1364/oe.16.008594.

[60] C. Arbore, L. Perego, M. Sergides, and M. Capitanio, “Probing force in living cells with optical tweezers: from single-molecule mechanics to cell mechanotransduction,” *Biophysical Reviews*, vol. 11, no. 5, pp. 765–782, 2019, doi: 10.1007/s12551-019-00599-y.

[61] N. Rezaei, B. P. B. Downing, A. Wieczorek, C. K. Y. Chan, R. L. Welch, and N. R. Forde, "Using optical tweezers to study mechanical properties of collagen," *Photonics North 2011*, vol. 8007, no. May 2014, p. 80070K, 2011, doi: 10.1117/12.905714.

[62] H. Zhang and K. K. Liu, "Optical tweezers for single cells," *Journal of the Royal Society Interface*, vol. 5, no. 24, pp. 671–690, 2008, doi: 10.1098/rsif.2008.0052.

[63] S. A. Klemuk, S. Jaiswal, and I. R. Titze, "Cell viability viscoelastic measurement in a rheometer used to stress and engineer tissues at low sonic frequencies," *The Journal of the Acoustical Society of America*, vol. 124, no. 4, pp. 2330–2339, 2008, doi: 10.1121/1.2973183.

[64] Y. J. Li *et al.*, "A microfluidic micropipette aspiration device to study single-cell mechanics inspired by the principle of wheatstone bridge," *Micromachines*, vol. 10, no. 2, 2019, doi: 10.3390/mi10020131.

[65] L. M. Lee and A. P. Liu, "The application of micropipette aspiration in molecular mechanics of single cells," *Journal of Nanotechnology in Engineering and Medicine*, vol. 5, no. 4, pp. 1–6, 2015, doi: 10.1115/1.4029936.

[66] G. Fu *et al.*, "Shear assay measurements of cell adhesion on biomaterials surfaces," *Materials Science and Engineering C*, vol. 29, no. 4, pp. 1293–1301, 2009, doi: 10.1016/j.msec.2008.10.026.

[67] Y. Cao, R. Bly, W. Moore, Z. Gao, A. M. Cuitino, and W. Soboyejo, "On the measurement of human osteosarcoma cell elastic modulus using shear assay experiments," *Journal of Materials Science: Materials in Medicine*, vol. 18, no. 1, pp. 103–109, 2007, doi: 10.1007/s10856-006-0667-8.

[68] C.J. Ani, J.D. Obayemi, V.O. Uzonwanne, O. S. Danyuo, Y Odusanya, J. Hu, K. Malatesta, and W. O. Soboyejo, "A Shear Assay Study of Single Normal/Breast Cancer Cell Deformation and Detachment from Poly-Di-Methyl-Siloxane (PDMS) Surfaces," *Journal of the Mechanical Behavior of Biomedical Materials*, 2018, doi: 10.1016/j.jmbbm.2018.11.012.

[69] K. Onwudiwe *et al.*, "Actin cytoskeletal structure and the statistical variations of the mechanical properties of non-tumorigenic breast and triple-negative breast cancer cells," *Journal of the Mechanical Behavior of Biomedical Materials*, vol. 119, no. May 2020, p. 104505, 2021, doi: 10.1016/j.jmbbm.2021.104505.

[70] L. Guillou *et al.*, "Measuring Cell Viscoelastic Properties Using a Microfluidic Extensional Flow Device," *Biophysical Journal*, vol. 111, no. 9, pp. 2039–2050, 2016, doi: 10.1016/j.bpj.2016.09.034.

[71] L. M. Lee and A. P. Liu, "A microfluidic pipette array for mechanophenotyping of cancer cells and mechanical gating of mechanosensitive channels," *Lab on a Chip*, vol. 15, no. 1, pp. 264–273, 2015, doi: 10.1039/c4lc01218f.

[72] S. A. Vanapalli, M. H. G. Duits, and F. Mugele, "Microfluidics as a functional tool for cell mechanics," *Biomicrofluidics*, vol. 3, no. 1, pp. 3–5, 2009, doi: 10.1063/1.3067820.

[73] Z. Chen, T. F. Yip, Y. Zhu, J. W. K. Ho, and H. Chen, “The method to quantify cell elasticity based on the precise measurement of pressure inducing cell deformation in microfluidic channels,” *MethodsX*, vol. 8, no. January, p. 101247, 2021, doi: 10.1016/j.mex.2021.101247.

[74] M. Dao, C. T. Lim, and S. Suresh, “Mechanics of the human red blood cell deformed by optical tweezers,” *Journal of the Mechanics and Physics of Solids*, vol. 51, no. 11–12, pp. 2259–2280, 2003, doi: 10.1016/j.jmps.2003.09.019.

[75] A. Ravetto, P. D. A. Anderson, C. V. C. Bouten, and J. M. J. den Toonder, “Microfluidics for Single Cell Mechanical Characterization: A Review,” *SM Journal of Biomedical Engineering*, vol. 3, no. 2, p. 1016, 2017.

[76] J. Mehanna, F. G. H. Haddad, R. Eid, M. Lambertini, and H. R. Kourie, “Triple-negative breast cancer: Current perspective on the evolving therapeutic landscape,” *International Journal of Women’s Health*, vol. 11, pp. 431–437, 2019, doi: 10.2147/IJWH.S178349.

[77] M. A. Medina *et al.*, “Triple-Negative Breast Cancer: A Review of Conventional and Advanced Therapeutic Strategies,” pp. 1–32, 2020.

[78] Y. Shen *et al.*, “Detecting heterogeneity in and between breast cancer cell lines,” *Cancer Convergence*, vol. 4, no. 1, pp. 1–11, 2020, doi: 10.1186/s41236-020-0010-1.

[79] J. Guck *et al.*, “Optical deformability as an inherent cell marker for testing malignant transformation and metastatic competence,” *Biophysical Journal*, vol. 88, no. 5, pp. 3689–3698, 2005, doi: 10.1529/biophysj.104.045476.

[80] Y. Nematbakhsh, K. T. Pang, and C. T. Lim, “Correlating the viscoelasticity of breast cancer cells with their malignancy,” *Convergent Science Physical Oncology*, vol. 3, no. 3, p. 034003, 2017, doi: 10.1088/2057-1739/aa7ffb.

[81] M. Tabatabaei, M. Tafazzoli-Shadpour, and M. M. Khani, “Correlation of the cell mechanical behavior and quantified cytoskeletal parameters in normal and cancerous breast cell lines,” *Biorheology*, vol. 56, no. 4, pp. 207–219, 2019, doi: 10.3233/BIR-190214.

[82] S. Suresh, “Biomechanics and biophysics of cancer cells,” *Acta Biomaterialia*, vol. 3, no. 4, pp. 413–438, 2007, doi: 10.1016/j.actbio.2007.04.002.

[83] E. L. Bearer, “Role of actin polymerization in cell locomotion: molecules and models.,” *American journal of respiratory cell and molecular biology*, vol. 8, no. 6, pp. 582–591, 1993, doi: 10.1165/ajrcmb/8.6.582.

[84] H. Kubitschke, J. Schnauss, K. D. Nnetu, E. Warmt, R. Stange, and J. Kaes, “Actin and microtubule networks contribute differently to cell response for small and large strains,” *New Journal of Physics*, vol. 19, no. 9, 2017, doi: 10.1088/1367-2630/aa7658.

[85] H. Babahosseini, A. N. Ketene, E. M. Schmelz, P. C. Roberts, and M. Agah, “Biomechanical profile of cancer stem-like/tumor-initiating cells derived from a progressive ovarian cancer model,” *Nanomedicine: Nanotechnology, Biology, and Medicine*, vol. 10, no. 5, pp. e1013–e1019, 2014, doi: 10.1016/j.nano.2013.12.009.

[86] Y. Nematbakhsh, K. T. Pang, and C. T. Lim, "Correlating the viscoelasticity of breast cancer cells with their malignancy," *Convergent Science Physical Oncology*, vol. 3, no. 3, p. 034003, 2017, doi: 10.1088/2057-1739/aa7ffb.

[87] S. E. Cross, Y. S. Jin, J. Rao, and J. K. Gimzewski, "Nanomechanical analysis of cells from cancer patients," *Nature Nanotechnology*, vol. 2, no. 12, pp. 780–783, 2007, doi: 10.1038/nnano.2007.388.

[88] A. Nagelkerke, J. Bussink, A. E. Rowan, and P. N. Span, "The mechanical microenvironment in cancer: How physics affects tumours," *Seminars in Cancer Biology*, vol. 35, pp. 62–70, 2015, doi: 10.1016/j.semcancer.2015.09.001.

[89] P. Sajeesh, A. Raj, M. Doble, and A. K. Sen, "Characterization and sorting of cells based on stiffness contrast in a microfluidic channel," *RSC Advances*, vol. 6, no. 78, pp. 74704–74714, 2016, doi: 10.1039/c6ra09099k.

[90] M. Nikkhah, J. S. Strobl, E. M. Schmelz, and M. Agah, "Evaluation of the influence of growth medium composition on cell elasticity," *Journal of Biomechanics*, vol. 44, no. 4, pp. 762–766, 2011, doi: 10.1016/j.jbiomech.2010.11.002.

[91] F. S. Quan and K. S. Kim, "Medical applications of the intrinsic mechanical properties of single cells," *Acta Biochimica et Biophysica Sinica*, vol. 48, no. 10, pp. 865–871, 2016, doi: 10.1093/abbs/gmw081.

[92] S. Kumar and V. M. Weaver, "Mechanics, malignancy, and metastasis: The force journey of a tumor cell," *Cancer and Metastasis Reviews*, vol. 28, no. 1–2, pp. 113–127, 2009, doi: 10.1007/s10555-008-9173-4.

[93] R. Takahashi, K. Kuribayashi-Shigetomi, M. Tsuchiya, A. Subagyo, K. Sueoka, and T. Okajima, "High-throughput measurements of cell mechanics using atomic force microscopy with micro-patterned substrates," *2013 International Symposium on Micro-NanoMechatronics and Human Science, MHS 2013*, vol. 0, pp. 7–9, 2013, doi: 10.1109/MHS.2013.6710471.

[94] M. E. Grady, R. J. Composto, and D. M. Eckmann, "Cell elasticity with altered cytoskeletal architectures across multiple cell types," *Journal of the Mechanical Behavior of Biomedical Materials*, vol. 61, pp. 197–207, 2016, doi: 10.1016/j.jmbbm.2016.01.022.

[95] A. N. Ketene, E. M. Schmelz, P. C. Roberts, and M. Agah, "The effects of cancer progression on the viscoelasticity of ovarian cell cytoskeleton structures," *Nanomedicine: Nanotechnology, Biology, and Medicine*, vol. 8, no. 1, pp. 93–102, 2012, doi: 10.1016/j.nano.2011.05.012.

[96] H. Ghaffari, M. S. Saidi, and B. Firoozabadi, "Biomechanical analysis of actin cytoskeleton function based on a spring network cell model," *Proceedings of the Institution of Mechanical Engineers, Part C: Journal of Mechanical Engineering Science*, vol. 231, no. 7, pp. 1308–1323, 2017, doi: 10.1177/0954406216668546.

[97] E. Fuchs and D. W. Cleveland, "A structural scaffolding of intermediate filaments in health and disease," *Science*, vol. 279, no. 5350, pp. 514–519, 1998, doi: 10.1126/science.279.5350.514.

[98] G. R. Sant, K. B. Knopf, and D. M. Albala, “Live-single-cell phenotypic cancer biomarkers-future role in precision oncology ?,” *npj Precision Oncology*, no. April, pp. 1–6, 2017, doi: 10.1038/s41698-017-0025-y.

[99] A. Burgess, S. Vigneron, E. Brioudes, J. C. Labbé, T. Lorca, and A. Castro, “Loss of human Greatwall results in G2 arrest and multiple mitotic defects due to deregulation of the cyclin B-Cdc2/PP2A balance,” *Proceedings of the National Academy of Sciences of the United States of America*, vol. 107, no. 28, pp. 12564–12569, 2010, doi: 10.1073/pnas.0914191107.

[100] O. Gavet and J. Pines, “Progressive Activation of CyclinB1-Cdk1 Coordinates Entry to Mitosis,” *Developmental Cell*, vol. 18, no. 4, pp. 533–543, 2010, doi: 10.1016/j.devcel.2010.02.013.

[101] S. Moreno-Flores, R. Benitez, M. D. M. Vivanco, and J. L. Toca-Herrera, “Stress relaxation and creep on living cells with the atomic force microscope: A means to calculate elastic moduli and viscosities of cell components,” *Nanotechnology*, vol. 21, no. 44, 2010, doi: 10.1088/0957-4484/21/44/445101.

[102] B. R. Brückner, H. Nöding, M. Skamrahl, and A. Janshoff, “Mechanical and morphological response of confluent epithelial cell layers to reinforcement and dissolution of the F-actin cytoskeleton,” *Progress in Biophysics and Molecular Biology*, vol. 144, pp. 77–90, 2019, doi: 10.1016/j.pbiomolbio.2018.08.010.

[103] L. Ramms, Fabris, Gloria, Windoffer, Reinhard, Schwarz, Nicole, Springer, Ronald, Zhou, Chen, azar, Jaroslav, Stiefel Simone, Hersch Nils, Schnakenberg Uwe, Magin Thomas M., Leube Rudolf E., Merkel Rudolf, Hoffmann Bern. “Keratins as the main component for the mechanical integrity of keratinocytes,” *Proceedings of the National Academy of Sciences of the United States of America*, vol. 110, no. 46, pp. 18513–18518, 2013, doi: 10.1073/pnas.1313491110.

[104] A. Malandrino, R. D. Kamm, and E. Moeendarbary, “In Vitro Modeling of Mechanics in Cancer Metastasis,” *ACS Biomaterials Science and Engineering*, vol. 4, no. 2, pp. 294–301, 2018, doi: 10.1021/acsbiomaterials.7b00041.

[105] H. Kim, K. Ishibashi, T. Okada, and C. Nakamura, “Mechanical property changes in breast cancer cells induced by stimulation with macrophage secretions in vitro,” *Micromachines*, vol. 10, no. 11, 2019, doi: 10.3390/mi10110738.

[106] G. Runel, N. Lopez-Ramirez, J. Chlasta, and I. Masse, “Biomechanical Properties of Cancer Cells,” *Cells*, vol. 10, no. 4, pp. 1–14, 2021, doi: 10.3390/cells10040887.

[107] K. Onwudiwe, J. Hu, J obayemi, V. Uzonwanne, C. Ani, C. Nwazojie, C. Onyekanne, T. Ezenwafor, S. Odunsanya, W. Soboyejo. “Actin cytoskeletal structure and the statistical variations of the mechanical properties of non-tumorigenic breast and triple-negative breast cancer cells,” *Journal of the Mechanical Behavior of Biomedical Materials*, vol. 119, no. May 2020, p. 104505, 2021, doi: 10.1016/j.jmbbm.2021.104505.

[108] X. Li and J. Wang, “Mechanical tumor microenvironment and transduction: Cytoskeleton mediates cancer cell invasion and metastasis,” *International Journal of Biological Sciences*, vol. 16, no. 12, pp. 2014–2028, 2020, doi: 10.7150/ijbs.44943.

[109] A. Teti, “Regulation of cellular functions by extracellular matrix,” *Journal of American society of Nephrology*, 1992.

[110] Elgundi Zehra, Papanicolaou Michael, Major Gretel, Cox Thomas R., Melrose james, Whitelock John M. Farrugia Brooke L. “Cancer Metastasis: The Role of the Extracellular Matrix and the Heparan Sulfate Proteoglycan Perlecan,” *Frontiers in Oncology*, vol. 9, no. January, 2020, doi: 10.3389/fonc.2019.01482.

[111] W. H. Goldmann, “Mechanosensation: A Basic Cellular Process,” *Progress in Molecular Biology and Translational Science*, vol. 126, pp. 75–102, Jan. 2014, doi: 10.1016/B978-0-12-394624-9.00004-X.

[112] X. Peng, E. S. Nelson, J. L. Maiers, and K. A. DeMali, “New Insights into Vinculin Function and Regulation,” *International Review of Cell and Molecular Biology*, vol. 287, pp. 191–231, Jan. 2011, doi: 10.1016/B978-0-12-386043-9.00005-0.

[113] X. F. Walboomers and J. A. Jansen, “Cell and tissue behavior on micro-grooved surfaces,” *Odontology*, vol. 89, no. 1, pp. 2–11, 2001, doi: 10.1007/s10266-001-8178-z.

[114] Allison L. Berrier and Kenneth M. Yamada, “Cell–matrix adhesion.pdf.” Journal of cell physiology, 2007. doi: 10.1002/jcp.21237.

[115] H. Stephen and E. H. J. Danen, “adhesion signaling. pdf.” Journal of cell science, pp. 1059–1069, 2009. doi: 10.1242/jcs.039446.

[116] R. M. Saunders *et al.*, “Role of vinculin in regulating focal adhesion turnover,” *European Journal of Cell Biology*, vol. 85, no. 6, pp. 487–500, 2006, doi: 10.1016/j.ejcb.2006.01.014.

[117] J. L. Coll, A. Ben-Ze’ev, R.M Ezzell, J.L. Rodriguez Fernandez, H. Baribault, R.G Oshima, E.D Adamson “Targeted disruption of vinculin genes in F9 and embryonic stem cells changes cell morphology, adhesion, and locomotion,” *Proceedings of the National Academy of Sciences of the United States of America*, vol. 92, no. 20, pp. 9161–9165, 1995, doi: 10.1073/pnas.92.20.9161.

[118] M. Heidari-Rarani and A. R. Ghasemi, “Appropriate shape of cohesive zone model for delamination propagation in ENF specimens with R-curve effects,” *Theoretical and Applied Fracture Mechanics*, vol. 90, pp. 174–181, 2017, doi: 10.1016/j.tafmec.2017.04.009.

[119] D. Baruffaldi, G. Palmara, C. Pirri, and F. Frascella, “3D Cell Culture: Recent Development in Materials with Tunable Stiffness,” *ACS Applied Biomaterials*, vol. 4, no. 3, pp. 2233–2250, 2021, doi: 10.1021/acsabm.0c01472.

[120] J. Y. Park, S. J. Yoo, E. J. Lee, D. H. Lee, J. Y. Kim, and S. H. Lee, “Increased poly(dimethylsiloxane) stiffness improves viability and morphology of mouse fibroblast cells,” *Biochip Journal*, vol. 4, no. 3, pp. 230–236, 2010, doi: 10.1007/s13206-010-4311-9.